# Revealing the Analytical Potential of FcγRIa (CD64) as a Ligand Molecule for IgG1 Capture and Antigen Sensing: Evaluation of FcγRIa ectodomain via Molecular Dynamics

by Eda ÇAPKIN

Submitted to the Graduate School of Engineering
and Natural Sciences in partial fulfillment of
the requirements for the degree of Doctor of Philosophy

Sabancı University
July 2023

Revealing the Analytical Potential of FcγRIa (CD64) as a Ligand Molecule for IgG1 Capture and Antigen Sensing: Evaluation of FcγRIa ectodomain via Molecular Dynamics

Eda ÇAPKIN

Molecular Biology, Genetics, and Bioengineering Program,
Ph.D. Thesis, JULY 2023

Thesis Supervisor: Assoc.Prof. Meral YÜCE

Keywords: Fc gamma receptor I, IgG1 capture, Surface Plasmon Resonance, Molecular Dynamics, D3 domain

## ABSTRACT

Monoclonal antibodies are widely used in many fields such as research, diagnostic, and therapeutic applications. the clinically approved monoclonal antibodies predominantly belong to the IgG1 sub-type. Generally, Protein A ligand is used to capture monoclonal antibodies, but it non-specifically interacts with other molecules. FcγRI plays a vital role in the immune system by triggering ADCC and or ADPC. It specifically interacts with a high affinity toward the lower hinge region of the Fc region of IgG1 sub-type antibodies. In this study, we evaluated the potential of Fc gamma receptor I (FcγRI) in terms of site-specific IgG1 capture and controlled orientation of IgG1 molecules on the sensor surface to detect their target antigens by SPR assays. Furthermore, we integrated the experimental approaches with computational methods to understand the structure and functional information of Fc and FcγRI interactions.

The first part of the study consisted of a comprehensive characterization of FcγRIa as an affinity ligand for IgG1-type monoclonal antibody binding. The antibody binding potential of FcγRIa was assessed with the SPR technique using different immobilization

techniques. Assays were performed in parallel with Protein A ligand to compare the antibody binding capacity of FcγRIa ectodomain. The final part of the study performed the classical molecular dynamics simulations to investigate the structural features, conformational dynamics, and interactions between FcγRIa with the Fc region of IgG1 in the presence and absence of the D3 domain within FcγRIa ectodomain.

.

IgG1 Yakalama ve Antijen Algılama için Ligand Molekülü Olarak FcγRIa'nın (CD64) Analitik Potansiyelinin Ortaya Çıkarılması: FcγRIa ekto bölgesinin Moleküler Dinamikler Yoluyla Değerlendirilmesi

Eda ÇAPKIN

Moleküler Biyoloji, Genetik ve Biyomüendislik
DOKTORA TEZİ, TEMMUZ 2023

Tez Danışmanı: Doç. Dr. Meral YÜCE

Anahtar Kelimeler: Fc gama reseptör protein I, IgG1, Yüzey Plazmon Rezonansı, Moleküler Dinamik, D3 domain

## ÖZET

Monoklonal antikorlar, araştırma, teşhis ve tedavi uygulamaları gibi birçok alanda yaygın olarak kullanılmaktadır. Klinik olarak onaylanmış monoclonal antikorlar ağırlıklı olarak IgG1 alt tipine aittir. Genel olarak Protein A ligandı, monoklonal antikorları yakalamak için kullanılır, ancak diğer moleküllerle spesifik olmayan bir şekilde etkileşime girer. FcγRI, ADCC ve/veya ADPC'yi tetikleyerek bağışıklık sisteminde hayati bir rol oynar. Spesifik olarak, IgG1 alt tipi antikorların Fc bölgesinin alt menteşe bölgesine doğru yüksek bir afinite ile etkileşime girer. Bu çalışmada, Fc gama reseptörü I'in (FcγRI) potansiyelini bölgeye özgü IgG1 yakalama ve sensör yüzeyinde IgG1 moleküllerinin hedef antijenlerini SPR testleri ile saptamak için kontrollü yönlendirme açısından değerlendirdik. Ayrıca, Fc ve FcγRI etkileşimlerinin yapısını ve fonksiyonel bilgilerini anlamak için deneysel yaklaşımları hesaplamalı yöntemlerle entegre ettik.

Çalışmanın ilk bölümü, IgG1 tipi monoklonal antikor bağlanması için bir afinite ligandı olarak FcγRIa'nın kapsamlı bir karakterizasyonundan oluşuyordu. FcγRIa'nın antikor bağlama potansiyeli, farklı immobilizasyon teknikleri kullanılarak SPR tekniği ile değerlendirildi. Analizler, FcγRIa ekto bölgesinin antikor bağlama kapasitesini karşılaştırmak için Protein A ligandı ile paralel olarak yapıldı. Çalışmanın son kısmı,

FcyRIa dış etki alanı içinde D3 alanının varlığında ve yokluğunda yapısal özellikleri, konformasyonel dinamikleri ve FcyRIa ile IgG1'in Fc bölgesi arasındaki etkileşimleri araştırmak için klasik moleküler dinamik simülasyonlarını gerçekleştirildi.

# ACKNOWLEDGEMENTS

First, I would like to thank my supervisor, Assoc. Prof. Meral Yüce for her mentorship and scientific contributions during my Ph.D. I would like to thank Assoc. Prof Hasan Kurt for his valuable feedback, discussion, and scientific contributions. Special thanks to Asst. Prof. Aslı Kutlu. We have studied with her for one year and she made me enjoy Molecular Dynamics study field with comprehensive knowledge and great patience. I would like to express my appreciation to jury members, Asst. Prof. Stuart Lucas and Asst. Prof. Morteza Ghorbani, for their contributions.

Secondly, I want to express my great appreciation to İlko R & D Biotechnology team. Especially Dilan Bıçak, Sibel Akgün Baş, and İlyas Koçak, I have learned many things from them and also enjoyed in our free time activities. I always feel like a team player while working in the DSP group. Also, it was a pleasure to work with Görkem Cemali, Meltem Çorbacıoğlu Pala, and Aylin Özkan. Besides work, we shared beautiful moments all together.

I feel so lucky to have friends that share beautiful memories and overcome difficulties together. Everything becomes easier with them. Ayşe Nur Ayan, Didem Aksu, Ayşe Nur Cin. I am grateful for our friendship over the years. They always listen, care, and encourage me. Their presence in my life has provided I want to thank my labmates, Begüm Balkan, Sümeyra Vural Kaymaz, Beyza Nur Günaydın, and Monireh Esmaili Rad. Besides their encouragement, motivation, and support, it was a privilege to meet these amazing researchers with good personalities and work discipline. I want to thank my last roommate, Gülşah Sevimli. I appreciate her patience, kindness, and her energy with odd songs. Thanks to Nilufer Çakır and Fatme Sert, we tried to motivate, encourage, and survive in every difficulty that we encountered. Thanks to my oldest friends, Asuman Güleç, Dilek Alan, and Sinan Gökçe, we shared countless memories, and I am grateful for them being in my life.

Lastly, Thanks to my family, Akide Çapkın, Hasan Çapkın, and Aysel Çapkın, they have always surrounded me with their love, support, and unwavering belief. They are always there for me whenever and wherever I need them.

*To my dear family…*

# TABLE OF CONTENTS

# LIST OF TABLES

# LIST OF FIGURES

# LIST OF ABBREVIATIONS

**ADA** Adalimumab

**ADCC** Antibody-Dependent Cellular Cytotoxicity

**ADCP** Antibody-Dependent Cellular Phagocytosis

**AVT** Avastin

**EDC** 1-Ethyl-3-(3-Dimethylaminopropyl)Carbodiimide

**FcγRs** Fc Gamma Receptors

**HER** Herceptin

**Ig** Immunoglobulin

**IgG** Immunoglobulin G

**ITAM** Immunoreceptor Tyrosine-Based Activation Motif

**ITIM** Immunoreceptor Tyrosine-Based Inhibitor Motif

**$k_a$** Association Rate Constant

**$k_d$** Dissociation Rate Constant

**$K_D$** Equilibrium Dissociation Constant

**kDa** Kilodalton

**MD** Molecular Dynamics

**NHS** N-hydroxysuccinimide

**nM** Nanomolar

**PDB** Protein Data Bank

**RMSD** Root-mean Square Deviations

**RMSF** Root-mean Square Fluctuations

**RU** Response Unit

**SEC-HPLC** Size exclusion high-performance liquid chromatography

**SPR** Surface Plasmon Resonance

**TNF-α** Tumor Necrosis Factor-alpha

**VEGF** Vascular Endothelial Growth Factor

**VMD** Visual Molecular Dynamics

# 1.    INTRODUCTION

## 1.1 Immune System and Immunoglobulins

The immune system is composed of many cell types and organs that collectively work to protect the body from invading pathogens or destructive self-cell types such as cancer cells.  Further, the immune system is classified as an innate and adaptive immune system.  The innate immune system provides the first line of defense by physical barriers (i.e., mucosal membrane), the cells (neutrophils, macrophages, Natural killer cells, dendritic cells, etc.), and secreted molecules (i.e., cytokine) for invading pathogens. The adaptive immune system gives a response specifically to the foreign antigen and activates the signaling cascade to combat the antigen. Recognition of the antigen occurs through the cell receptors of the cell ( B and T cells) and the antigen. The response is more durable and can be recognized quickly when it encounters the same antigen another time. Due to its specificity, the adaptive immune system could discriminate the self-molecules vs non-self-molecules and activate the response(Murphy and Weaver. 2017).

All cell types in the immune system are derived from hematopoietic stem cells in the bone marrow and further divided into either myeloid or lymphoid progenitor cells. Myeloid-derived progenitor cells which are T and B lymphocytes (T and B cells) are the main components in the adaptive immune systems. T cells are responsible for the cell-mediated immune response via interacting with the antigen through their T cell receptors (TCRs) on their cell surface. Upon the activation of B cells, they secrete soluble immunoglobulin (Ig) molecules to blood and body fluids for the neutralization of T-cell mediated destruction of the antigen(Murphy and Weaver. 2017).

In humans, there are 5 isotypes of Igs which are IgD, IgM, IgG, IgA, and IgE. Table 1 is given for the summary of all Ig isotypes. They are classified depending on the

1

varied heavy chain (HC) types including μ, δ, γ, α, or ε. The Light chain (LC) could be found in κ or λ type without affecting its antigen-binding activity. Both HC and LC contain the variable and constant regions in the upper region in Fab and the lower Fab/Fc regions, respectively. Fc regions possess branched glycans and they are attached through asparagine (Asn) residue forming N-linked glycans or serine (Ser), threonine (Thr), and tyrosine (Tyr) residues forming O-linked glycans. The profile of glycans affects various properties in an Ig function such as stability, effector function, and immunogenicity(Murphy and Weaver. 2017; Upton et al. 2016; Vidarsson, Dekkers, and Rispens 2014).

Table 1. Overview of the Ig isotypes and their properties. Adapted from (Murphy and Weaver. 2017).

| Antibody Isotype | IgD | IgM | IgG | IgA | IgE |
|---|---|---|---|---|---|
| | Membrane-bound | Monomer and pentamer | Monomer | Monomer and dimer | Monomer |
| Heavy chain | δ | μ | γ | α | ε |
| Subclass | | | IgG1 to IgG4 | IgA1 and IgA2 | |
| Abundance in bloodstream | + | ++ | ++++ | ++ | + |

| Function | B cell activation | high avidity for antigens and activation of the complement system | long-term protection via opsonization, ADCC, complement system activation, etc. | Protection for mucosal surfaces | Allergic response and parasite infections |
|---|---|---|---|---|---|

IgD has a unique property that is usually found in the membrane-bound form in the mature B cell surface. The function of IgD in the cell surface is capturing antigens and recruiting the downstream signaling effects in the cell(Schroeder and Cavacini 2010).

IgM is the earliest antibody produced in either the membrane-bound or secreted form in B cells. Mostly, it is linked by disulfide bonds through the Fc region to form a pentameric structure. The multiple binding sites provide increased avidity for antigen binding. Also, the pentameric IgM form enhances the effector function responses by interacting specifically with the C1q protein for the activation of the complement system in the early phase of infection(Murphy and Weaver. 2017; Schroeder and Cavacini 2010).

IgA can be found in monomeric or dimeric forms in the blood and mucosal membrane areas. Its primary role serves to protection over mucosal membranes (lungs, gastrointestinal tract, etc.) from an invading pathogen(Ding et al. 2022). IgE has a specific role in response to an allergen or parasite. It interacts with a high affinity with Fc epsilon receptor FcεR on the mast and basophil cell surface to trigger the release of histamine and other molecules for the elimination of the allergen(Schroeder and Cavacini 2010).

Immunoglobulin G (IgG) has the highest concentration and highest half-life in human serum (21 days compared to other Ig types. It consists of 2 heavy chains (HC) and 2 light chains (LC) which are bound by disulfide bonds in the hinge region. The fragment of antigen binding region (Fab) specially interacts with an antigen and triggers the downstream signaling in the target cell. In the Fab region, the antigen is recognized

through Complementary Determining Regions (CDRs) and each chain within the Fab region has 3 CDRs. The Fragment of crystallizable (Fc) region engages with varied receptors (Neonatal receptor-FcRn, Fc gamma receptor-FcγR, Complement protein 1q-C1q, etc.) to recycle the antibody molecules and/or initiate effector functions. IgGs are divided into 4 sub-classes which are IgG1, IgG2, IgG3, and IgG4. Among them, IgG1 is predominantly found in human serum. Even though they share high sequence similarity with a 90% ratio, they varied for the number of disulfide linkages in the hinge region, the length of the hinge region, and the effector function mechanism(Forest-Nault et al. 2021; Kiyoshi et al. 2015).
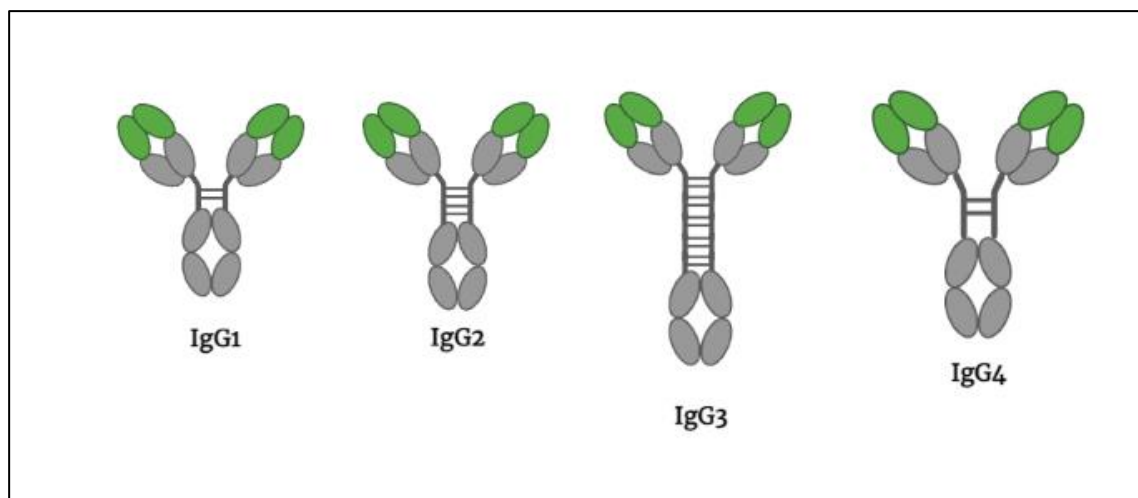


Figure 1. Schematic illustration of IgG sub-classes. The illustration was created with BioRender. Green represents variable region and gray parts represent constant region in the antibody structure. Figure adapted from(Vidarsson, Dekkers, and Rispens 2014).

## 1.2 Monoclonal Antibody

A monoclonal antibody is produced from a single B cellcolony that targets specifically one antigen and binds with a high affinity. Due to their enhanced specificity and affinity, monoclonal antibodies have a great application range, especially in the treatment of diseases (cancer, autoimmune disease, viral infection, etc.). The number of clinically approved monoclonal antibodies has been reported to be about 162 based on June 2022 reports and this number increases every year. Besides this number, there are a vast number of ongoing studies and first approval steps in the field of monoclonal antibodies. Antibody Society reported that this year

4

10 monoclonal antibody candidates were supported for the first approvals either from U.S.A or Europe. Expected selling numbers in the field of monoclonal antibody is indicated as 445 billion USD by 2028(The Antibody Society 2022). According to 2018 selling profit, top 10 clinically approved monoclonal antibodies were reported as Adalimumab (Humira), Nivolumab (Opdivo), Pembrolizumab(Keytruda), Trastuzumab (Herceptin), Bevacizumab (Avastin), Rituximab (Rituxan), Infliximab (Remicade), Ustekinumab (Stelara), Eculizumab (Soliris), and Omalizumab (Xolair) (Table 2)(R.-M. Lu et al. 2020). Due to the CoVID-19 pandemic in 2019, the best-selling clinically approved monoclonal antibody was replaced by the CoVID-19 vaccine (Pfizer/BioNTech) with a $55,918,791,640 profit(Kaplon et al. 2023).

Table 2. List of ten the most selling therapeutic monoclonal antibodies for 2018 (R.-M. Lu et al. 2020; Lyu et al. 2022)

| Product | Target | Disease | Antibody type | |
|---|---|---|---|---|
| Adalimumab | Tumor necrosis factor- alpha (TNF-α) | Crohn's disease Rheumatoid arthritis Ulcerative colitis Uveitis | IgG1 | Human |
| Nivolumab | Programmed cell death protein 1 (PD-1) receptor | Melanoma Non-small cell lung cancer Renal cell carcinoma | IgG4 | Human |
| Pembrolizumab | Programmed cell death protein 1 (PD-1) receptor | Melanoma Head and neck cancer Non-small cell lung cancer Lymphoma | IgG4 | Humanized |
| Trastuzumab | HER-2 receptor | Breast cancer Gastric cancer | IgG1 | Humanized |
| Bevacizumab | Vascular endothelial growth factor (VEGF) | Colorectal cancer Non-small cell lung cancer Breast ERB2 negative cancer Renal cell carcinoma Glioblastoma | IgG1 | Humanized |
| Rituximab | CD20 | Non-Hodgkin's lymphoma Chronic lymphocytic leukemia | IgG1 | Chimeric |

| | | Rheumatoid arthritis | | |
|---|---|---|---|---|
| Infliximab | TNF-α | Crohn's Disease Rheumatoid arthritis(RA) Ulcerative colitis Psoriasis | IgG1 | Chimeric |
| Ustekinumab | Interleukin (IL-12/IL-23) | Psoriasis Psoriatic arthritis Crohn's Disease | IgG1 | Human |
| Eculizumab | Complement protein C5 | Paroxysmal nocturnal hemoglobinuria Atypical hemolytic uremic syndrome | IgG2/4 hybrid | Humanized |
| Omalizumab | IgE | Asthma Chronic idiopathic urticaria | IgG1 | Human |

Therapeutic monoclonal antibodies are mostly produced in the form of IgG1 type. Technology for monoclonal antibody production is preferred by hybridoma and bacteriophage display techniques. Hybridoma technique is the first method that is performed by the fusion of antibody-producing B cells with immortalized myeloma cells. Bacteriophage is a virus that infects bacteria. This technique is generally used to produce single-chain variable fragments (scFv) at the coat surface glycoprotein of bacteria(Alejandra et al. 2023).

The specific antigen is injected into a mouse (called the immunization process) and B cells that produce monoclonal antibodies are recovered from the host. Then, they are fused with myeloma cells to produce monoclonal antibodies continuously. Depending on their origin and composition, the recombinant production of a monoclonal antibody could be murine, chimeric, humanized, or human types as shown in Figure 2. The first produced form of it was the murine monoclonal antibody that both Fab and Fc regions originated from mice. However, this type of antibody gives an immunogenic response when it is injected into a different host (i.e. human). Therefore, the production of a monoclonal antibody is genetically developed for the reduced immune response and higher binding activity in humans. For this purpose, a second monoclonal antibody type, chimeric, was developed in that variable chain in the Fab region originated from mice and other parts contain human amino acid

sequence. Further, a humanized monoclonal antibody was generated by integrating mouse-derived CDRs only in the Fab region to human frameworks in the antibody structure. This type is characterized by a lower immunogenicity and enhanced therapeutic properties compared to murine and chimeric monoclonal antibody forms. Human monoclonal antibodies originated in full human sequence in a whole antibody structure providing the lowest immunogenicity for a human host(Alejandra et al. 2023; Irani et al. 2015; R.-M. Lu et al. 2020).
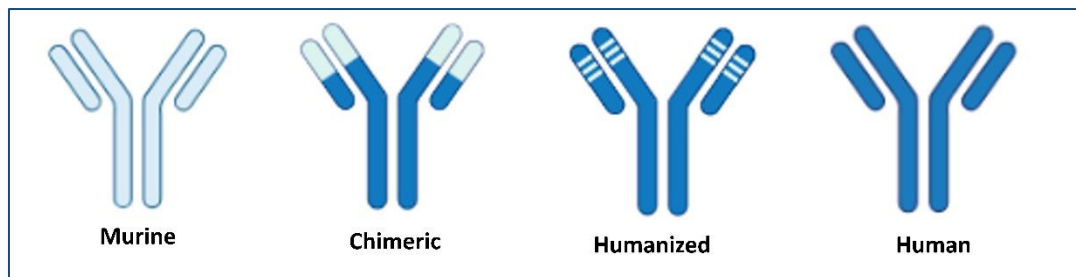


Figure 2. Schematic illustration for monoclonal antibody types from murine to human types. Light blue represents the sequence derived from mouse while blue represents the sequence originating from humans. Figure adapted from(R.-M. Lu et al. 2020).

Genetic engineering techniques are developed for the recombinant production of monoclonal antibodies in different hosts (mammalian, bacteria) for large-scale production. The CHO cell line (Chinese Hamster Ovary) is commonly used for the recombinant production of humanized monoclonal antibodies. CHO cells have been optimized for the correct folding of the protein, glycosylation, and titer capacities. They secrete antibodies to the media and after completion of the production bioprocess, they are recovered from this cell harvest. A general scheme is shown in Figure 3 to summarize the purification process of monoclonal antibodies. The purification process aims for the highest recovery of the target product while maintaining the highest product quality. Several filtration and chromatography steps are employed to remove impurities(Alejandra et al. 2023).
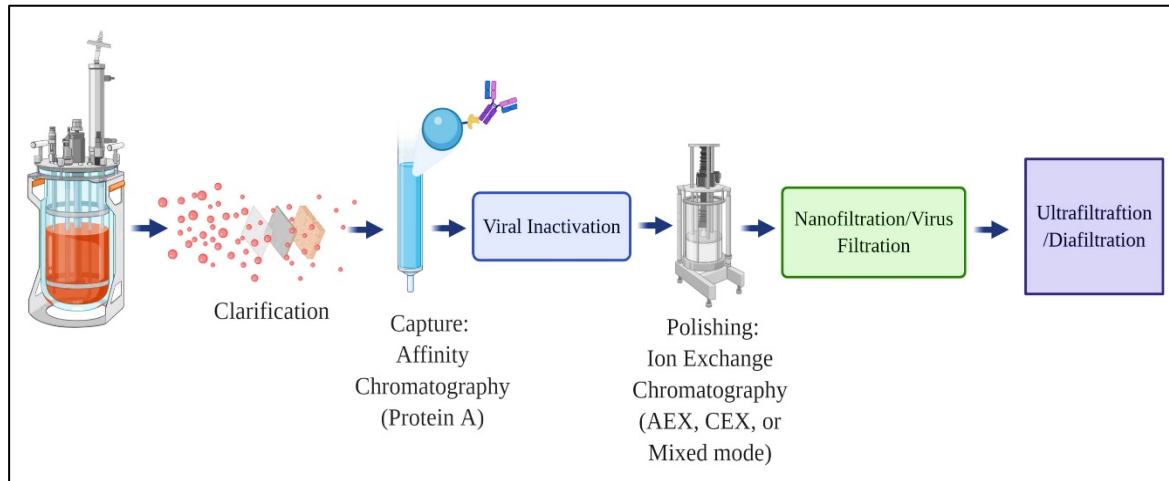
Figure 3. General flow chart for the recovery of monoclonal antibodies. The illustration was created with BioRender.

The application area of IgG1 is diverse including therapeutics, diagnosis, and research. In the field of therapeutics, the oriented capture of IgG1 is a significant role in the development phase of a therapeutic monoclonal antibody. Their characterization analysis is performed in all steps in a bioprocess through many analytical assays to ensure their efficacy and safety. IgG1-type monoclonal antibodies have great importance in the diagnosis of a disease. For instance, a cancer biomarker could be diagnosed with its targeting antibody in an immunoassay. Also, the progression of the disease and efficacy of the therapy could be monitored through the concentration analysis of the antigen and IgG1. Another example of the application of IgG1 in the diagnosis is the detection of infectious agents such as bacteria, viruses, and other pathogens. They could rapidly sense the presence of the agents and their amount in different samples. The widespread use of IgG1 has made it necessary and important to develop methods for their production, isolation, and selection from complex samples(Alejandra et al. 2023; Cain et al. 2023; Irani et al. 2015; Taeye, Rispens, and Vidarsson 2019).

## 1.3 Affinity Ligands

The capture or immobilization strategies are a key determinant in terms of binding efficiency which should not alter the binding ability of the antibody. Amine coupling

is a frequently used immobilization method in immunoassays. The coupling chemistry occurs through amide bond formation between the free primary amine group of the protein and a carboxyl group on the surface. Since this technique relies on random coupling, the binding activity of the biomolecules could be affected and diminish the performance of immunoassays(Brown et al. 2018; Forest-Nault et al. 2021). Amino acids that contain free primary amine groups in their R-group such as lysine (Lys), asparagine (Asn), and glutamine (Gln) could be conjugated through either in their  N terminal free amine groups or R- groups.

Alternatively, affinity ligands are utilized for the capture of antibodies. Commonly used antibody ligands are bacteria-originated Protein A, Protein G, Protein G/A, and Protein L. They are used in immunoassays, antibody purification, and immunoprecipitation assays.

Protein A is produced in the cell wall of Staphylococcus aureus *(S. aureus)*.  The binding occurs through the Fc region of IgGs in neutral pH conditions. Also, It could bind human, mouse, and rabbit IgGs. The structure of Protein A is composed of a single polypeptide. It has approximately 42 kDa and 5 Ig binding domains. Due to the steric hindrance, it is indicated as a 2 to 3 antibody binding ratio. Protein A ligand is frequently used in the purification process of monoclonal antibodies. However, it has some drawbacks, including ligand leaching with the treatment of the regeneration step, non-specific binding with other molecules in the cell supernatant, interaction with the Fab region of antibodies, and cost(Ghose, Hubbard, and Cramer 2006a).

Protein G is produced in *Streptococci* (Group G). Similar to Protein A, Protein G consists of a single polypeptide chain. The major difference with Protein A, Protein G has a high affinity toward all IgG subclasses. The recovery of IgGs is obtained with more acidic conditions than that of Protein A.

Protein L is obtained from Pepto streptococcus magnus (*P. magnus)*. It interacts with kappa light chain in Fab region of IgGs. Mostly it is used for the capture of antibodies that are not recovered with Protein A and Protein G ligands. It has 4 Ig binding domains and can bind with IgA, IgD, IgM, and IgE antibodies. The major restriction for Protein L is limited to antibodies that contain kappa light chains(Chen et al. 2020; Patel et al. 2015).

Protein G/ A or A/G is a combination of Protein G and Protein A ligands. It is fused to enhance antibody binding capacity for different antibody types from different species(Ghose, Hubbard, and Cramer 2006a; Taeye, Rispens, and Vidarsson 2019).

## 1.4 Fc Gamma Receptors

Fc gamma receptors (FcγRs) are expressed on varied immune cell surfaces and could trigger different immune responses by engaging the Fc region of the IgGs. Depending on the signaling molecule in the cytoplasmic region, it can be classified activator or inhibitory type. Activator type FcγRs have an ITAM domain (Immunotyrosine activator motif), and inhibitor type has an ITIM domain, an immunoreceptor tyrosine-based inhibitory motif. In humans, FcγRI, FcγRIIa, and FcγRIIIa are activator-type receptors while FcγRIIb is an inhibitory type receptor(Figure 4.). They can initiate and trigger varied immune responses such as antibody-dependent cellular cytotoxicity, antibody-dependent cellular phagocytosis, B-cell and dendritic cell activation, the release of proinflammatory molecules, etc. Binding interactions between FcγRs and IgGs depend on the antibody isotypes (IgG1, IgG2, IgG3, and IgG4) and the glycosylation profile of the antibody. FcγRIIIb is a different version of FcγRs which has a glycosylphosphatidylinositol (GPI) anchor to the cell membrane of neutrophils and does not possess a signaling molecule in its cytoplasmic part. The activator and inhibitor type FcγRs are expressed on the same cell surface to balance the immune response. In certain diseases i.e. arthritis, the alteration of the FcγRs structure and expression on the cells have been shown to cause the deviation of the immune responses(Cambay et al. 2020; Champion and Beck 2013; Forest-Nault et al. 2021; Hayes et al. 2016; Macri et al. 2021; Takakura, Tada, and Ishii-Watabe 2017; W. Wang and Chen 2022).
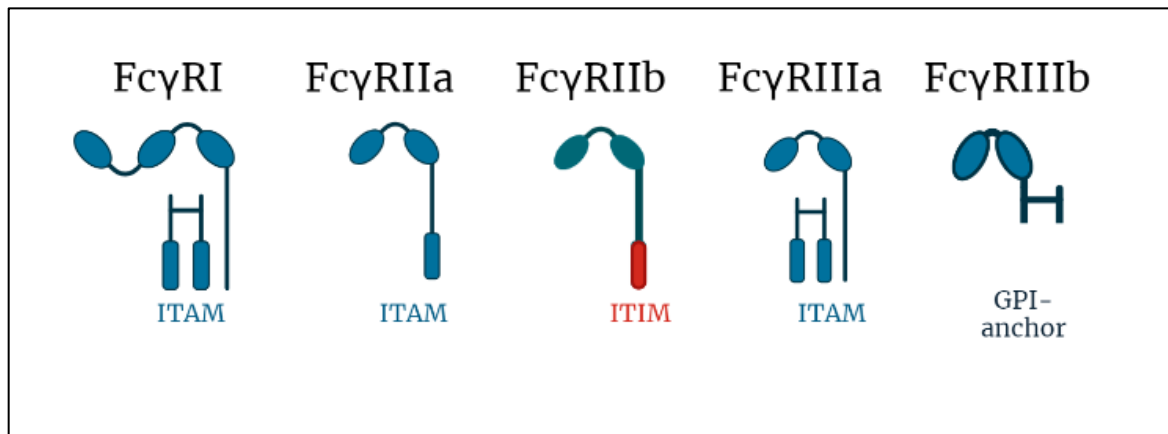
Figure 4. Schematic illustration of FcγRs. The illustration was created with BioRender.

### 1.4.1 Fc Gamma Receptor I

Among the FcγRs, the highest affinity toward IgGs occurs with FcγRI. It is expressed on the cell surface of macrophages, dendritic cells, and neutrophils. FcγRI is triggered by the engagement of the antibody on the target cell and leads to antibody-dependent cellular cytotoxicity (ADCC), complement-dependent cytotoxicity (CDC), or antibody-dependent cellular phagocytosis (ADCP). The immune response could be altered depending on the glycosylation profile of the monoclonal antibody(Anderson et al. 2022; J. Lu et al. 2011, 2015; van der Poel et al. 2011; Shields et al. 2001). The structure of the FcγRI possesses an ectodomain, a transmembrane domain, and an intracellular domain consisting of the activator motif signaling molecule. The binding interaction occurs with a 1: 1 binding ratio through the lower hinge region of IgGs. Binding affinity is different depending on the IgG sub-classes and such that IgG1 and IgG3 interact greater affinity with FcγRI than IgG4 and IgG2. Only FcγRI could bind to monomeric IgGs while other FcγRs could interact with antibody-antigen complexes.

FcγRI has 3 domains in its ectodomain part which are D1, D2, and D3(Figure 5). The D3 domain is found in only FcγRI; other FcγRs contain D1 and D2 domains. This variation is suggested as contributing to the higher affinity for IgGs than FcγRIIa and FcγRIIIa. Most of the binding interaction between FcγRI and IgG occurs through the

D1 and D2 domains. Especially, KHR motif in FG loop within the D2 domain contributes a significant stabilization with the IgG. The D3 domain in the FcγRI ectodomain is reported as serving a linker molecule which has no direct role in the binding interaction with IgG(Kiyoshi et al. 2015; J. Lu et al. 2011, 2015).
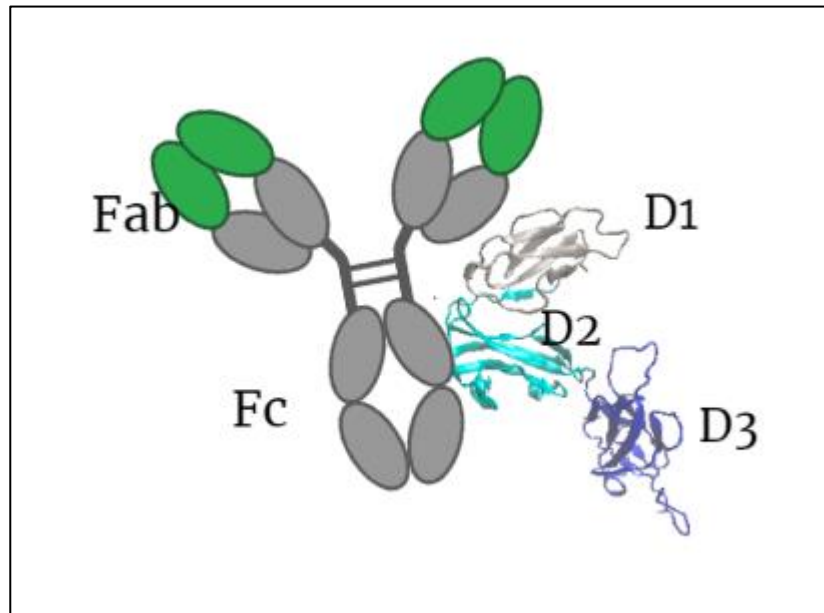


Figure 5. Structure of Fc and FcγRI complex. FcγRI domains represent grey, cyan, and blue D1, D2, and D3 domains respectively (PDB ID: 4X4M) in New Cartoon formats by Visual Molecular Dynamics (VMD) tools.

Many studies in the literature have focused on the therapeutic effects of the interactions between IgGs and FcγRs by Surface Plasmon Resonance (SPR) which is frequently used for binding analysis(Boesch et al. 2018; Dorion-Thibaudeau et al. 2014; Jefferis and Lund 2002b; Thomann et al. 2015b). It is reported by varied immunoassays that FcγRI interacts with a high affinity ($10^{-8}$ -$10^{-9}$) with IgG1-type antibodies. However, the configuration of FcγRs and IgGs on the chip surface has an impact on the value of $K_D$ in SPR assays. The anti-His capture method is commonly used to study binding interaction analysis with FcγRs and IgGs. Other assays involve amine coupling of either FcγRs and IgGs, a Biotin capture kit, and Protein A.

The binding interaction between FcγRs and IgGs is monitored to evaluate the quality attributes of therapeutic monoclonal antibodies. A few studies reported recombinant production of FcγRI ectodomain for IgG capture as an affinity ligand(Y Asaoka et al. 2012;

Hatayama et al. 2012; Jung, Kang, and Georgiou 2010; Kiyoshi et al. 2018).

## 1.5     Thesis Approach

Since the importance of IgG1 antibodies in varied biomedical and diagnostic applications, it is a need to develop alternative ligands with a high precision and specificity. In this thesis, we aim to reveal the ligand potential of FcγRI for IgG1 subtype antibody capture. The first part of the study covered the evaluation of binding interactions between FcγRI and IgG1 antibodies via SPR assays. Three clinically approved IgG1 monoclonal antibodies were utilized for assessing the potential of the FcγRI ectodomain. In parallel, the antibody binding potential was compared with the Protein A ligand in both on-surface (amine-coupling, His capture, and Biotin-streptavidin) and in-solution (via Protein L ligand) configurations in the SPR method.

In the second part, antigen sensing property was studied through site-specific IgG1 capture utilizing FcγRI ectodomain as an antibody capture ligand. SPR assays were performed to test FcγRI and Protein A ligands in terms of antibody and antigen binding responses. Binding affinity & kinetics, concentration analysis, and specificity assays were conducted in both captured FcγRI and amine-coupled Protein A ligand surfaces.

Moreover, computational methods were applied to analyze the structure and functional properties of FcγRI ectodomain complexed with the Fc region of an IgG1-type monoclonal antibody. To unravel the D3 domain impact within the FcγRI structure, Molecular Dynamics (MD) approach was studied with and without the presence of the D3 domain in the FcγRI ectodomain- Fc complex over 100 ns and 200 ns simulation runs. Critical residues in the binding site of FcγRI and Fc were assessed with analysis including root-mean-square deviation (RMSD), root-mean-square fluctuations (RMSF), intramolecular interactions, secondary structure, and unfolding tendency. Visual Molecular Dynamics (VMD) was utilized for the preparation of the system and the analysis of MD outputs.

## 2   Revealing the Analytical Potential of FcγRIa (CD64) as a Ligand Molecule for IgG1 Capture

### 2.1 Introduction

One unique property of FcγRIa is its high affinity for monomeric IgG, in contrast to other Fc receptors such as FcγRII and FcγRIII, which bind efficiently to the complex IgGs (dimer or aggregates) (Paetz et al. 2005; van de Winkel and Capel 1993). Despite the overwhelming amount of data published about the effector function of FcγRIa with therapeutic monoclonal antibodies, only a limited number of studies reported the FcγRIa protein as a potential affinity ligand (Bailey et al. 2018; Bruggeman et al. 2017; Robinett et al. 2018; Temming et al. 2021). In the study conducted by Boesch *et al*. (Boesch et al. 2018), the authors developed prototypes of FcγRs-conjugated (Ia, IIa, and IIIa) affinity chromatography columns to separate IgGs of different isotypes or glycan profiles from pooled human serum. The coupling of FcγRs was performed using EDC-NHS chemistry, which randomly constitutes a covalent bond between free carboxylic acid and primary amine groups. FcγRIIa and FcγRIIIa-coupled affinity columns accomplished the recovery of varied IgG subclasses and were further tested for their effector functions. However, the covalently-coupled FcγRIa affinity column was not as effective as the others due to regeneration problems. In another study by Kim *et al*. (C. Kim et al. 2014), FcγRIa was used to conjugate IgG-type antibodies to nanoparticles for biosensing purposes. The His-tagged FcγRIa proteins were first immobilized to the lipid-coated quantum dots using Ni-NTA conjugation chemistry. Four target-specific antibodies were later conjugated to the nanoparticles through FcγRIa-antibody interactions and evaluated further to detect cancer biomarkers, including Claudin-4, Mesothelin, Mucin-4, and Cadherin-11. FcγRIa was proposed as a universal antibody linker in this study. However, the authors did not conduct a complete analytical characterization study for the FcγRIa-antibody interaction. Despite the overwhelming amount of data published about the effector function of the FcγRIa with therapeutic monoclonal antibodies, only a few studies reported the FcγRIa protein as a potential affinity ligand with limited analytical performance information (Bailey et al. 2018; Bruggeman et al. 2017; Robinett et al. 2018; Temming et al. 2021).

A comprehensive analytical characterization of the FcγRIa as an alternative ligand molecule for site-directed IgG1 capture is covered in the current study. A systematic approach was adopted to evaluate the potential of FcγRIa as an alternative affinity ligand for IgG1-type monoclonal antibody binding. The SPR technique was used to monitor and compare the binding interactions obtained from different immobilization techniques. Then, cell supernatants of a biosimilar mAb product obtained from different purification steps were used to compare FcγRIa and Protein A-immobilized surfaces for IgG1 binding. Finally, we revealed the in-solution binding affinity of free FcγRIa to IgGs. The initial results promise a bright future for FcγRIa in analytical chemistry, especially in site-oriented IgG1 capture on surfaces and interfaces for biosensing applications.

## 2.2    Method

### 2.2.1 In-surface Configuration of FcγRIa and Protein A for IgG1 Binding Capacity Analysis

The IgG1 binding capacity analysis of immobilized FcγRIa and Protein A for three monoclonal antibodies ─ Adalimumab (ADA), Avastin (AVT), and Herceptin (HER) ─ was carried out on a CM5 type dextran chip by applying a standard EDC/Sulpho-NHS primary amine coupling procedure using a Biacore T200 SPR system (Cytiva). Later, two alternative conjugation methods were implemented.

First, His capture method was performed for FcγRIa binding analysis. A commercially available FcγRIa protein which includes a 6XHis tag at its C-terminal was studied for His capture assay (R&D systems). An amine coupling kit was used to apply the anti-His IgG1 antibody immobilization procedure based on the manufacturer's guide (Cytiva). The chip surface was activated by a 1:1 mixture of EDC-NHS reagents for Protein A immobilization. Then, Protein A was diluted to 25 µg/mL in 10 mM pH 5.0 acetate buffer and coupled through their primary amine groups to one flow cell. The residual activated carboxyl groups were blocked with 1M ethanolamine-HCl (Cytiva) on the dextran matrix. The final

immobilization level for the active flow cells reached approximately 200 response units (RU). FcγRIa at 10 µg/mL solution in HBS-EP 1X was captured on the active flow cells for 60 s with a 10 µL/min flow rate at 22 °C. Three different concentrations (10 nM, 30 nM, 90 nM) of monoclonal antibody samples were injected on both flow cells (active and blank) with 60 s association and 600 s dissociation with 30 µL/min flow rate at 22 °C. The surface was regenerated with 10 mM glycine (pH 1.5) for 60 s. Results were obtained with the double referencing method, where the presented data was subtracted from the zero-concentration sample and the blank surface. The SPR data were presented as the mean value obtained from at least three sample measurements. The kinetic parameter $k_a$, $k_d$, and equilibrium dissociation constants $(K_D)$ ─ were calculated by Biacore Evaluation Software using either the 1:1 Langmuir binding model (for FcγRIa) or the heterogeneous binding model (for Protein A). $K_D$ values from affinity analysis were performed with steady-state by Biacore Evaluation Software.

The second method was performed with biotinylated FcγRIa (Acro Biosystems) on the streptavidin-coated chip (SA) (Cytiva) chip. For the non-covalent immobilization of the FcγRIa ligand, the procedure was applied based on the manufacturer's guide (Cytiva). Biotinylated FcγRIa was prepared in HBS-EP 1X buffer solution at 100 nM concentration. The active flow cell was conditioned with 1M NaCl in 50 mM NaOH for 60 s. Then, FcγRIa was immobilized on the active flow channel at a 200 RU level. The wash step was performed with 50% isopropanol in 1 M NaCl and 50 mM NaOH. Binding analysis was performed with AVT at 30 nM concentration into both flow cells (active and blank) with 60 s association and 600 s dissociation with 30 µL/min flow rate at 22 °C. The surface was regenerated with 100 mM phosphoric acid pH 3.0 solution for 30 s. Results were obtained with double referencing, subtracted from zero concentration samples and blank surfaces. The SPR data were presented as the mean value, calculated from at least three measurements per sample.

### 2.2.2 IgG1 Binding Capacity Analysis with FcγRIa and Protein from Harvest Samples

An anti-VEGF biosimilar harvest product from the ILKO ARGEM Biotechnology R&D Center was purified with Protein A affinity chromatography (GE) using an AKTA FPLC instrument. Elution and clean-in-place (CIP) fractions were also collected for analysis. The sample solution was exchanged to HBS-EP five times with a 10 kDa protein filter unit

(Amicon Ultra-0.5, EMD-Millipore). Finally, the concentration of all samples was adjusted to 15 nM with 1X HBS-EP buffer.

The purity level of monoclonal antibody fractions was quantified with a size exclusion high-performance liquid chromatography (SEC) system (Waters e2695) on a TSK-GEL G3000SWxL (7.8 x 300 mm, Tosoh Biosciences) column. Reference sample (Avastin, AVT), a biosimilar harvest supernatant, and monoclonal antibody fractions (Elution, CIP) diluted in distilled water were loaded. All SEC-HPLC system buffers were filtered with a polyether sulfone membrane filter (0.2 μm) and degassed before use. The samples were monitored by UV absorbance at 280 nm. The monomeric monoclonal antibody level was obtained by determining the peak area of each species as a percentage of the total peak area (J. A. J. Lee et al. 2019; Seo et al. 2018; Xie et al. 2020).

Protein A, anti-His antibody, and FcγRIa was immobilized on the CM5 chip using the amine coupling reaction on the second, third, and fourth flow cells for two different CM5 chips. FcγRIa (14 nM and 30 nM) was captured on the third flow cell for the 60 s with a flow rate of 10 μL/min at 22 °C. Monoclonal antibody samples were injected at 15 nM for the 60 s with a flow rate of 10 μL/min.

The results were obtained with double referencing, where the presented response was subtracted from the zero-concentration sample (buffer) and blank surface (either naïve CM5 surface or Ethanolamine-coated surface). The mean value and standard deviation were calculated from at least three measurements per sample.

### 2.2.3 On-surface Configuration of FcγRIa, FcγRIIa, and FcγRIIIa for IgG1 Binding Assay

The binding analysis of recombinant FcγRIa, FcγRIIa, and FcγRIIIa (R&D systems) for three different monoclonal antibodies was performed with a Biacore T200 SPR system (Cytiva). Protein L (Pierce) was immobilized on two flow channels of the CM5 chip by applying a standard amine coupling reaction (Cytiva). First, the chip surface was activated by a 1:1 mixture of EDC-NHS reagents. Then, Protein L was diluted to 25μg/mL in 10 mM pH 4.0 acetate buffer and coupled through their primary amine groups to two flow cells. The residual activated carboxyl groups were blocked with 1M ethanolamine-HCl (Cytiva) on the dextran matrix. The final immobilization level for the flow cells reached approximately 300 response units (RU). FcγRs and three monoclonal antibodies, Adalimumab (Abbvie, HumiraPen, 1126059), Avastin( Roche, B8703H35), Herceptin

(Roche, Herceptin, N7377B51U1) were prepared with 1x HBS-EP running buffer. Single-cycle kinetic analyses were conducted at a 30 µL/mL flow rate at 22 °C (Karlsson, Pol, and Frostell 2016). Adalimumab, Avastin, and Herceptin at 6 nM concentrations were captured on the active flow cells for the 60 s with a 10 µL/mL flow rate at 22 °C. Three different concentrations (1.66 nM, 5 nM, 15 nM) of FcγRIa, FcγRIIa, and FcγRIIIa samples were injected through both flow cells (active and blank) with 60 s association and 600 s dissociation with a flow rate of 30 µL/mL at 22 °C. The surface was regenerated with 10 mM glycine buffer at pH 1.5 for 60 s. Results were obtained with double referencing, subtracting the active surface response from the zero-analyte concentration sample (buffer) and blank surface (either naïve CM5 surface or Ethanolamine-coated surface). The SPR data were presented as the mean value and standard deviation, calculated from at least three measurements per sample. One-way analysis of variance, ANOVA, was used to reveal the statistically significant data ($p < 0.05$ was considered significant and $p < 0.005$ was considered highly significant).

### 2.2.4 On-surface Configuration of FcγRIa and Protein A for IgG1 Binding Capacity Analysis

The binding analyses of the FcγRIa and Protein A (Sigma Aldrich) in solution were carried out on a Protein L-immobilized dextran-coated CM5 chip (Cytiva). The immobilization procedure was applied as previously described in section 2.1.3. FcγRIa, Protein A, and selected monoclonal antibodies (Adalimumab, Avastin, and Herceptin) were prepared with 1X HBS-EP running buffer. Single-cycle kinetic analyses were conducted at a flow rate of 30 µL/min at 22 °C. Adalimumab, Avastin, and Herceptin were captured on the active flow cells for the 60 s with a flow rate of 10 µL/min at 22 °C. Five different concentrations (0.37 nM, 1.11 nM, 3.33 nM, 10nM, 30 nM) of FcγRIa and Protein A samples were injected on both flow cells (active and blank) with 60 s association and 600 s dissociation with a flow rate of 30 µL/min at 22 °C. The surface was regenerated with 10 mM glycine (pH 1.5) for 60 s. Results were obtained with double referencing and subtracted from zero concentration sample and blank surface. The SPR data were presented as the mean value, calculated from at least three measurements per sample. One-way analysis of variance, ANOVA, revealed the statistically significant differences between the sample pairs ($p < 0.05$ was considered significant and $p < 0.005$ was considered highly significant). The equilibrium dissociation constants ($K_D$) were calculated by Biacore Evaluation Software using a 1:1 Langmuir

binding model.

## 2.3    Results&Discussion

### 2.3.1  In-surface Configuration of FcγRI and Protein A for IgG1 Binding Capacity Analysis

Antibody binding performances of FcγRIa and Protein A were first assessed with direct coupling of FcγRIa ectodomain and Protein A on different CM5 type dextran chip channels by EDC/Sulpho-NHS reaction(Figure 6A). Despite several attempts, the amine coupling method did not perform successfully for FcγRIa; it resulted in a few RU of IgG binding with considerable variations among technical repeats (Figure 6B). A similar result for EDC/NHS coupling of FcγRIa was also reported in the literature (Dorion-Thibaudeau et al. 2014).

In the chip configuration presented in Figure 6C, the biotinylated FcγRIa ectodomain was tested on a streptavidin-coated chip surface, aiming for a site-directed immobilization of FcγRI ectodomain to the streptavidin surface for subsequent studies. Initially, the method was optimized for the best regeneration conditions. SPR assays were conducted on a low consumption mode with AVT antibody at 90 nM. As seen in Figure 6D, the optimum conditions were screened for the most stable baseline and the highest sample response by testing many different buffer solutions. According to the results, the best regeneration conditions were chosen as 50 mM citrate at pH 3.0 and 50 mM phosphoric acid solution, and the binding analysis was performed with these regeneration solutions. However, the binding analysis results were not reproducible. IgGs were not efficiently recovered from the FcγRIa-immobilized surface, leading to the IgGs' accumulation on the surface and an increase in the baseline response for the subsequent cycles. Therefore, only AVT was tested

in the binding analysis with 100 mM phosphoric acid as the regeneration buffer for 20 cycles. As seen in Figure 6E, the sample response decreased from 360 RU to 60 RU between the first and the last cycle. Also, the baseline increased gradually till the last cycle. Similar results were also reported by Boesch *et al.* (2018), who conjugated the FcγRs to a chromatography resin to recover different IgG subtypes from the human serum. Elution of the IgGs was accomplished with glycine buffer, but FcγRIIa and FcγRIIIa maintained their IgG binding activity while FcγRIa could not be used after the buffer treatment (Boesch et al. 2018). In our study, Glycine buffer also disrupted the FcγRIa structure after the first injection, and the Protein could not bind the antibodies for the following cycle (data not shown). In addition, some molecular modeling studies indicated that the glycan structure stabilizes the interaction between the FcγRIa and the IgG, and thus It is hard to disrupt the interaction without harming the ligand  (Anderson et al. 2022; Dorion-Thibaudeau et al. 2014). Our findings with regeneration scouting were similar to the studies, which reported that the regeneration of FcγRIa-IgG from the chip surface was complex due to high affinity (Dorion-Thibaudeau et al. 2014). Eventually, further experiments were carried out with the His-tag capture method.
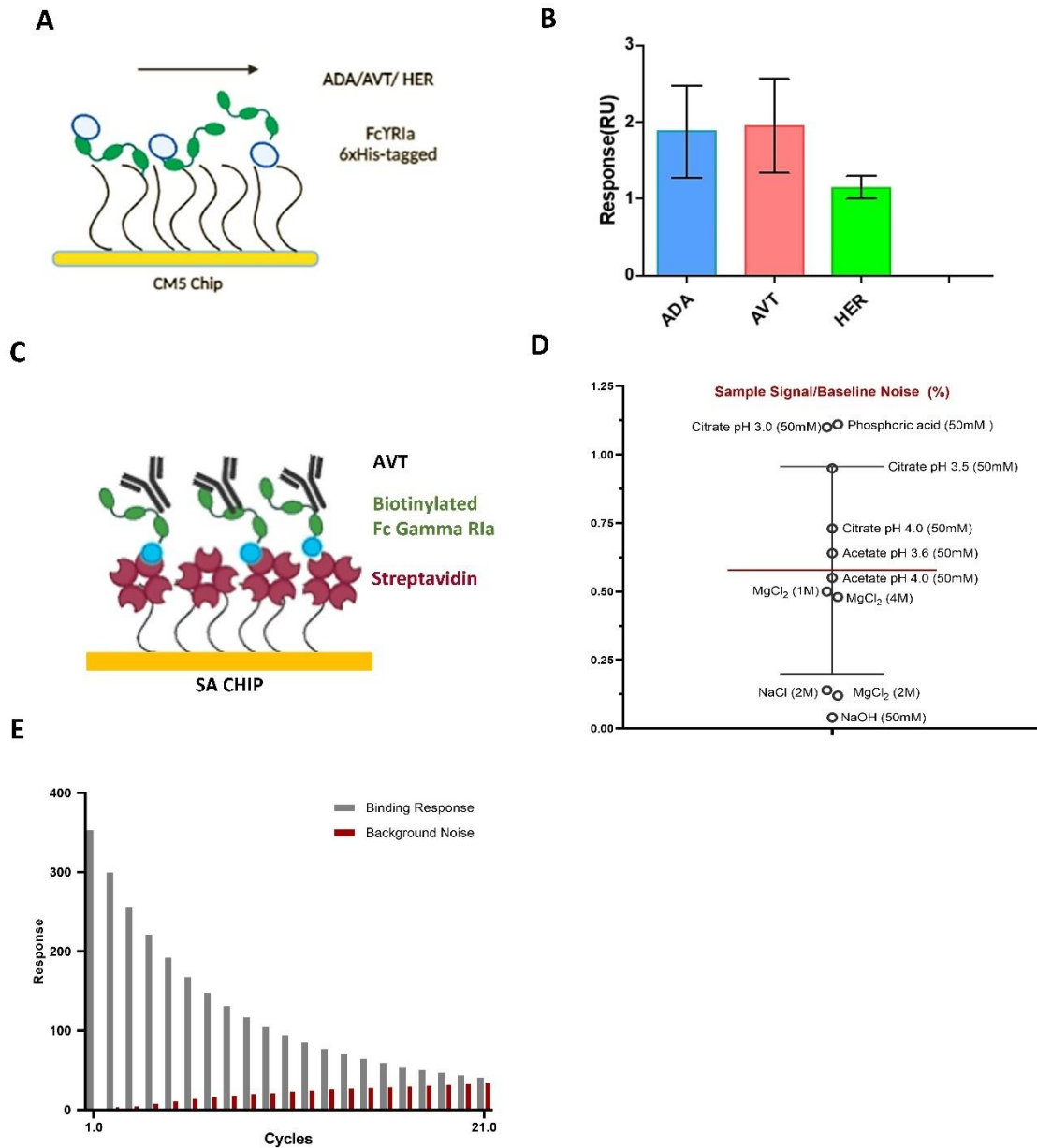
Figure 6. Evaluation of FcγRI and IgG binding response on amine coupled and biotin captured configurations A) Illustration of chip configuration for amine coupled FcγRI on CM5 chip B) Binding response graphs of three IgG1-type monoclonal antibodies, Adalimumab (ADA), Avastin (AVT), and Herceptin (HER) on amine coupled FcγRI on CM5 chip. C) Illustration of chip configuration for the binding assay with biotinylated FcγRI captured on the streptavidin (SA) chip surface D) Various regeneration buffer conditions were tested for the biotinylated FcγRI assay. The plot was obtained by normalizing the response of the antibody sample and baseline responses based on the control run. E) Repeatability assay which was performed with SA chip surface and Biotinylated FcγRIa with 20 cycles at a single concentration of AVT sample. The Response bar is shown for sample response and background response for each cycle.  Illustrations were created with BioRender program.

In the chip configuration presented in Figures 7A and 7B, anti-His antibodies and Protein A were directly coupled to the CM5 chip surface with EDC/NHS coupling method. FcγRIa was later captured through its His-tag at each experiment. IgG1-type monoclonal antibodies (ADA, AVT, and HER) were compared in terms of the binding response levels, and immobilized Protein A and captured FcγRIa levels were kept constant at 200 RU. As presented in Figure 7C, the monoclonal antibody binding response of FcγRIa was dramatically lower than that of Protein A, in sharp contrast to the in-solution binding analysis results, where those proteins were employed as analytes rather than ligands. However, the results were not surprising because Protein A has five IgG binding domains that give rise to an interaction beyond 1:1 when used as a ligand. As reported previously, the binding stoichiometry between monoclonal antibodies and Protein A was calculated at 2.4–3.1 (ratio) in a solution analysis (Ghose, Hubbard, and Cramer 2006a). Real-time interactions of IgGs and FcγRIa displayed a fast decline at the dissociation phase for each monoclonal antibody on the anti-His antibody immobilized surface. It is known that kinetics and affinity values could vary significantly depending on the SPR assay configuration. His capture method presented a non-stable sensorgram profile during the dissociation phase. Alternative to the His capture method, Protein A, E/K coil peptides, and biotin capture studies were reported for the FcγRIa-IgG interaction analysis (Forest-Nault et al. 2021). ADA and HER always showed higher response levels in two data sets than AVT (Figure 7D and Figure 7E).
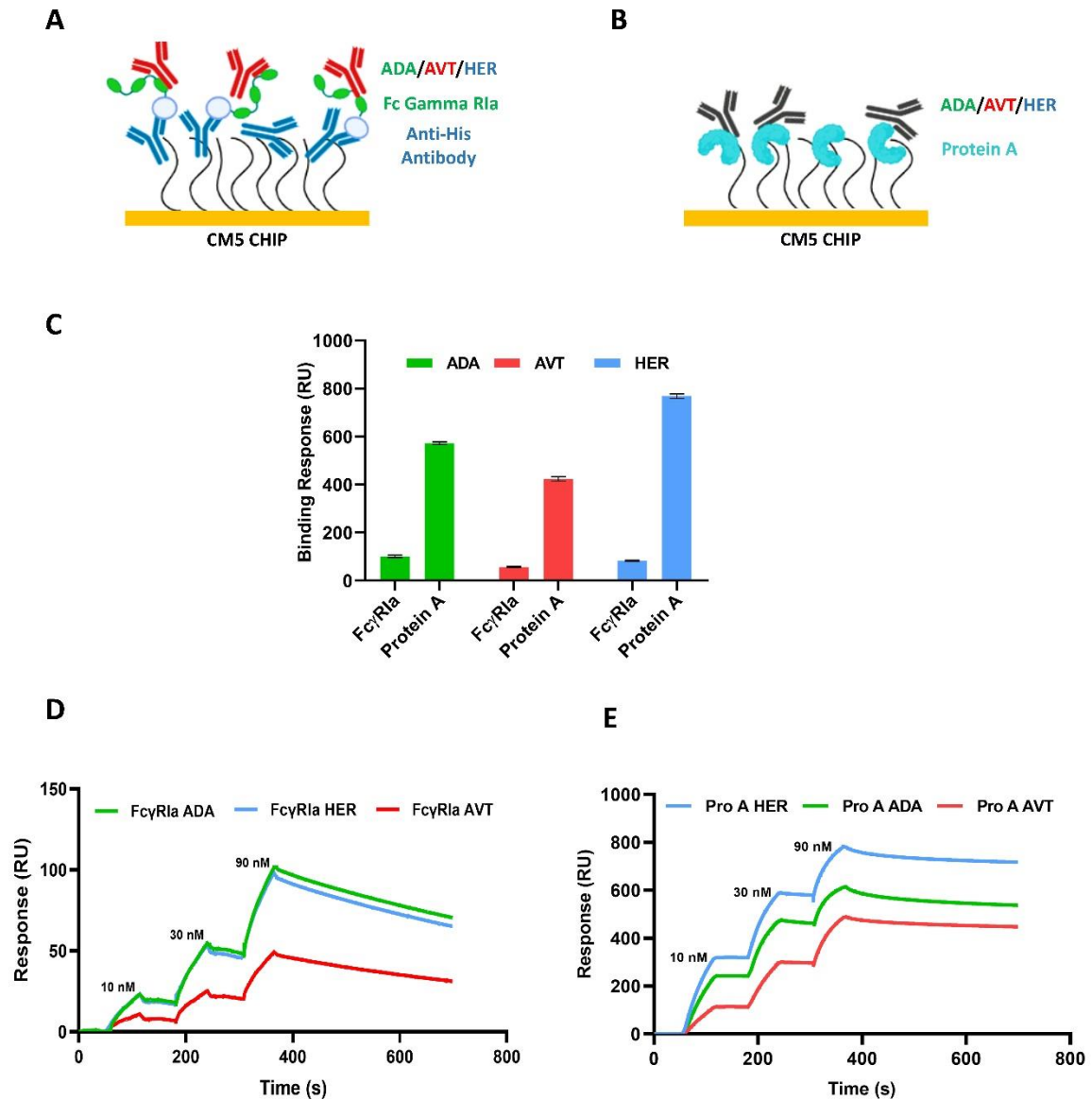
Figure 7. Evaluation of monoclonal antibody binding capacity on FcγRI captured surface and Protein A immobilized surface in SPR. A) The antibody binding assay steps were illustrated with BioRender, presenting the binding assay through the anti-His and Protein A ligands on the CM5 chip. FcγRI (His tagged at C-terminal) was captured on an anti-His antibody immobilized surface. B) Protein A was directly coupled to the CM5 chip surface by EDC/NHS conjugation chemistry. ADA, AVT, and HER were injected at 10 nM, 30 nM, and 90 nM concentrations with a single-cycle kinetics model. C) The binding response graph for three IgG1 sub-type monoclonal antibodies on both ligand surfaces. The data were presented as the mean value obtained from at least three measurements. D) Representative SPR sensorgrams indicating the binding responses for ADA, AVT, and HER on the FcγRIa captured surface. E) Representative SPR sensorgrams indicating the binding responses for ADA, AVT, and HER on the Protein A surface.

The kinetic parameters were analyzed with a 1:1 Langmuir interaction model for FcγRIa and a heterogeneous ligand model chosen for Protein A (Table 3). The steady-

state $K_D$ values were in the range of 77.1 - 106.6 nM for FcγRIa binding analysis (Table 4). These findings were similar to the IgG-FcγRIa interaction results that were reported previously in the literature (Forest-Nault et al. 2021; Hatayama et al. 2012; Hayes et al. 2016; Jefferis and Lund 2002a). Protein A sensorgrams were not globally analyzed with 1:1 interaction due to the presence of five potential target-binding domains. The steady-state $K_D$ values for Protein A were in the range of 10.67 - 35.28 nM.

Table 3. Kinetics and affinity parameters related to FcγRIa or Protein A interactions with ADA, AVT, and HER. For FcγRIa, the kinetic parameters were calculated by Biacore Evaluation Software using a 1:1 Langmuir binding model, and the heterogeneous model was utilized for Protein A.

| | | FcγRIa | | | Protein A | | | | | |
|---|---|---|---|---|---|---|---|---|---|---|
| | | $k_a \times 10^5$ (M$^{-1}$s$^{-1}$) | $k_d \times 10^{-4}$ (s$^{-1}$) | $K_D$ (nM) | $k_{a1} \times 10^5$ (M$^{-1}$s$^{-1}$) | $k_{a2} \times 10^5$ (M$^{-1}$s$^{-1}$) | $k_{d1} \times 10^{-4}$ (s$^{-1}$) | $k_{d2} \times 10^{-4}$ (s$^{-1}$) | $K_{D1}$ (nM) | $K_{D2}$ (nM) |
| **KINETICS** | **ADA** | 2.4±0.15 | 9.5±0.3 | 3.9±0.1 | 8.1±6.0 | 4.4±5.9 | 4±6.16 | 6.7±5.4 | 13.9±21 | 22.2±23 |
| | **AVT** | 1.9±0.19 | 10.4±0.7 | 5.5±0.4 | 12.8±12 | 11.9±13 | 18±25.6 | 15.9±24 | 0.8±0.7 | 0.5±0.8 |
| | **HER** | 2.4±0.13 | 10.6±0.5 | 4.3±0.1 | 4.9±5.9 | 14.4±5.7 | 2.4±1.17 | 0.4±1.05 | 1.0±0.5 | 0.16±0.4 |

Table 4. Affinity parameters related to FcγRIa or Protein A interactions with ADA, AVT, and HER. The Steady-state model was utilized for affinity values.

| | | FcγRIa | | Protein A | |
|---|---|---|---|---|---|
| | | $R_{max}$ | $K_D$ (pM) | $R_{max}$ | $K_D$ (pM) |
| **AFFINITY** | **ADA** | 169.7 | 78.0±5.2 | 936.7 | 10.7±0.5 |
| | **AVT** | 90.9 | 106.6±13.8 | 749.4 | 35.3±2.5 |
| | **HER** | 156.5 | 77.1±6.9 | 1038.5 | 15.3±0.2 |

## 2.3.2 IgG1 Binding Capacity Analysis with FcγRI and Protein from Harvest Samples

The IgG binding performance of FcγRIa protein was also evaluated with a biosimilar's crude samples. For this purpose, a biosimilar candidate harvest was utilized and purified with Protein A affinity chromatography to collect monoclonal antibodies with various monomer purity (elution and clean-in-place (CIP) fractions). SEC analysis was

conducted to reveal the monomer content of the samples. AVT was utilized as a control reference sample with a high purity level (99%). The monomer levels were 48.50%, 98.45%, and 39.98% for harvest, elution, and CIP fractions, respectively (Figure 8A). All samples were buffer exchanged to HBS-EP system solution and adjusted to 15 nM concentration with the same buffer for SPR assays. The chip configuration for SPR assays was illustrated in Figures 8B and 8C. Protein A was directly coupled to the CM5 chip surface via EDC/NHS chemistry, and FcγRIa was captured on an anti-His antibody immobilized surface. As stated in the method section, immobilized Protein A and captured FcγRIa levels were kept constant at 200 RU and 300 RU, respectively. For the reliability of the assay, it was repeated on two different CM5 chips. Since we aimed to compare monoclonal antibody binding capacity, we checked the monoclonal antibody binding response with 200 RU and 300 RU surfaces. For the FcγRIa-captured surface, monoclonal antibody purity levels did not significantly alter the binding to FcγRIa. The highest binding response levels were 81.8 RU with AVT sample (99% purity). Even in the CIP fraction with 40% monomer IgG content, the antibody binding response was 59.9 RU. Dorion-Thibaudeau et al. (2017) performed a similar SPR analysis with FcγRIa ectodomains to examine monoclonal antibody titer and its binding activities from the cell culture. The authors stated that the FcγRIa ectodomain maintained a stable ligand performance during SPR monitoring of monoclonal antibody samples from the harvest (Dorion-Thibaudeau, Durocher, and De Crescenzo 2017). As presented in Figure 8D, Protein A responses were considerably higher than that of FcγRIa. The binding to Protein A surface was in correlation with the purity level of the samples. AVT sample presented a nearly 1.77-fold higher monoclonal antibody binding response than FcγRIa. CIP fraction presented the lowest monoclonal antibody response with a value of 64.5 RU.
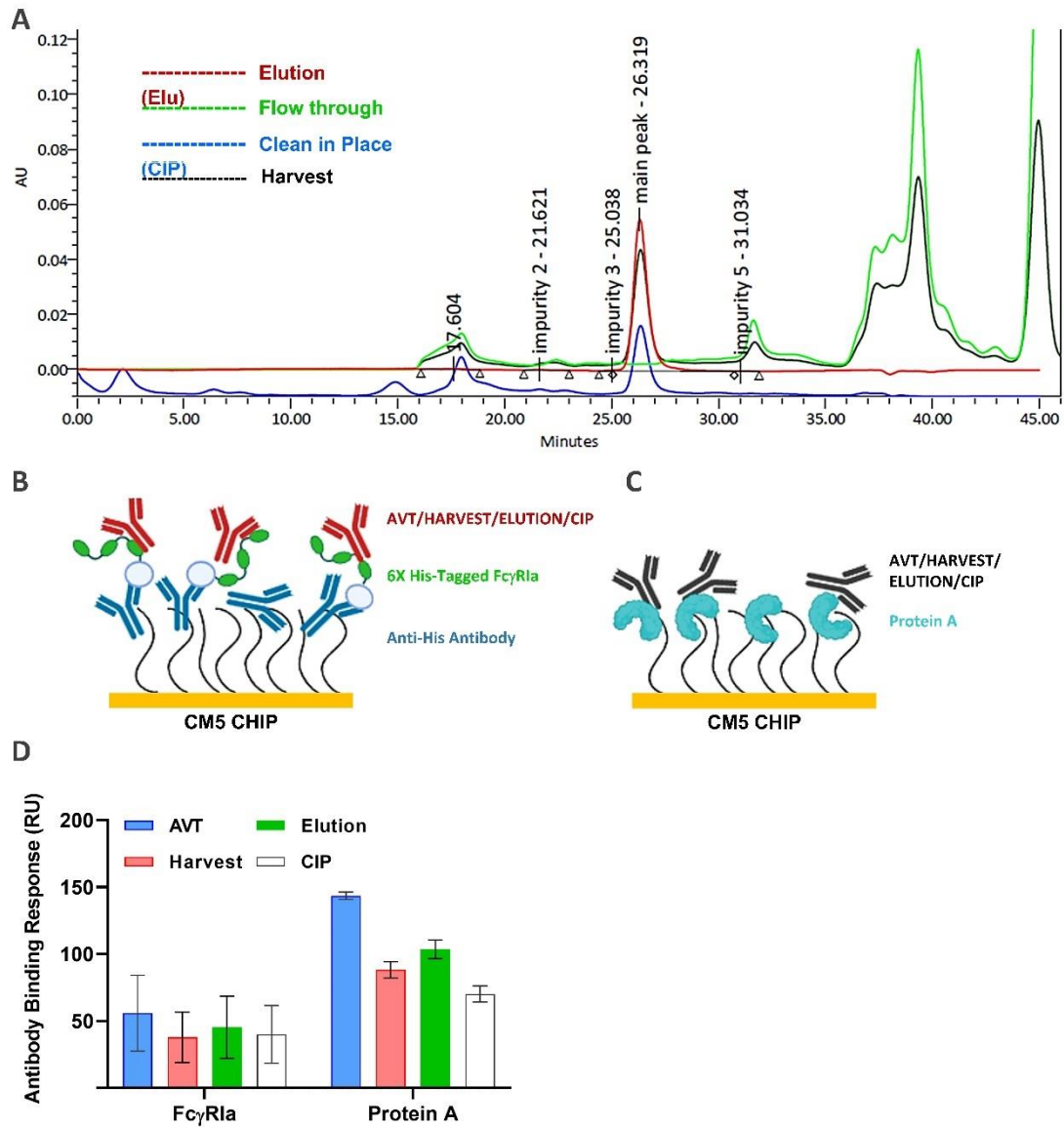
Figure 8. Evaluation of binding response with varied purity levels of monoclonal antibody samples from a biosimilar harvest on FcγRI captured surface and Protein A immobilized surface A) Chromatogram profile of AVT, harvest, elution, and CIP samples obtained from SEC-HPLC analysis. B) Schematic illustration of the binding analysis with anti-His antibody surface. FcγRIa was captured on the anti-His antibody immobilized surface. C) Schematic illustration of the binding analysis with Protein A surface. Protein A was coupled by EDC/NHS conjugation chemistry. All samples were injected at 15 nM concentration. The illustration has been created with BioRender. D) The graph Antibody binding responses were evaluated for AVT, harvest, elution, and CIP fractions with FcγRIa and Protein A ligands(n>3).

## 2.3.3 On-surface Configuration of FcγRI, FcγRIIa, and FcγRIIIa for IgG1 Binding Assay

An alternative approach was used to reveal the in-solution IgG1 binding characteristics of

FcγRIa, FcγRIIa, and FcγRIIIa on the Protein L-immobilized chip. Protein L binds to the kappa light chain in the Fab region of monoclonal antibodies. It is an effective ligand for an oriented capture of molecules on surfaces or particles (Chen et al. 2020; Patel et al. 2015). With this assay configuration, model IgG1-type monoclonal antibodies (ADA, AVT, HER) were captured on the Protein L-immobilized surface through their Fab regions and the Fc regions of the antibodies that bind to FcγRs were left exposed to the solution for target binding. (Figure 9A).

The FcγRs (Ia, IIa, and IIIa) were injected onto the antibody-captured surfaces to monitor the IgG1 binding behavior of free FcγRs proteins. In Figure 9B, IgG1 binding characteristics of free FcγR proteins (used as analytes) were compared for three monoclonal antibodies (used as ligands). The highest binding response level was found with FcγRIa. Binding response levels of ADA, AVT, and HER to FcγRIa were 89±5, 52±2, and 77±1 RU, respectively. The lowest binding response level was obtained with FcγRIIa which was 3±0.2, 2±1, and 3±2 RU for ADA, AVT, and HER. FcγRIIIa binding response analysis for ADA, AVT, and HER were 10±0.5, 4±0.5, and 9±0.2 RU, respectively. The binding levels differed depending on the captured monoclonal antibodies on the Protein L surface. HER mediates a mechanism of action through its Fc region resulting in ADCC activities on the target cells; ADA possesses both CDC (Complement Dependent Cytotoxicity) and ADCC activities (Horiuchi et al. 2010a; Xie et al. 2020). AVT is not capable of inducing either CDC or ADCC activity. In addition to that, the distinct glycan profile of the monoclonal antibodies probably affected the interactions with FcγRs (J. Lu et al. 2015). This is a critical quality attribute of IgGs that rely on a CDC-based mechanism. The major glycan profile of HER contains Man5, G0F,-GN, G0, G0F, G1F, and G2F (S. Kim et al. 2017; Xie et al. 2020). Predominant glycan forms of ADA are high galactose glycans which are G0F, G1F, and G2F. Other glycan forms include afucosylated (≤ 1.7%), high mannose (<10%), and sialylated (≤0.3%) (J. A. J. Lee et al. 2019; Liu et al. 2016; Zhang et al. 2020). AVT contains mainly G0F, G1F, and G2F N-glycan types. Minor glycan forms include afucosylated (≤1.7%), high mannose (≤1.3%), and sialylated (<0.2%) (Seo et al. 2018). Several studies reported N-glycans' effect on the FcγR-IgG interactions (Cambay et al. 2020; Jefferis and Lund 2002a; S. Kim et al. 2017; Thomann et al. 2015a; Upton et al. 2016; Zhang et al. 2020). Lack of core fucose (Afucosylation) in the IgG structure was indicated as a main inducer for the ADCC activity, and it led to enhanced binding affinity to FcγRIIIa (S. Kim et al. 2017; Upton et al. 2016). Most therapeutic

monoclonal antibodies include less than 15% afucosylation. The efficacy of ADCC or a CDC-based mechanism could be altered with engineered afucosylation levels (Upton et al. 2016).
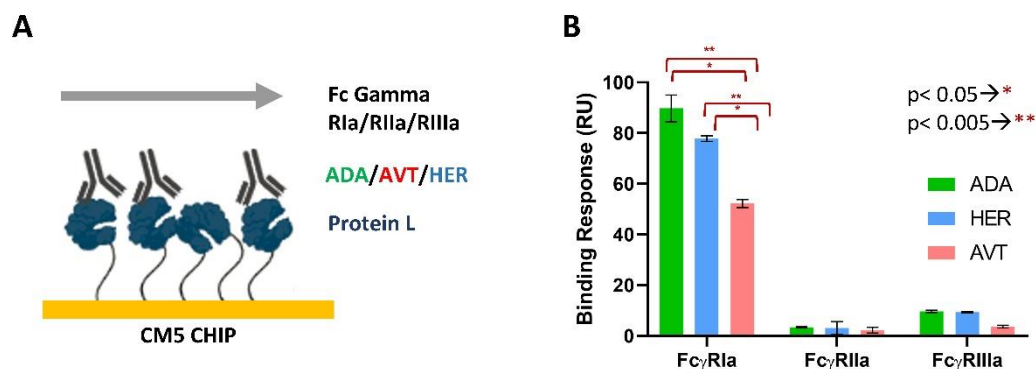


Figure 9. In-solution configuration binding analysis for FcγRI, FcγRIIa, and FcγRIIIa A) Three IgG1 sub-type monoclonal antibodies were used as ligands and captured on Protein L immobilized surface. Schematic illustration of the in-solution binding assay on SPR. As the samples FcγRIa, FcγRIIa, or FcγRIIIa were injected as samples at 1.66 nM, 5 nM, and 15 nM into the chip surface. The Illustration was created with BioRender. B) The binding response of in-solution configuration of FcγRIa, FcγRIIa, and FcγRIIIa on IgG1 captured surface. Data were presented as the mean value obtained from at least three measurements.

## 2.3.4 On-surface Configuration of FcγRI and Protein A for IgG1 Binding Capacity Analysis

Upon successful IgG1 binding performance of FcγRIa over the other Fc receptors tested, the IgG1 binding potential was compared with Protein A in-solution configuration. Based on the in-solution binding kinetics results obtained in this study, further investigation of FcγRIa as an alternative ligand molecule seemed viable. First, different IgG1 type monoclonal antibodies (ADA, AVT, HER) of the same concentration (6 nM) were captured on a Protein L-immobilized chip surface (Figure 10A). Then, the FcγRIa and Protein A samples prepared at five different concentrations were injected onto the antibody-captured surfaces and evaluated for the final binding response at equilibrium and the binding kinetics. The antibody binding capacity of free FcγRIa and free Protein A were compared for ADA, AVT, and HER binding, as presented in Figure 10B. The equilibrium binding responses of ADA, AVT, and HER were $101\pm5$, $57\pm2$, and $83\pm3$ RU for FcγRIa, and $48\pm2$, $26\pm0.2$, and $54\pm1$ RU for Protein A, respectively. In agreement with the His capture data set in-surface configuration, the IgG1 binding capacity of free FcγRIa was statistically significantly greater than the IgG1 binding capacity of free

Protein A.
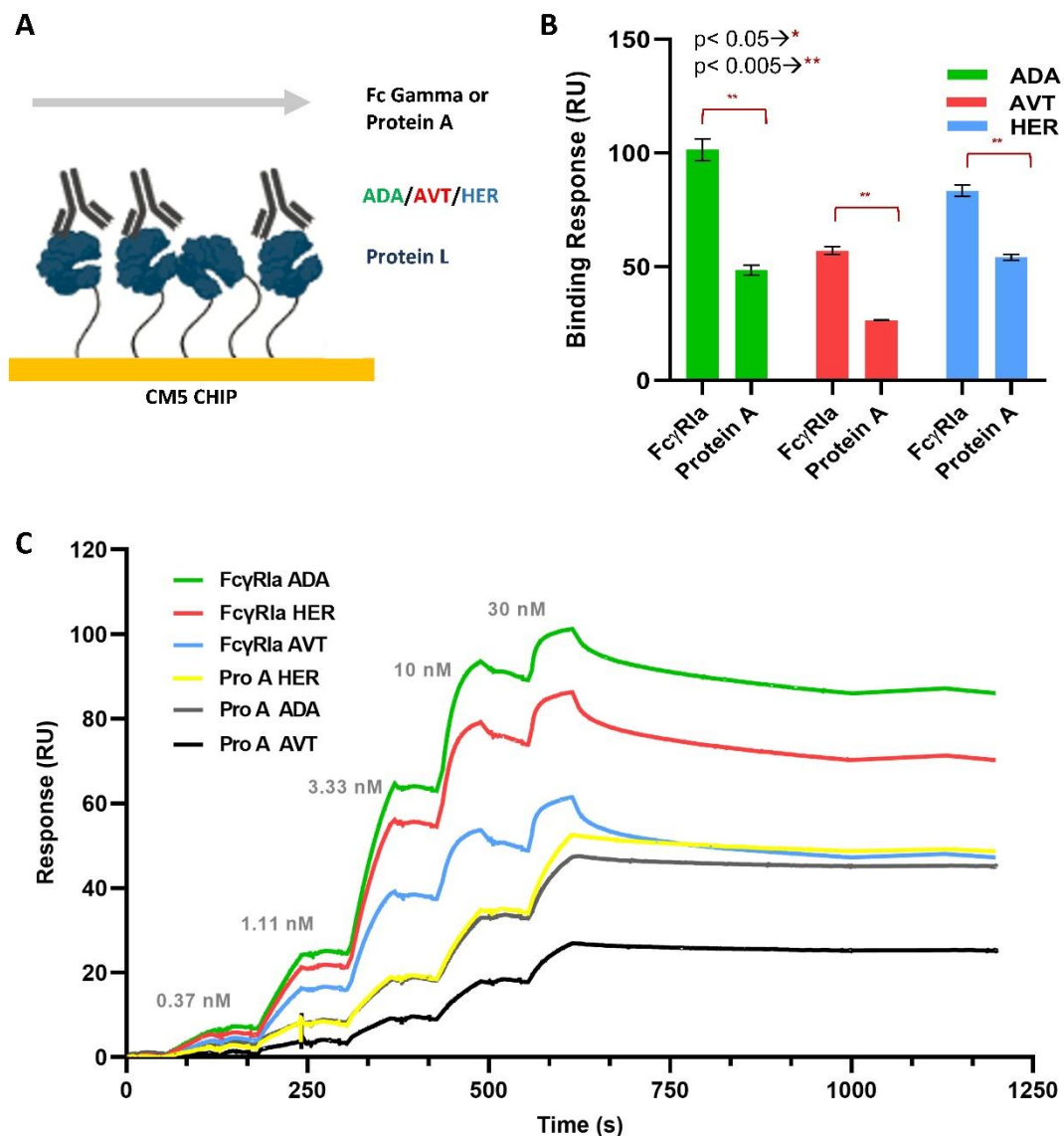


Figure 10. Comparison of FcγRIa and Protein A for IgG1 binding with an in-solution orientation where these molecules were used as analytes instead of ligands, A) Schematic illustration of the in-solution binding assay on SPR ADA, AVT, or HER (6 nM) was captured on Protein L-immobilized surface and the samples (FcγRIa or Protein A) were injected with five concentrations (0.37 nM, 1.11 nM, 3.33 nM, 10nM, 30 nM) using single-cycle kinetics mode. The Illustration was created with BioRender. B) Results of in-solution IgG1 binding response for FcγRIa and Protein A. Data were presented as the mean value obtained from at least three measurements. C) Representative SPR sensorgrams of FcγRIa or Protein A binding to ADA, AVT, or HER captured surface.

On the other hand, the IgG binding capacity of FcγRIa and Protein A varied for all tested antibodies, indicating a glycosylation-dependent binding variation, as previously reported by research groups (Cambay et al. 2020). Increased concentrations of FcγRIa displayed a fast association profile in the sensorgram over the monoclonal antibody-captured surface (Figure 10 C). However, the response declined over the dissociation phase. The sensorgram of Protein A did not reach a saturation profile at the same concentration range for the association step, but it maintained a more stable interaction during the dissociation phase. The kinetics and affinity parameters presented in (Table 5 and Table 6) were obtained using Langmuir 1:1 binding interaction model and steady-state model. In the kinetic analysis, the $k_a$ value was found to be remarkably higher for FcγRIa (51.7- 83.5 $\times$ 10$^5$ M$^{-1}$s$^{-1}$) than Protein A (13$\times$10$^5$ M$^{-1}$s$^{-1}$). However, the $k_d$ value for Protein A was almost half of that for FcγRIa. Once we take the five IgG binding sites of Protein A into consideration, a lower $k_d$ for Protein A-IgG interaction is reasonable since any IgG leaving the binding site on Protein A could easily find another binding site nearby. This naturally led to a more stable interaction between the monoclonal antibody and Protein A during the dissociation phase. The $K_D$ values obtained from kinetic parameters were between 37.5 - 46.2 pM for FcγRIa, and 45.1 - 103.8 pM for Protein A. On the other hand, steady-state affinity values were similar for both ligands within the range of 2.1 - 10.3 pM.

Previous FcγRIa-IgG characterization studies reported $K_D$ values ranging from 0.1 to 100 nM with diverse immobilization strategies in which FcγRIa was usually immobilized to the surface as a ligand (Cambay et al. 2020; Champion and Beck 2013; Forest-Nault et al. 2021; W. Wang and Chen 2022). Our SPR studies indicate that the $K_D$ values vary significantly depending on the FcγRIa protein orientation and are susceptible to the conjugation chemistry. Here, we identified the in-solution binding affinity of free FcγRIa to IgGs in the low pM range. The oriented configuration of IgGs on the Protein L surface provided an equal comparison of FcγRIa and Protein A for the IgG binding, where the FcγRIa presented a better performance than Protein A when they were used as analytes rather than ligands.

Table 5. Kinetics and affinity parameters related to FcγRIa or Protein A interactions with ADA, AVT, and HER. The kinetic parameters were calculated by Biacore Evaluation Software using a 1:1 Langmuir binding model.

| | | FcγRIa | | | Protein A | | |
|---|---|---|---|---|---|---|---|
| | | $k_a \times 10^5$ (M$^{-1}$s$^{-1}$) | $k_d \times 10^{-5}$ (s$^{-1}$) | $K_D$ (pM) | $k_a \times 10^5$ (M$^{-1}$s$^{-1}$) | $k_d \times 10^{-5}$ (s$^{-1}$) | $K_D$ (pM) |
| KINETICS | ADA | 72.4±10.79 | 27.7±0.49 | 38.9±5.68 | 13.2±0.455 | 13.7±0.19 | 103.8±3.19 |
| | AVT | 51.7±6.07 | 24.2±7.60 | 46.2±13.45 | 12.4±0.34 | 6.5±0.26 | 52.7±2.51 |
| | HER | 83.5±10.89 | 30.7±5.37 | 37.5±9.26 | 13.1±0.65 | 5.0±3.55 | 45.1±20.12 |

Table 6. Affinity parameters related to FcγRIa or Protein A interactions with ADA, AVT, and HER. The Steady-state model was utilized for affinity values.

| | | FcγRIa | | Protein A | |
|---|---|---|---|---|---|
| | | $R_{max}$ | $K_D$ (pM) | $R_{max}$ | $K_D$ (pM) |
| AFFINITY | ADA | 129.1 | 2.33±0.045 | 59.15 | 9.39±0.52 |
| | AVT | 73.62 | 2.11±0.163 | 35.12 | 10.32±0.33 |
| | HER | 109.12 | 10.03±0.52 | 69.65 | 2.11±0.15 |

## 3 . Site-oriented IgG capture with Fc Gamma receptor I for Tumor Necrosis Factor-alpha (TNF -α) Detection

### 3.1 Introduction

Tumor necrosis factor-a (TNF-α) is a cytokine that exerts its biological activity in homotrimer form by engaging Type 1 and 2 TNF receptors (TNFR-1 and TNFR-2). TNF-α could be either in transmembrane (26 kDa) or soluble form (17 kDa). Transmembrane TNF-α is expressed in the cell membranes of macrophages, lymphocytes, and other cell types(Horiuchi et al. 2010b). Upon activation of macrophages, it is cleaved by TACE (TNF-α converting enzyme) to produce a soluble form of TNF-α. Both TNF-α types are in homotrimer protein form. In normal cells, it regulates many immune responses including intracellular pathogen responses, cytotoxicity, and local inflammation. However, its overexpression in tissues is related to inflammatory responses and may result in diseases such as Crohn's disease and rheumatoid arthritis. The TNF-α levels in serum have been studied for the indication of autoimmune diseases, the monitoring of the treatment, and the alleviation effect of anti-TNF-α agents(Horiuchi et al. 2010b; Jang et al. 2021; Marušič et

al. 2012).

Various biosensor formats have been developed for the detection of TNF-α(Arya and Estrela 2017; Barhoumi et al. 2018; Baydemir et al. 2016; Deng, Qiao, and Li 2022; Gao et al. 2022; Ghosh et al. 2018; B. Y. Kim, Lee, and Lee 2019; Li et al. 2021; Martinez-Perdiguero et al. 2014; Pruna et al. 2018; Vargas et al. 2022; Y. Wang et al. 2021). Generally, ELISA assay is the most preferred format for the detection of TNF-α from serum(Baydemir et al. 2016). However, it takes many manual steps and has a longer duration. In addition, other disadvantages are the single-use ELISA kits, which require labeled secondary antibodies for the detection(Arya and Estrela 2017; Barhoumi et al. 2018; Ghosh et al. 2018). Secondary antibodies in ELISA assays are usually conjugated with a fluorophore molecule to detect the binding signal via a spectrophotometer. To detect signals with high sensitivity and specificity, the assay should be optimized for the concentration of the secondary antibody solution.(Schroeder and Cavacini 2010) To overcome these drawbacks, studies continued with alternative detection methods such as optical, electrochemical, fluorescent, etc. Yagati et al. developed an electrochemical-based immunoassay obtaining a 0.78 pg/mL LOD by gold nanoparticles with graphene in human serum samples(Yagati, Lee, and Min 2018). Despite their low LOD values, electrochemical-based immunoassays possess complex steps in terms of fabrication, surface functionalization, and proper orientation of the ligand(Vargas et al. 2022). As an optical-based method, Surface Plasmon Resonance (SPR) has been studied for the detection and binding interaction analysis of TNF-α even in complex samples (serum, cells, and cell supernatant) (Cytiva n.d.). For instance,  Ogura *et al*. investigated the binding interactions of different anti-TNF agents between transmembrane TNF-α and Jurkat cells by SPR analysis(Ogura, Tanaka, and Toyoda 2016).

Many studies for TNF-α sensing strategy were based on the direct conjugation of TNF-α antibodies and DNA aptamers to the surface with EDC/NHS coupling chemistry(Arya and Estrela 2017; Barhoumi et al. 2018; Ghosh et al. 2018; Martinez-Perdiguero et al. 2014; Pruna et al. 2018; Yagati, Lee, and Min 2018). Recently, A Fc-specific aptamer was studied for the proper orientation of proteins. The study performed an oriented receptor capture, which contains an Fc tag at its C-terminal, via an Fc-specific aptamer on magnetic nanoparticles for the detection of a target biomarker (Leukocyte cell-derived chemotaxin 2). The study reported that oriented capture provided an enhanced SPR signal in comparison to the random immobilization strategy(Zhu et al. 2022). Brown *et al*. (Brown et al. 2017, 2018)

developed an Fc-based array containing antigen-conjugated beads to capture target antibodies in a polyclonal sample solution. Then, they evaluated the effector functions of the specified antibodies through streptavidin-biotin conjugated FcγRs on multiplex fluorescent beads. FcγRI has been utilized as a probe for imaging purposes 4 cancer biomarkers in-vitro studies(C. Kim et al. 2014). Even with limited studies of FcγRI as an affinity ligand, it promises potential in terms of site-specific capture of IgG and antigen-sensing applications.

The current study evaluated FcγRI as an alternative affinity ligand for TNF-α antigen detection via SPR analysis. The binding interactions were assessed with the SPR technique using His capture method for FcγRI and amine-coupled Protein A on the CM5 chip surface. First, Adalimumab was bound on FcγRI captured anti-His surface and Protein A immobilized chip surface. Subsequently, binding kinetics, concentration analysis, and specificity analysis were performed and compared with the Protein A surface. Finally, spiked TNF-α samples in BSA-containing HBS EP buffer were analyzed for their antigen-sensing properties on both surfaces.

## 3.2    Method

### 3.2.1   Adalimumab  Binding Capacity Analysis for FcγRIa and Protein A Ligands

Adalimumab (ADA) Binding assays were conducted simultaneously on FcγRI captured and Protein A immobilized surfaces using a Biacore T200 instrument. For FcγRI captured surface, anti-His antibody was directly amine coupled through EDC/NHS chemistry. It was performed based on the assay guideline (Cytiva, His capture kit). Also, Protein A was immobilized through direct amine coupling. For this, EDC and sulpho-NHS mixture were injected into the CM5 chip surface for the activation of the carboxyl group. Subsequently, Protein A which was diluted to 25 µg/mL in 10 mM pH 5.0 acetate buffer injected into the chip surface. As a final step, Ethanolamine solution were injected into the chip surface to block the residual activated carboxyl groups. A blank immobilization was performed for the first flow cell (FC1) for double referencing which is the binding response was subtracted from the zero-concentration sample (HBS-EP 1X solution) and the blank surface. The procedure for this assay is the same as the amine coupling method (EDC/NHS) except there is no protein injection. The activated carboxy groups on the CM5 chip surface were blocked with ethanolamine solution.

FcγRI had a 6xHis tag at its C-terminal and was captured on an anti-His immobilized surface for 60s  at with a 10 µL/min flow rate at 22 °. Following that, ADA solution at 15 nM concentration was injected on both active (FcγRI captured and Protein A immobilized surfaces) and blank flow cells. TNF-α protein samples were injected at 3.33 nM, 10 nM, and 30 nM concentrations into both flow cells (active and blank) with 60 s association and 300 s dissociation with 50 µL/min flow rate at 22 °C. 10 mM glycine (pH 1.5) was injected for  60 s to the regenerate the surfaces. Results were obtained with the double referencing method. The SPR data were presented as the mean value obtained from at least three sample measurements. The kinetic parameters were calculated by Biacore Evaluation Software using the two-state binding model. $K_D$ values from affinity analysis were performed with the steady state by Biacore Evaluation Software.

### 3.2.2 Concentration analysis for FcγRIa and Protein A ligands

For concentration analysis, FcγRI was captured at 250 RU on the active flow cell for 60 s with a 10 µL/min flow rate at 22 °C. ADA was injected on both surfaces as a 500 RU final response level. TNF-α sample solutions were prepared with HBS-EP 1X system buffer and were injected at five different concentrations (1.11 nM, 3.33 nM, 10 nM, 30 nM, 90, 270 nM) in multi-cycle on blank, FcγRI, Protein A surfaces with 60 s association and 300 s dissociation with 50 µL/min flow rate at 22 °C. The surface was regenerated with 10 mM glycine (pH 1.5) for 60 s. Results were obtained with the double referencing method, where the presented data was subtracted from the zero-concentration sample and the blank surface. The calibration plots were fitted by non-linear regression to the four-parameter logistic(4-PL) equation (GraphPad Prism 5.0). The limit of detection (LOD) is calculated from the three-time standard deviation (SD) of replicate measurements on blank samples. The Accuracy/recovery value is obtained from the formula as stated below.

Accuracy/recovery%= (Calculated mean [ TNF-α])/(Theoretical mean [TNF-α])×100

The coefficient of variation (CV%) values in the concentration analysis were calculated as the formula below:

Coefficient of variation % (CV%)%= (SD of sample solution [ TNF-α])/(Theoretical mean [TNF-α])×100

### 3.2.3 Specificity analysis for FcγRIa and Protein A ligands

Specificity analysis was performed with 0.02% BSA in 1X HBS-EP system buffer. Sample dilutions were prepared in 5% BSA in 1X HBS-EP. Four different proteins (C1q, thrombin, IL-1β, and TNF-α) were prepared in 0.02% BSA in 1X HBS-EP system buffer at 30 nM concentration. Sample solutions were injected on active surfaces (FcγRI and protein A) and blank surfaces with 60 s association and 300 s dissociation with a 50 µL/min flow rate at 22 °C. The surface was regenerated with 10 mM glycine (pH 1.5) for 60 s. Results were obtained with the double referencing method, where the presented data was subtracted from the zero-concentration sample and the blank surface.

## 3.3 Results & Discussion

### 3.3.1 Adalimumab and TNF-α Binding Capacity Analysis for FcγRIa and Protein A Ligands

Adalimumab (Humira) is an IgG1-type monoclonal antibody that interacts with TNF-α with a high affinity ($K_D$ $10^{-11}$). Therefore, it is effectively involved in the treatment of autoimmune diseases such as RA, Crohn's disease, Behçet disease, and Psoriasis. It blocks soluble TNF-α antigens for the exaggerated inflammatory response in the tissue. Adalimumab recruits effector functions (Complement-dependent Cell Cytotoxicity, Antibody-Dependent Cell Cytotoxicity) upon engagement with transmembrane TNF-α on the target cell membrane(Jang et al. 2021; Tebbey et al. 2015).

The target antigen (TNF-α) was detected with SPR analysis by comparing two IgG1 capture ligands, FcγRI and Protein A. For this purpose, the binding interactions were analyzed in terms of Antibody (ADA) and antigen (TNF-α) binding responses. The FcγRI ectodomain was captured on the anti-His antibody immobilized surface without affecting its binding activity (Figure 11A). Protein A was directly conjugated with EDC/NHS chemistry to the chip surface (Figure 11B). Immobilized Protein A and captured FcγRI levels were kept constant at 200 RU. As presented in Figure 11C, the Protein A surface presented a 2.5-fold higher antibody binding response than the FcγRI surface. This result could be explained by the Protein A structure which possesses 5 Ig binding domains. Even though Protein A has 5 Ig-binding domains, studies indicated that it could bind 2.1 to 3 IgG in solution due to the steric hindrance of IgG molecules(Ghose, Hubbard, and Cramer 2006b). In addition to that, amine coupling randomly immobilizes the protein through its free primary amines. Thus, the antibody binding capacity is affected by both a steric hindrance and the immobilization strategy. The TNF-α binding response was nearly 2-fold higher on the Protein A surface than that of FcγRI (Figure 11D). As expected, Protein A surface captured more TNF-α antigen on ADA captured surface than that of FcγRI. 2-fold FcγRI or ADA should be injected to reach equally same antigen binding response of Protein A surface. A study performed with SPR analyzed the efficiency of the anti-TNF-α agents in RA patient samples. For this, TNF-α was immobilized with amine coupling to quantify anti-TNF-α (Adalimumab) molecules within RA patient samples. They reported that the SPR assay was correlated with the ELISA assay. According to the results, the TNF-α value for the control group was in 10 to 20 RU range and that of RA patient group

was in the range of 50 to 250 RU(Bustos et al. 2018).
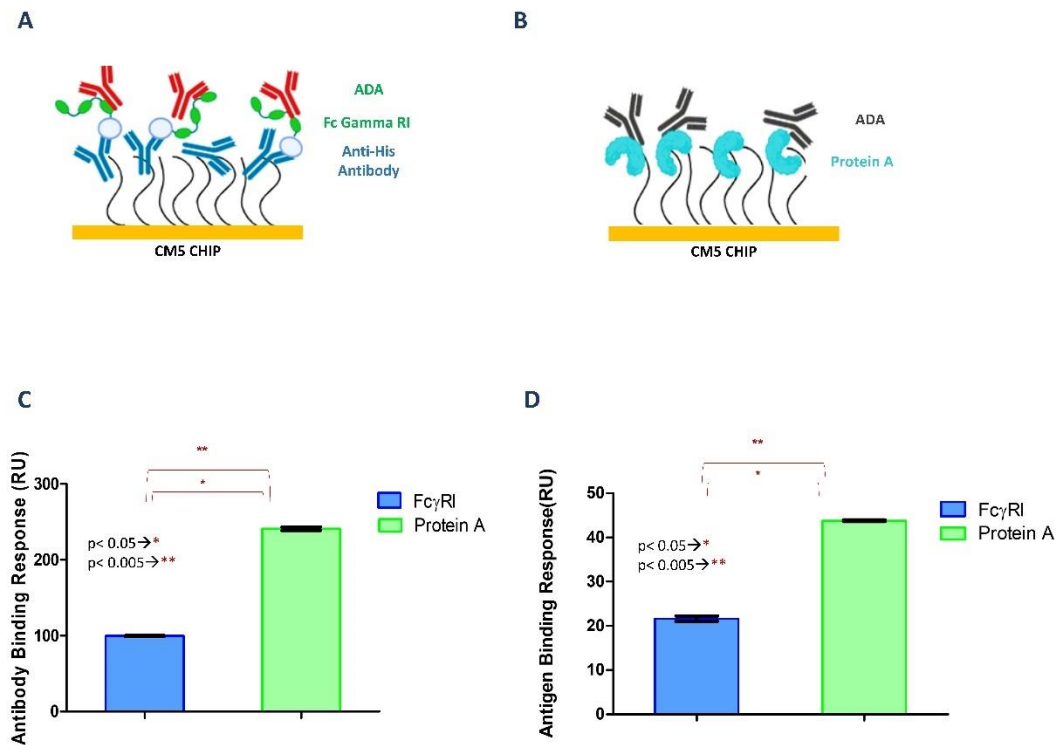


Figure 11. Antibody and Antigen Binding responses on FcγRI and Protein A ligand surface A) the chip conformation for the binding analysis. Schematic illustration created with BioRender. 6XHis tagged FcγRI was captured on anti-His antibody immobilized surface B)Amine coupled Protein A ligand surface C) The graphics represented the antibody (ADA) binding response on FcγRI and Protein A ligands. D) The graphics represented the antigen (TNF-α) binding response on FcγRI and Protein A ligands. Data were presented as the mean value obtained from at least three measurements. * $p < 0.05$, ** $p < 0.005$

The assay parameters were optimized in terms of ligand concentration, TNF-α flow rate, and TNF-α concentration range. Kinetic analyses were conducted at low ligand levels (150 RU). In addition to that, TNF-α sample solution was injected at 50 µL/min to reduce mass transport limitation on the chip surface(W. Wang, Thiemann, and Chen 2022). TNF-α samples were prepared with a concentration range of 3.33 to 30 nM (3-fold dilution). The $K_D$ values of kinetic analysis, which were obtained from the two-state binding model for both ligands, were 0.08-0.63nM range for ADA and TNF-α (Table 7). The steady-state $K_D$ values were 9.54 nM and 11.9 nM for FcγRI captured and Protein A surface, respectively (Table 8). Ogura et al. studied three anti-TNF-α agents (etanercept, infliximab, and adalimumab) for their binding to membrane-form TNF-α within Jurkat cells by SPR

analysis. One type of their assay was capturing anti-TNF-α agents with Protein A immobilized chip surface. They obtained $K_D$ values for soluble TNF-α in the pM range (5.66 to 277 pM) for three anti-TNF-α agents (Ogura, Tanaka, and Toyoda 2016).

In kinetic analysis, the ligand response must be low to ensure association and dissociation rates. The dissociation for the FcγRI surface presented a fast decline due to anti-His antibody whereas Protein A was more stable. This can be explained by more Ig binding domains that antigens could be captured if there is any dissociation from one binding site to another. However, Affinity analysis requires a higher ligand surface to obtain half of the maximum analyte response. Therefore, $K_D$ values differed between the steady-state and kinetic analysis. The dissociation phase measurements of Protein A suggested that it gave a stable interaction with IgG1. Even though there is a dissociation of IgG, the other Ig-binding domain will be available for the binding. Therefore, it seems that the dissociation phase presented stronger in Protein A assay in comparison to the FcγRI surface. TNF-α antigen is about 17 kDa and could interact with both Fab regions of ADA. Therefore, fitting parameters were chosen as a two-state model in kinetics.
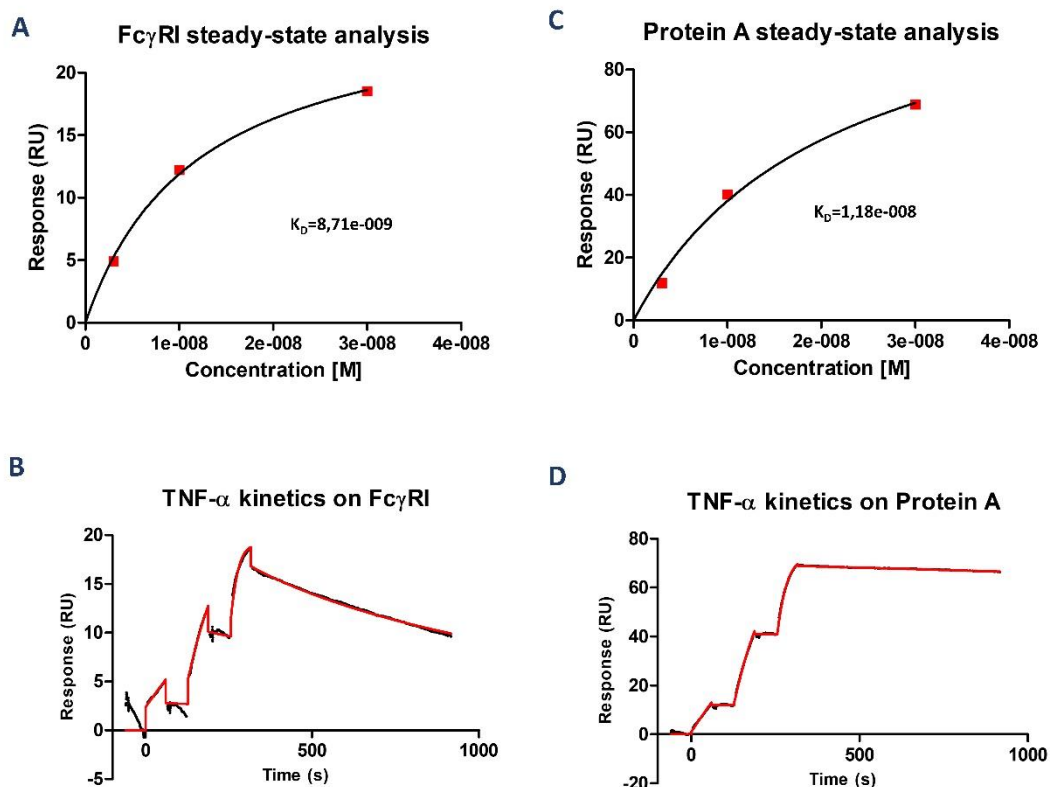


Figure 12. Affinity and Kinetic analysis sensorgrams A) Steady-state analysis of TNF-α on FcγRI captured surface B) ) Two-state kinetic analysis of TNF-α on FcγRI captured surface C) Steady-state analysis of TNF-α on Protein A surface D) Two-state kinetic analysis of TNF-α on Protein A surface.

Table 7. Kinetics parameter related to TNF-α for ADA on FcγRI captured and Protein A immobilized chip surface. Two-state binding model was utilized for kinetic parameters in Biacore Evaluation Software.

| KINETICS | | | | | | | |
|---|---|---|---|---|---|---|---|
| Ligand | $k_{a1} \times 10^5$ $(M^{-1}s^{-1})$ | $k_{a2}$ $(M^{-1}s^{-1})$ | $k_{d1} \times 10^{-4}$ $(s^{-1})$ | $k_{d2}(s^{-1})$ | $K_D$ (nM) | Chi$^2$ | kt× (10$^8$) |
| FcγRI | 15.8±3.6 | 0.013±0.016 | 16.45±6.7 | 0.045±0.05 | 0.63±0.08 | 0.25±0.04 | 5.55±0.08 |
| Protein A | 14.1±0.9 | 0.002±0.002 | 0.75±0.18 | 0.009±0.02 | 0.008±0.02 | 0.1±0.02 | 2.32±0.005 |

Table 8. Affinity parameters related to TNF-α for ADA on FcγRI captured and Protein A immobilized chip surface. The steady-state analysis was utilized in Biacore Evaluation Software.

| AFFINITY | | |
|---|---|---|
| Ligand | $R_{max}$ | $K_D$ (nM) |
| FcγRI | 24.1±2.3 | 9.54±0.6 |
| Protein A | 110±1.6 | 11.9±0.2 |

### 3.3.2 Concentration analysis for FcγRIa and Protein A ligands

A calibration curve for TNF-α was studied in multi-cycle mode with 6 different concentrations of TNF-α. Immobilized Protein A and captured FcγRI levels were kept constant at 300 RU. ADA were injected on these surfaces at 90 nM and 74 nM concentration for FcγRI and Protein A ligands, respectively. At this step, Antibody (ADA) binding response was nearly 500 RU for both ligand surfaces (data not shown). Then, TNF-α samples were injected from lowest to highest concentration. The binding response for the assays was obtained from double referencing where zero-concentration TNF-α (HBS-EP buffer) and TNF-α sample responses were subtracted from blank and FcγRI captured active chip surface. The response for anti-His immobilized surface was decreased over

time. This might be due to an unstable baseline with anti-His antibody and that is why lower concentrations of TNF-α samples were represented as a negative response. At higher concentrations of TNF-α presented a curvature in the sensorgram for both ligand surfaces (Figure 13A). A non-linear 4-parameter curve was obtained by plotting TNF-α concentration versus binding response. The results were analyzed with a non-linear 4-parameter equation with GraphPad (Figure 13B). The half response of the maximum response value, EC50, was found 13.2 nM for FcγRI and 18.4 nM for Protein A. Subsequently, the linearity was evaluated by plotting the TNF-α concentration of the sample against the calculated TNF-α concentration. As shown in Figure 13C, the correlation was higher with a good correlation efficient value ($R^2$: 0.9916 and $R^2$: 0.9927) for FcγRI and Protein A. LOD values were calculated as 1.93 nM for FcγRI captured surface and 0.84 nM for Protein A immobilized surface. In the SPR studies, detection ranges were indicated in the nM and pM range in various biological sample solutions (urine, serum, plasma, etc.)(Zhu et al. 2022) Our results were found in the nM range on both ligand surfaces.
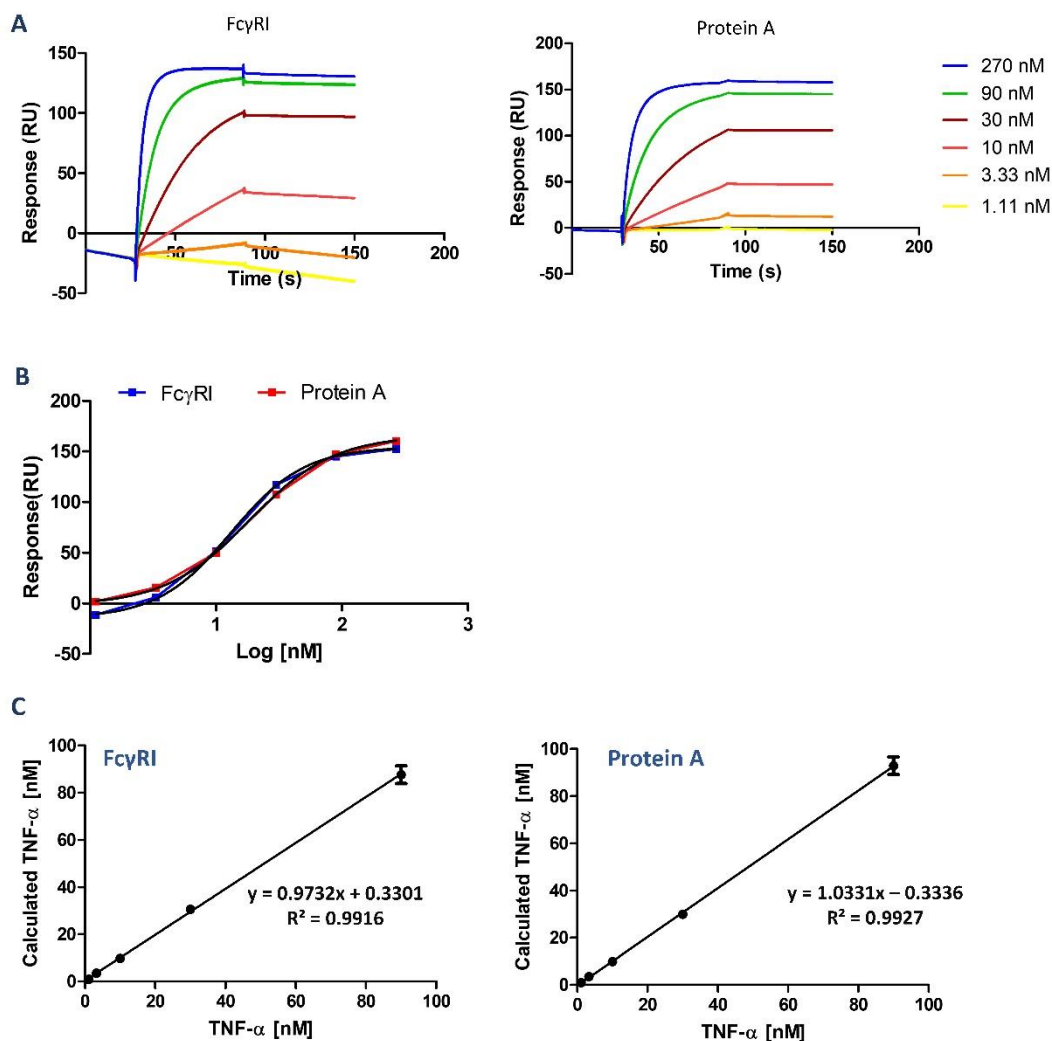
Figure 13. TNF-α Concentration analysis A) Representative SPR sensorgrams of TNF-α binding on ADA captured surface through FcγRI and Protein A chip surface, respectively. TNF-α sample solutions were injected into the chip surface from the lowest to the highest concentration in duplicates. For each cycle, the surface was regenerated with 10 mM glycine (pH 1.5) for 60 s. Results were obtained from double-referencing B) Calibration curve was plotted with a non-linear 4-parameter equation for FcγRI and Protein A ligand surface C) Linearity plots of TNF- α were calculated from the output of calibration curve analysis.

Table 9 and 10 indicates parameters accuracy/recovery and coefficient of variation (CV%) related to the concentration analysis of TNF-α. Parameters were evaluated based on the 80-120% accuracy/recovery and < 20 % CV value condition(Cytiva n.d.). According to these results, FcγRI captured surface good accuracy/recovery and low CV% value in the range of 3.33 to 90 nM TNF-α concentrations. Protein A ligand surface covered a similar concentration range in terms of good accuracy/recovery and low CV% value except for the highest TNF-α concentration.

Table 9. The parameters obtained from TNF-α concentration analysis in HBS-EP buffer on FcγRI captured surface

| Concentration(nM) | Calculated Concentration (nM) | SD | Accuracy/Recovery% | CV% |
|---|---|---|---|---|
| 1.11 | 0.95 | 0.12 | 85.4 | 12.2 |
| 3.33 | 3.52 | 0.10 | 105.8 | 2.86 |
| 10 | 9.83 | 0.09 | 98.3 | 0.87 |
| 30 | 30.6 | 0.26 | 102 | 0.87 |
| 90 | 87.6 | 7.51 | 97.3 | 8.57 |
| 270 | 349 | 223.6 | 130 | 34.0 |

Table 10. The parameters obtained from TNF-α concentration analysis in HBS-EP buffer on Protein A surface

| Concentration(nM) | Calculated Concentration (nM) | SD | Accuracy/Recovery% | CV% |
|---|---|---|---|---|
| 1.11 | 0.97 | 0.04 | 87.7 | 3.96 |
| 3.33 | 3.51 | 0.13 | 105.4 | 3.66 |
| 10 | 9.9 | 0.19 | 99.0 | 1.95 |
| 30 | 29.97 | 1.19 | 99.9 | 3.98 |
| 90 | 92.87 | 7.43 | 103.2 | 8.00 |
| 270 | 272.8 | 80.0 | 101.0 | 29.32 |

Following that, concentration analysis was conducted at 0.02%BSA containing HBS-EP buffer. Antibody (ADA) capture level was kept at 500 RU for both ligand surfaces as in the HBS-EP condition. TNF-α spiking samples were prepared in 1.25% BSA containing HBS-EP buffer to mimic real serum sample conditions. TNF-α spiking concentration range was 1.11 to 90 nM since previous concentration results presented a high standard deviation and CV% value at 270 nM. TNF-α spiked samples were injected from lowest to highest concentration on both antibody-captured ligand surfaces. The binding response was found

similar to the HBS-EP buffer condition in both FcγRI captured and Protein A surface (Figure 14A). The studies with real serum samples stated that serum has a complex medium and could interact with non-specific binding to the chip surface. As shown in the binding response graph, there is no non-specific binding to the chip surface. A calibration curve for TNF-α was presented in Figure 14B by plotting TNF-α concentration versus binding response. The graphs were fitted with a non-linear 4-parameter curve and the half response of the maximum response value was found 13.7 nM for FcγRI and 17.8 nM for Protein A. The linearity plots presented a high correlation value ($R^2$: 0.9816 and $R^2$: 0.9977) for FcγRI and Protein A. Table 11 and Table 12 indicate parameters accuracy/recovery and coefficient of variation (CV%) related to the concentration analysis of TNF-α(Cytiva n.d.). FcγRI captured surface presented a good accuracy/recovery and low CV% value in the range of 3.33 to 90 nM TNF-α concentrations. CV% was out of the acceptable range for CV% at the lowest TNF-α spiked sample solution. Protein A ligand surface covered a similar concentration range in terms of good accuracy/recovery and low CV% value.
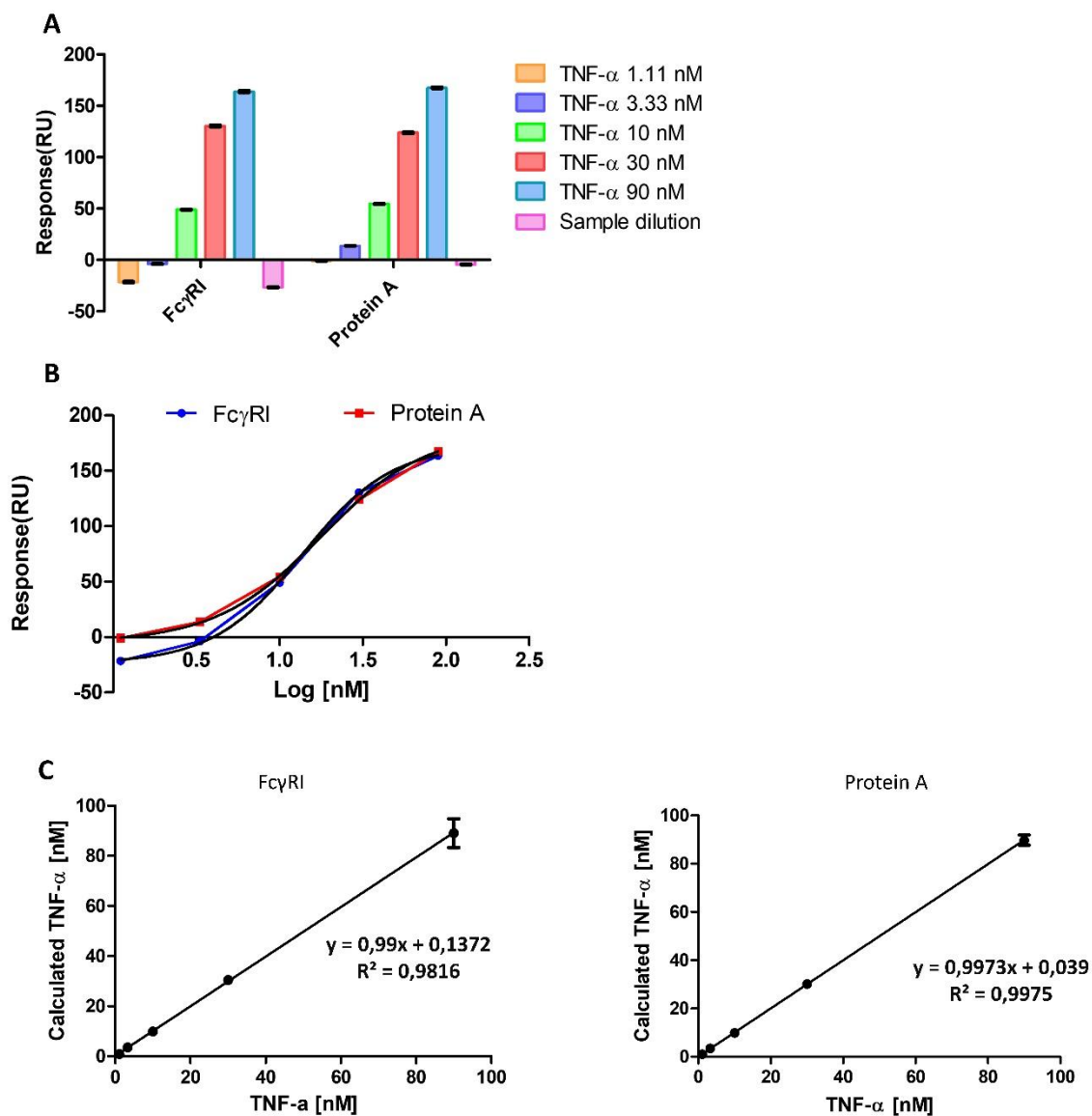
Figure 14. TNF-α Concentration analysis in BSA containing HBS-EP buffer A) Binding response graphs of TNF-α on ADA captured surface through FcγRI and Protein A chip surface. TNF-α spiked samples were prepared in 1.25 %BSA containing HBS-EP system buffer to mimic the real serum samples. The samples were injected from lowest to highest concentration in duplicates. For each cycle, the surface was regenerated with 10 mM glycine (pH 1.5) for 60 s. Results were obtained from double-referencing B) Calibration curve of FcγRI and Protein A ligand surface fitted with non-linear 4 parameter equation on GraphPad Prism. C) Linearity plots of TNF- α were calculated from the output of calibration curve analysis.

Table 11. The parameters obtained from TNF-α concentration analysis in BSA containing HBS-EP buffer on FcγRI surface

| Concentration (nM) | Calculated Concentration (nM) | SD | Accuracy/ Recovery% | CV% |
|---|---|---|---|---|
| 1.11 | 0.86 | 0.23 | 77.9 | 26.6 |
| 3.33 | 3.53 | 0.04 | 106.1 | 1.19 |
| 10 | 9.86 | 0.10 | 98.6 | 1.03 |
| 30 | 30.5 | 0.93 | 101.6 | 3.05 |
| 90 | 89.0 | 11.5 | 98.9 | 12.95 |

Table 12. The parameters obtained from TNF-α concentration analysis in BSA containing HBS-EP buffer on Protein A surface

| Concentration (nM) | Calculated Concentration (nM) | SD | Accuracy/ Recovery% | CV% |
|---|---|---|---|---|
| 1.11 | 1.02 | 0.09 | 91.7 | 8.88 |
| 3.33 | 3.45 | 0.02 | 103.5 | 0.50 |
| 10 | 9.91 | 0.13 | 99.1 | 1.29 |
| 30 | 30.16 | 0.79 | 100.5 | 2.61 |
| 90 | 89.74 | 4.20 | 99.7 | 4.68 |

### 3.3.3 Specificity analysis for FcγRIa and Protein A ligands

The specificity of the TNF-α binding assay was evaluated by injecting C1q, thrombin, and IL-1β protein samples. As shown in Figure 15A, only TNF-α sample specifically interacted with ADA captured surface in both ligands. The binding response of the non-specific proteins for the anti-His immobilized surface was represented as a negative response The reason for that could be explained by the unstable baseline occurring due to the Anti-His antibody immobilized surface and refractive index changes due to the different buffer solutions for the proteins. Also, binding response graphs were presented for each protein sample solution. Further, non-specific binding was checked for binding responses on the anti-His antibody immobilized flow cell via electrostatic interactions between analyte and

ligand(Arney and Weeks 2022). Anti-his immobilized two flow cells were tested at 30 nM TNF-α solution. There is no non-specific binding (<4 RU response level) with anti-His immobilized blank surface (data not shown). A recent study was conducted to minimize non-specific binding and enhance specificity via cell membrane coating. A bio affinity membrane layer was formed red blood cell and macrophage cell membrane onto the electrode substance. They reported that TNF-α sensing was obtained from a half-diluted serum sample without non-specific binding of the serum components. LOD value was calculated as 1.6 nM in this serum sample(Vargas et al. 2022). Another study performed a charged lipid membrane coating over Protein A conjugated chip surface in the SPR method. The charged lipid membrane (ethyl phosphocholine, EPC+) was utilized to prevent non-specific binding in undiluted serum samples. The assay proposed a sensitive detection of cholera toxin through the site-directed IgG orientation with Protein A ligand(Mckeating et al. 2019). It was reported that Protein A could bind non-specific interaction with the Fab region of antibodies and other proteins such as host cell proteins within the purification process of cell culture harvest(Ghose, Hubbard, and Cramer 2006b). Therefore, we suggested FcγRI is a potential ligand property in terms of antibody binding capacity, specificity, and antigen-sensing property.
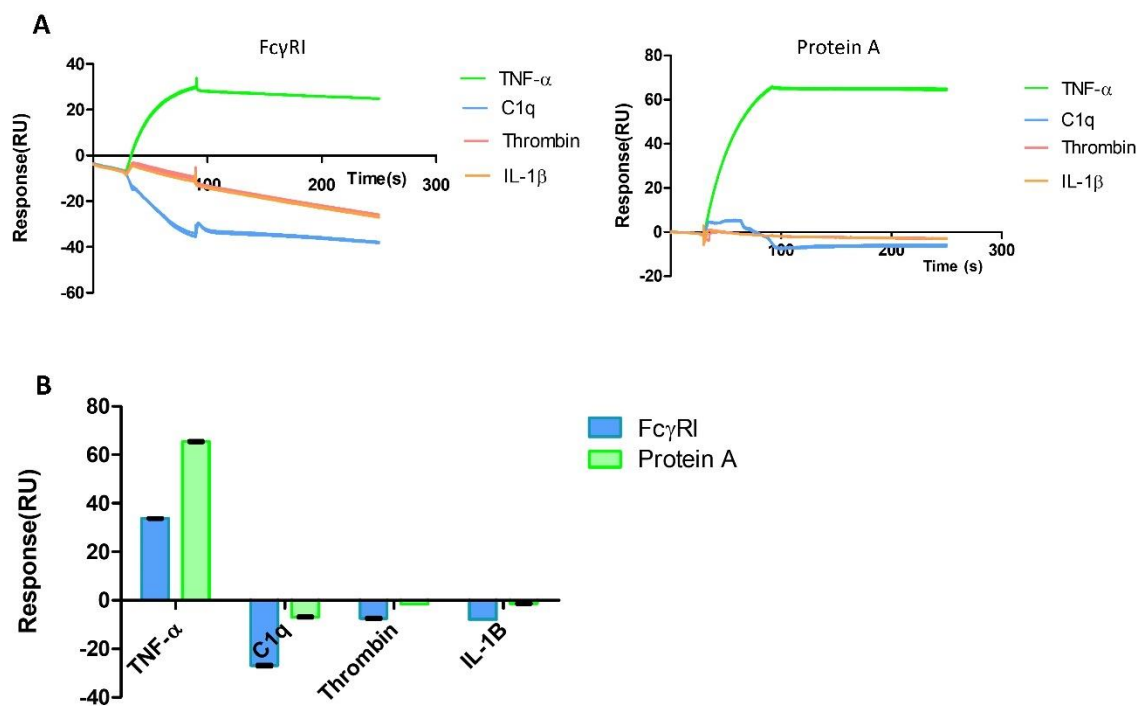


Figure 15. The specificity analysis for TNF-α binding assay on FcγRI captured and Protein A immobilized surface. A) Representative SPR sensorgrams of targeted (TNF-α) and non-targeted samples on ADA captured surface through FcγRI and Protein A

chip surface. All protein samples were injected at 15 nM concentration in duplicates. The surface was regenerated with 10 mM glycine (pH 1.5) for 60 s. Results were obtained from double-referencing  B) The plot of the binding response presented all protein samples for the specificity analysis.

To sum up, antigen sensing ability was evaluated through site-oriented IgG1 capture on FcγRI ligand by SPR assays. It is proposed that the FcγRI ligand provided an oriented IgG1 capture on the chip surface for antigen sensing.  The methods were analyzed for parameters including kinetics, affinity, accuracy/recovery, CV%, and specificity. FcγRI surface indicated good performance in the range of 3.33 to 90 nM TNF-α sample solution with a high accuracy/ recovery and low CV% values. FcγRI captured surface indicated antigen binding specifically to TNF-α solution. However, the concept possesses some drawbacks with FcγRI ligand due to the coupling and or capture strategy.  The low concentration of TNF-α solution presented a negative response in the sensorgram due to the unstable anti-his antibody surface and led to higher CV% and poor accuracy/recovery values. In comparison to the Protein A ligand, antibody binding and antigen binding responses were comparably low to that of the FcγRI ligand. In future work, an alternative coupling or capture configuration could enhance the IgG1 and antigen capture performance for FcγRI ligand such as biotin-streptavidin capture. Also, genetic alterations in FcγRI ectodomain structure without disrupting IgG1 binding ability could improve the FcγRI ligand potential, especially in the field of sensing, analytical, and purification of IgG1 monoclonal antibodies.

# 4. Evaluation of Impact of D3 domain within FcγRIa ectodomain on the interactions between FcγRIa and Fc via Molecular Dynamics

## 4.1 Introduction

The structural analysis suggested that the D3 domain within the ectodomain region in FcγRI provides higher affinity in comparison to FcγRIIa and FcγRIIIa. The first characterization study for FcγRI proposed that the D3 domain was positioned away from the binding site and put the hinge region of IgG in a straight conformation toward the cell surface(Kiyoshi et al. 2015). Furthermore, the KHR motif in the D2 domain provides a positive charge on the FcγRI and stabilizes the interaction for Fc chains. The glycans within

the Fc chains contribute to binding interactions forming H-bonds or salt bridges(Hayes et al. 2017; J. Lu et al. 2011, 2015). (Oganesyan et al. 2015). studied the structure of the Fc: FcγRI ectodomain complex and reported that glycans in the Fc chains did not directly involve in the binding interactions. In addition to that, they investigated the binding affinity for IgG1 by generating different variants in the FcγRI extracellular domain. The D3 truncated variant caused a slightly decreased activity in comparison to the full form of it. The effect of glycans on the binding affinity is reported in many studies including other FcγRs(Anderson et al. 2022; Helena et al. 2018; J. Lu et al. 2015; van der Poel et al. 2011). MD studies for FcγRI focused on the effect of glycans in the binding interactions with IgGs and the allosteric effects of antigen binding for the FcγRI ectodomain(Anderson et al. 2022; Zhao, Nussinov, and Ma 2019). However, there is no study for detailed information about the D3 domain function by Molecular Dynamics.

Characterization of a protein structure is usually conducted by X-ray and/or NMR methods which provide high-resolution 3-dimensional information. Molecular Dynamics (MD) reveals conformational dynamics over a period from the characterized structure via X-ray or NMR(Karplus and Kuriyan 2005). Thus, they provide functional information from the structure. In this study, we evaluated the dynamics of the Fc: FcγRI system with and without the presence of the D3 ectodomain as the full and truncated model, respectively. To achieve it, we use molecular dynamics simulations to calculate the changes in intramolecular interactions that also imply structure-based functional alterations. Specific residues for the molecular interactions between Fc and FcγRI were compared between the full and truncated models. For this purpose, the protein complex and its domains were evaluated for the backbone structure (RMSD), flexibility (RMSF), salt bridge interactions, and dihedral angle properties. Finally, the change in the stabilization tendency compared between the full and truncated model.

## 4.2 Method

### 4.2.1 Preparation of the Systems for Molecular Dynamics Simulation

4X4M Protein Data Bank (PDB) file was chosen to conduct MD simulations(J. Lu et al. 2015). Before the simulations, the protein complex and glycan systems within the

48

pdb file were prepared via CHARMM GUI input generator(Brooks et al. 2009; Jo et al. 2011; J. Lee et al. 2016; S. Park et al. 2017; S. J. Park et al. 2019). Also, the mutated residues in the 4X4M file were modified to the native FcγRI ectodomain (UNIPROT: P12314) sequence to mimic biological conditions during the input generator step. The solvation of the whole system was performed by adding transferable intramolecular potential 3P (TIP3P) water models and then the system was neutralized by adding 0.15 mM NaCl. Two different models were constructed; (1) full model of Fc: FcγRI and (2) truncated Fc: FcγRI model by excluding the D3 ectodomain.

NAMD program with CHARMM 36 all-atom force fields was used to carry out MD simulations. Electrostatic interactions were calculated by the particle mesh Ewald (PME) method(Darden, Lee, and Pedersen 2005; Essman et al. 1993). To control pressure at 1 atm, Langevin dynamic was used for NpT ensembles. Prior to production simulations, the system was minimized in 10,000 steps via Greedy Algorithm, and it was followed by equilibration of the whole system for 1 ns at 298 K as NpT. For all simulations, the periodic boundary conditions were applied in all dimensions (x,y,z). Along 200 ns, the production simulations were collected as NpT ensemble with 2 fs/step integration velocity at 310 K.

### 4.2.2 Analysis of the Systems

MD trajectory data of the systems were analyzed for the calculation of RMSD, RMSF, salt-bridge interactions, and dihedral angle via VMD(Humphrey, Dalke, and Schulten 1996). The critical residues in the binding interfaces were analyzed for the single residue RMSD&RMSF through the vmdICE 1.0 plugin in VMD(Knapp et al. 2010). FoldX program which was implemented as YASARA a plug-in was studied for the calculation of the changes in the destabilization tendencies in two systems(Guerois, Nielsen, and Serrano 2002; Krieger, Koraimann, and Vriend 2002; Schymkowitz et al. 2005). GraphPad Prism (v.5 ) and OriginPro (2021) programs were utilized for the graphics.

## 4.3    Results & Discussion

### 4.3.1  Evaluation of RMSD & RMSF properties between the full and truncated model

FcγRI structure has been characterized with X-ray and/or NMR method and reported in 4 PDB files which are 3RJD, 4W4O, 4X4M, and 4ZNE. The first study for the characterization of FcγRI structure was reported in 3RJD by X-ray crystallography. This study also compared the FcγRI ectodomain with FcγRIIa, FcγRIIIa, and Fc epsilon receptor I (FcεRI). The resolution value was indicated as 2.65 Å.in the optimized version. A study characterized the crystal structure of the Fc region of rituximab (humanized IgG1-type monoclonal antibody) bound to FcγRI ectodomain protein. The resolution value was indicated at 1.80 Å. To increase the thermal stability of the FcγRI ectodomain protein, 19 residues within the protein were mutated which are T20P, T25K, T38S, L46P, T63I, S69T, R71H, V77E, N78D, I100V, F114L, T160M, N163S, N195T, N206T, L207P, N240D, L283H, L285Q. The glycans were included within both FcγRI ectodomain and Fc chains. In addition to that, the 4W4O pdb file contains molecules such as Zn2+, acetate ions, and PEG. Another study revealed the complex with a high resolution (1.80 Å) for the Fc region of an IgG1 type antibody and FcγRI ectodomain. Only Fc chains contained glycans within the protein complex. The latest study about the Fc chain and FcγRI complex has been reported the overall structure with a 2.42 Å resolution value.
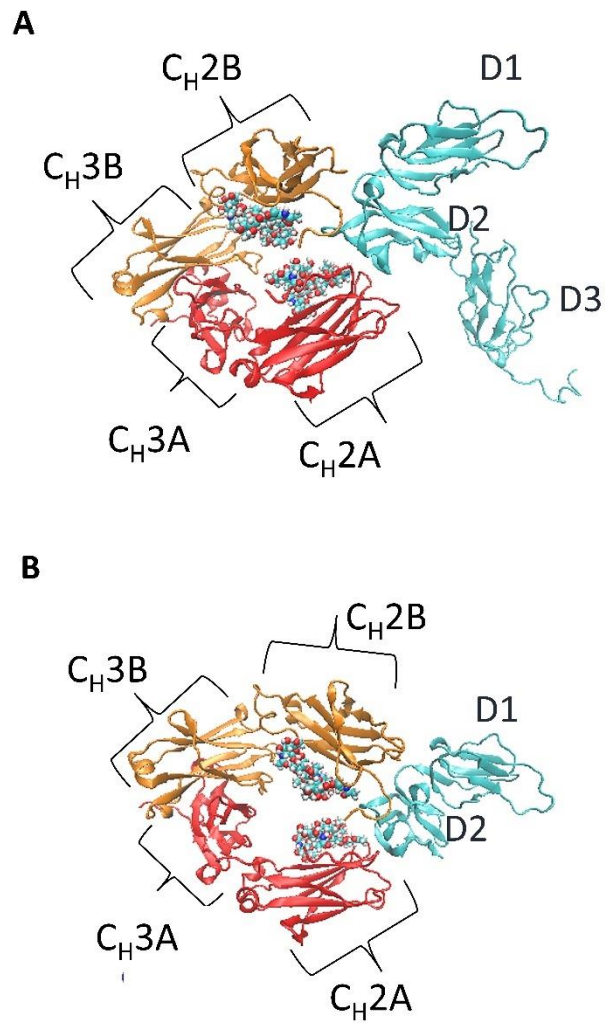
Figure 16. Structure of FcγRI and Fc chain(PDB ID: 4X4M). FcγRI domains are represented in cyan and the Fc region is shown as FcA (red) and FcB (orange) chains. The glycans were positioned at Asn297 of FcA (red) and FcB (orange). The protein domains are drawn in New Cartoon formats and the glycans are drawn in VDW format by Visual Molecular Dynamics (VMD) tools.
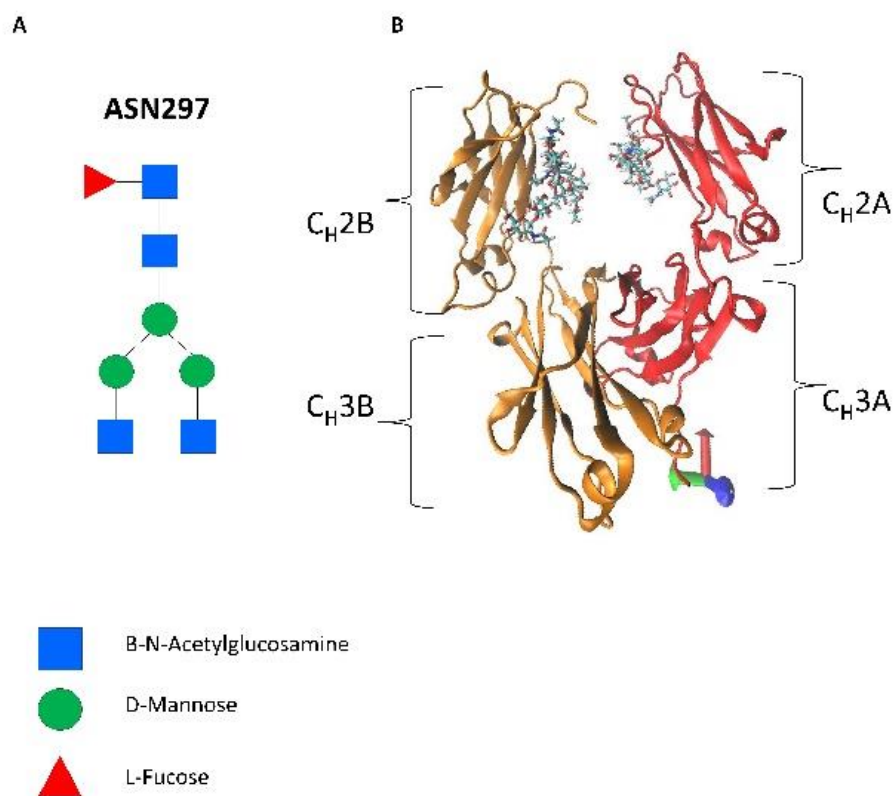
Figure 17. Illustration of the Fc region domains and their associated glycans. The protein domains are drawn in New Cartoon formats and the glycans are drawn in VDW format by Visual Molecular Dynamics (VMD) tools.

4X4M pdb file was uploaded to the Glycan reader system within CHARMM-GUI. Fc chains (A and B), their associated glycans, and a FcγRI ectodomain were selected from the file. Mutated residues within FcγRI ectodomain were converted to native residues and 6x His tag residues were added at the C-terminal of FcγRI ectodomain. As a first step, RMSD values were calculated over 200 ns trajectory outputs. RMSD plots for each protein structure are presented in Figure 18. Total protein within full FcγRI ectodomain (D1, D2, and D3) trajectories indicated higher RMSD values than FcA and FcB. Also, there is a variation between Fc chains (FcA and FcB chains) for Cα backbones. As can be seen in Figures 18A and 18B, RMSD values for truncated FcγRI ectodomain (D1 and D2) were found lower than the full form of it. RMSD plots within FcγRI domains were shown in Figure 19. As expected, Domain 3 gave the highest RMSD value and RMSD values were less than 3.0 Å for D1 and D2 domains within the truncated Fc structure.
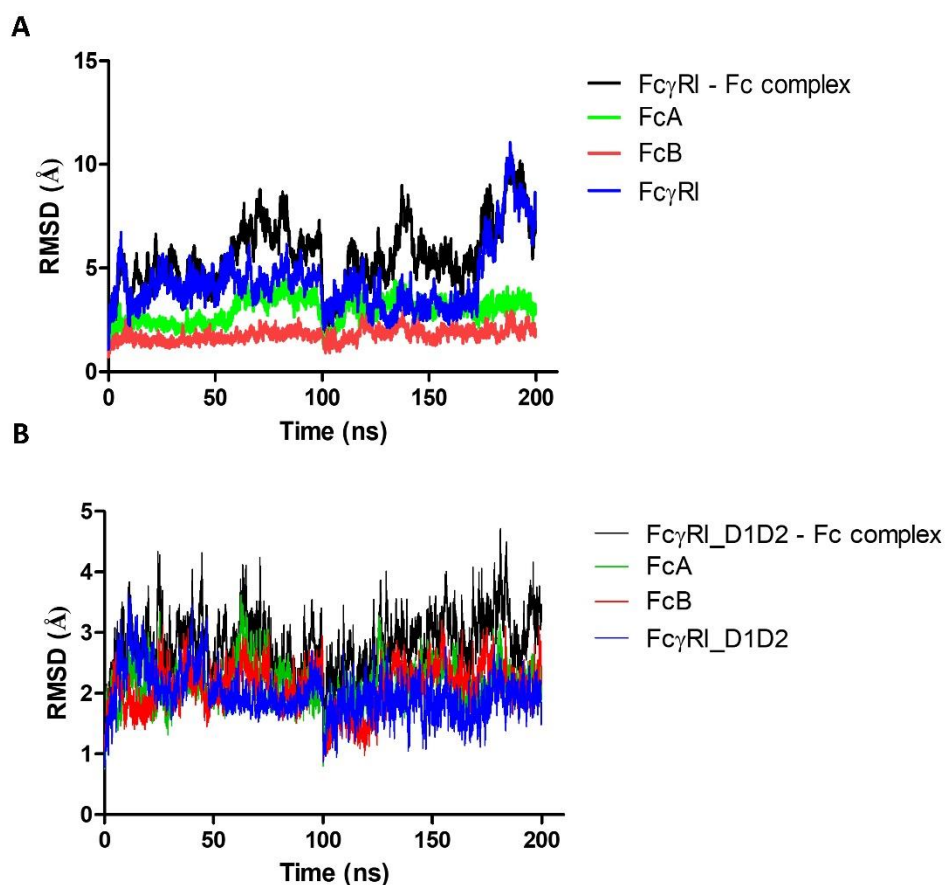
Figure 18. RMSD values of the FcγRI ectodomain protein and Fc region (FcA and FcB) over 200 ns A) RMSD values for the protein (FcγRI: Fc), FcγRI ectodomain, and Fc chains B) RMSD values for the protein, FcγRI ectodomain (D1 and D2) and Fc chains.

Recombinant FcγRI ectodomain protein is usually available with His tag to ease the recovery of the protein from the cell harvest. D3 domain with 6x-His tag residue dramatically increased RMSD value. Our findings correlated with the study in the literature in which FcγRI ectodomain (PDB ID: 3RDJ ) was docked to an Fc chain of IgG1 type antibody, and a noticeable change was observed with D3 domain(Kiyoshi et al. 2015). Asaoka et al(Yoshiharu Asaoka et al. 2013) compared the monoclonal antibody binding activity of full FcγRI ectodomain and truncated FcγRI (D1 and D2). According to SPR results, there is a comparable $K_D$ value between full and truncated forms of protein. Kinetics analysis indicated that the association rate constants were similar between the two forms of proteins. The difference occurred through the dissociation rate constant ($k_d$) which the absence of the D3 domain caused a faster dissociation phase in comparison to the full ectodomain.
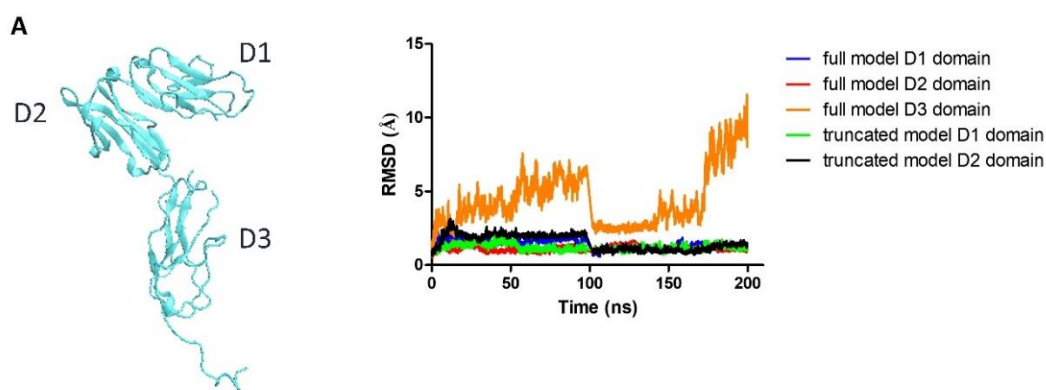
Figure 19. RMSD values of the FcγRI ectodomain (D1, D2, and D3) over 200 ns

RMSD values were shown for Fc chain domains, which are $C_H2$ and $C_H3$ regions, for both models. Full model RMSD values along 100ns were found 1.57 Å and 1.46 Å range for $C_H2A$ and $C_H2B$, respectively (Figure 20A). While the $C_H2A$ RMSD value slightly reduced to 1.35 Å, the $C_H2B$ RMSD value slightly increased to 1.59 Å for 200 ns (Figure 20B). RMSD values of the truncated FcγRI model along 100 ns were 1.44 Å and 1.68 Å for $C_H2A$ and $C_H2B$, respectively (Figure 20A). There was a slight increase in both $C_H2A$ (1.70 Å and $C_H2B$ (1.74 Å) for 200 ns within the truncated model (Figure 20B). $C_H3A$ domain RMSD values remained 0.97 Å and 1.10 Å range in the full model for 200 ns, respectively. The truncated model presented higher RMSD values in both simulation times which were 1.17 Å and 1.42 Å. In the $C_H3B$ results, the truncated model increased from 1.20 Å to 1.42 Å but the full form of it did not change over 200 ns (1.00 Å to 1.02 Å). Kiyoshi et al(Kiyoshi et al. 2015). reported that conformational change of $C_H2B$ within the FcB chain led to a high RMSD value (about 10 Å) upon binding with the FcγRI ectodomain. They explained these results by that most of the interactions occur through the D2 domain of FcγRI and the $C_H2B$ domain within FcB. In addition, they had not seen noticeable changes within the $C_H3$ domain in both Fc chains.

**A**



**B**
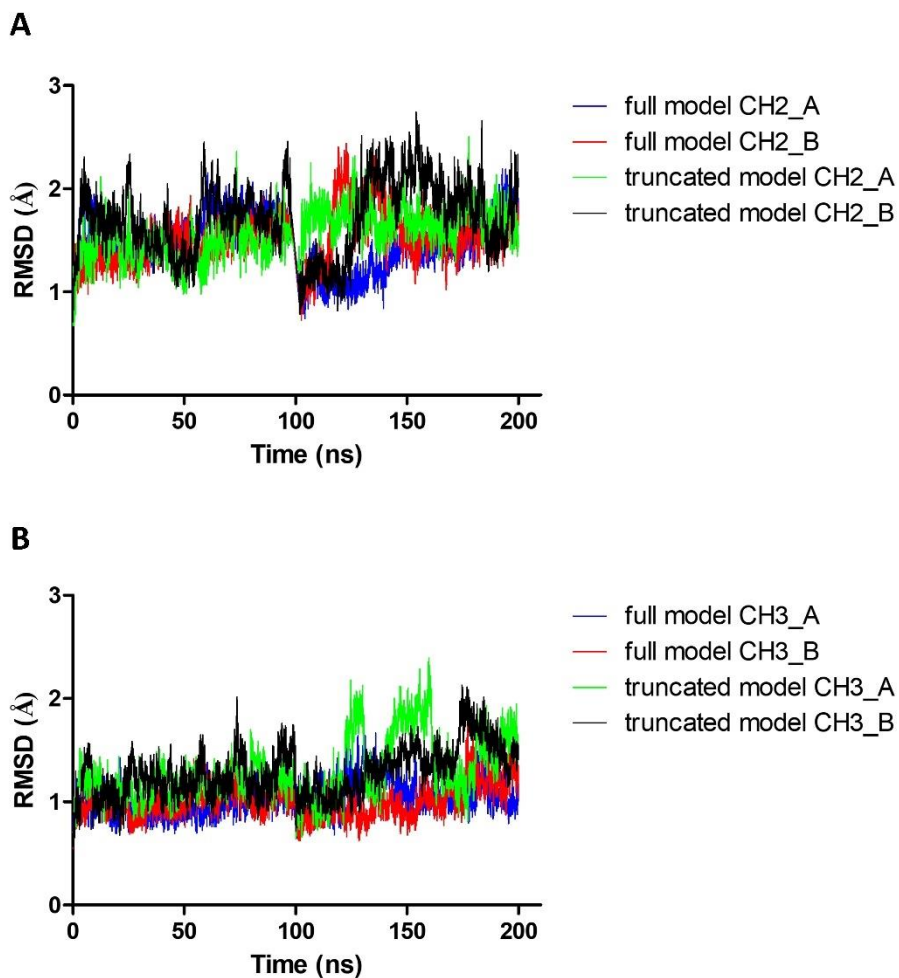


Figure 20 RMSD values of the Fc chains over 200 ns A) RMSD values for $C_H2$ domains within the Fc structure of full and truncated model B) RMSD values for $C_H3$ domains within Fc structure of the full and truncated model.

Moreover, RMSF calculation is performed within each protein and its domains. Figure 21 showed that the D3 domain has the highest RMSF value and flexibility over both simulation times in full-form FcγRI. This confirms the previous RMSD results for FcγRI. The D1 domain within the full model showed higher RMSF patterns for 200 ns simulation results. The truncated FcγRI model showed similar patterns and maintained its stability.

55
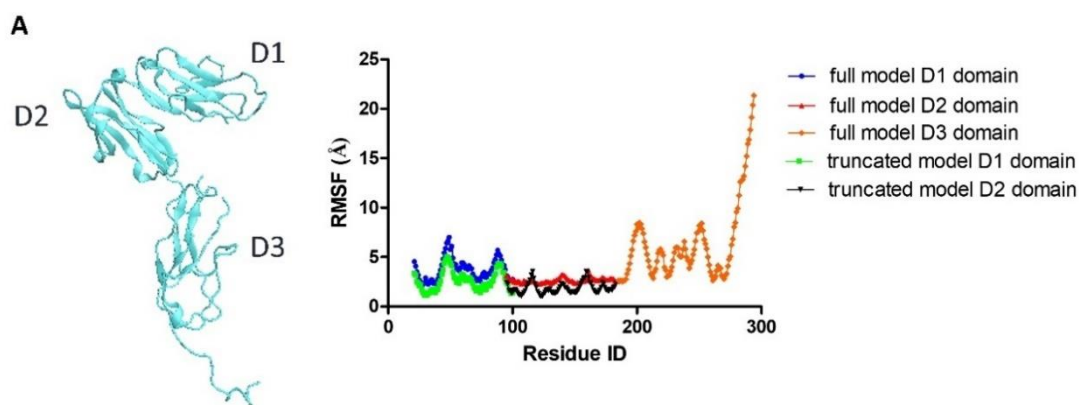
Figure 21 RMSF plots for the full and truncated model of FcγRI ectodomains over 200 ns.

RMSF patterns were analyzed separately for each domain within Fc chains (Figure 22). The full model RMSF plot for $C_H2A$ showed higher mobility in comparison to the truncated form of it over the simulation duration (Figure 22A). The RMSF plot of $C_H2B$ in both models presented similar patterns for 280 to 340 residues for 100 ns, but the 200 ns simulation results of the truncated model were comparatively lower than that of the full model. For the $C_H3$ domains (both A and B chains), the full model had higher flexibility for both simulation durations (Figure 22B). However, the truncated model showed similar patterns for both A and B chains whereas the full model presented dissimilarities within the chains. Zhao et al(Zhao, Nussinov, and Ma 2019). studied binding dynamics between Fc and FcγRI. They evaluated free antibody, free FcγRI, antibody: FcγRI bound complex, and target antigen: antibody: FcγRI bound complex. According to their results, RMSD patterns for Fc chains and the D3 domain were significantly altered upon binding an antibody to FcγRI. As stated in the literature, our results confirmed that there is an asymmetry in the same model between the domains of FcA and FcB chains.
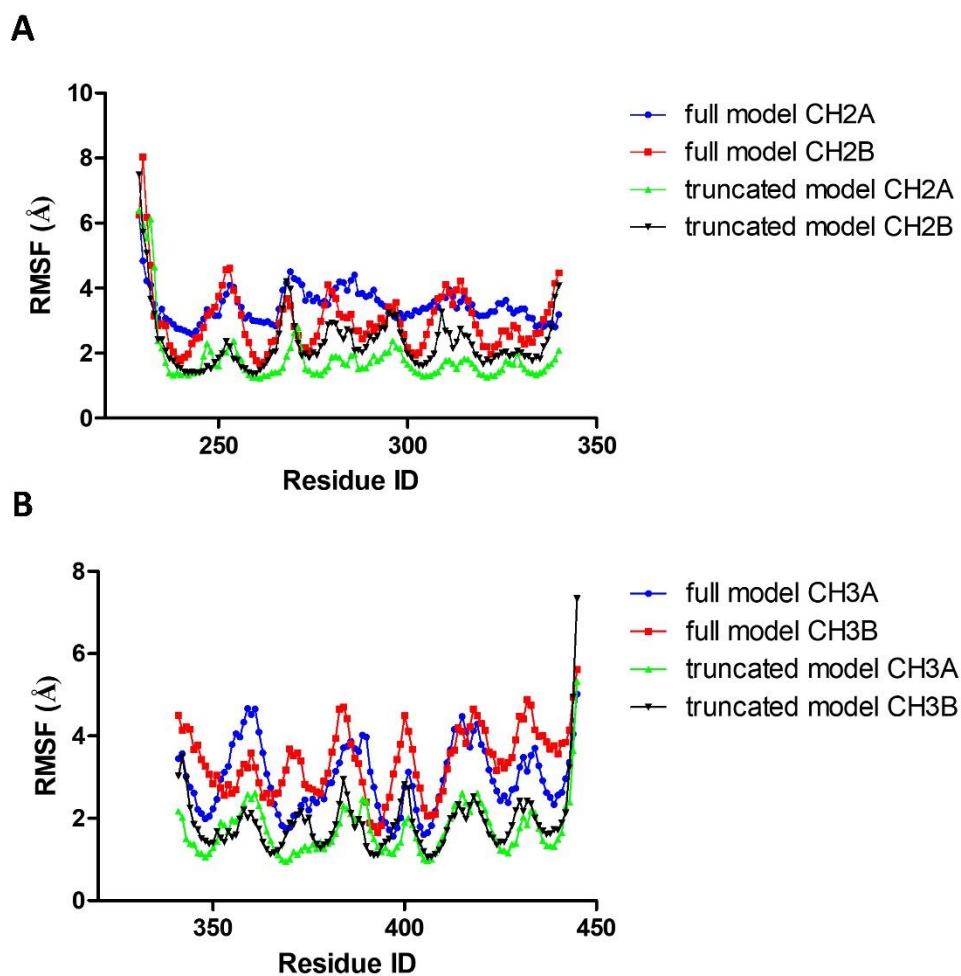
Figure 22. RMSF plots for the Fc chain domain in both the full and truncated model A) RMSF plots for the $C_H2$ domain within the Fc chains over 200ns B) RMSF plots for the $C_H3$ domain within the Fc chains over 200 ns.

### 4.3.2 Salt bridge interactions in the binding interface of FcγRI and Fc for the full and truncated model

The salt bridge analysis was evaluated between Fc: FcγRI ectodomain complex. Since the importance of the FG loop within the FcγRI ectodomain, key residues were initially chosen in this region for the salt bridge interaction results. KHR motif contributes a high affinity toward IgG antibodies and stabilizes the interaction between FcγRI and Fc region. LYS173: ASP265 FcB presented weaker interactions in the truncated model which fluctuated the distance more over time(Figure 23A). ARG175: ASP 265 FcA interactions had a higher distance at first but remained stable over a longer duration in both simulation runs. In the truncated model, this interaction started near 6 Å distance but resulted in a

57

similar distance (5 to 10 Å) with the full model (Figure 23B). Lu et al(J. Lu et al. 2015). evaluated the effect of the KHR motif on the binding affinity by performing mutations within the FG loop of the FcγRI ectodomain. The study showed that HIS174 caused a significant reduction in the binding affinity while ARG175 had a moderate effect on the binding affinity. In addition, the mutated version of the KHR motif disrupted the glycan interaction with the Fc region of the IgG.
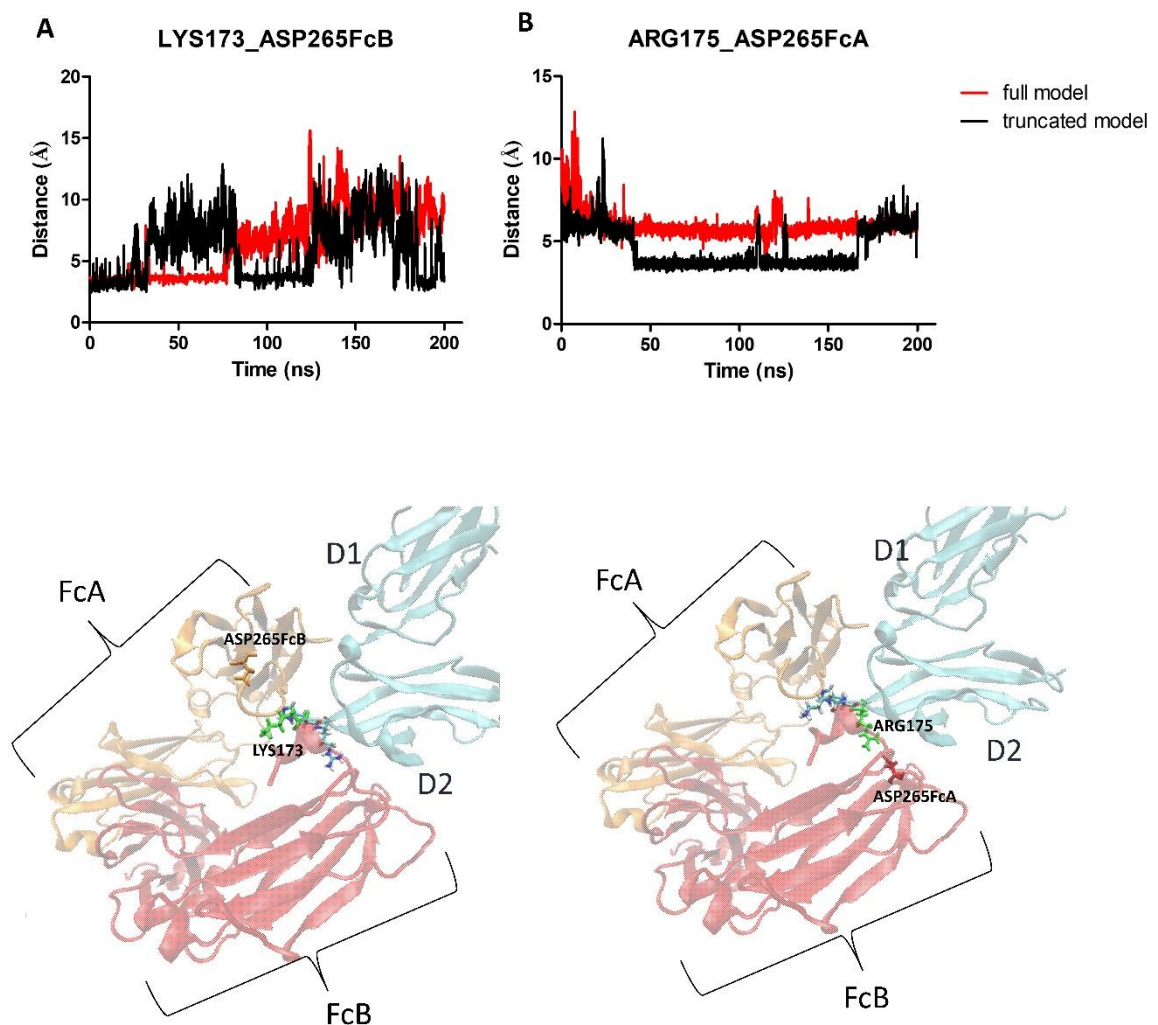


Figure 23.   The evaluation of LYS173: ASP265FcB and ARG175: ASP265FcA salt bridge interactions on full and truncated models.

LYS 128 and LYS130 are located in the binding surface area of the FcγRI ectodomain. Their salt bridge patterns were altered between the full and truncated models. LYS128:GLU269FcB interaction presented nearly 10 Å distance and stable pattern in

the full model (Figure 24A). The truncated model distance was altered over the simulation periods. LYS128:GLU270FcB interactions were comparably loosed over 200ns simulation runs in the truncated model. Besides, the distance increased nearly 2-fold around 125 ns but remained stable at 10 Å at the end of the simulation period (Figure 24B). LYS130:GLU269FcB interaction was stable in the full model and 5 to 10 Å distance while the truncated model showed weakened interaction and 10 to 15 Å distance (Figure 25A). The truncated model presented stable interaction for LYS130:GLU233 FcB interaction over the simulation run(Figure 25B).
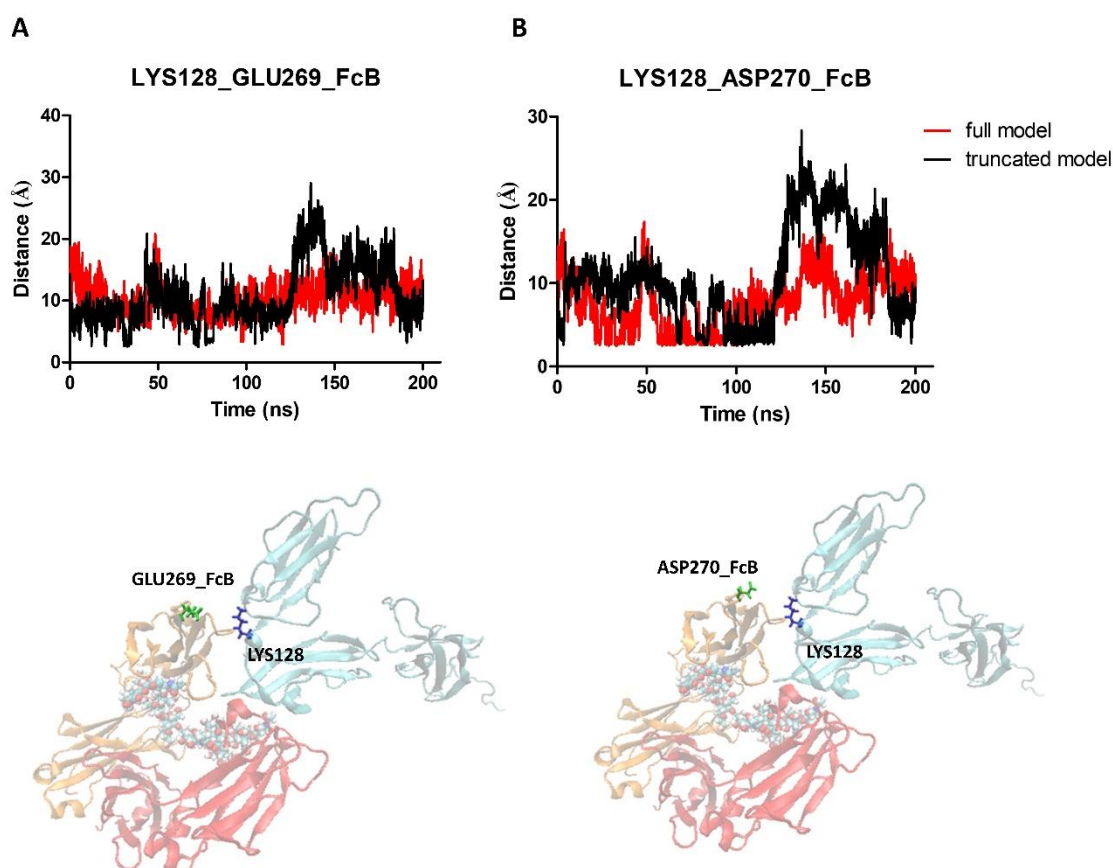


Figure 24. The evaluation of LYS128: GLU269FcB and LYS128: ASP270FcB salt bridge interactions on full and truncated models.
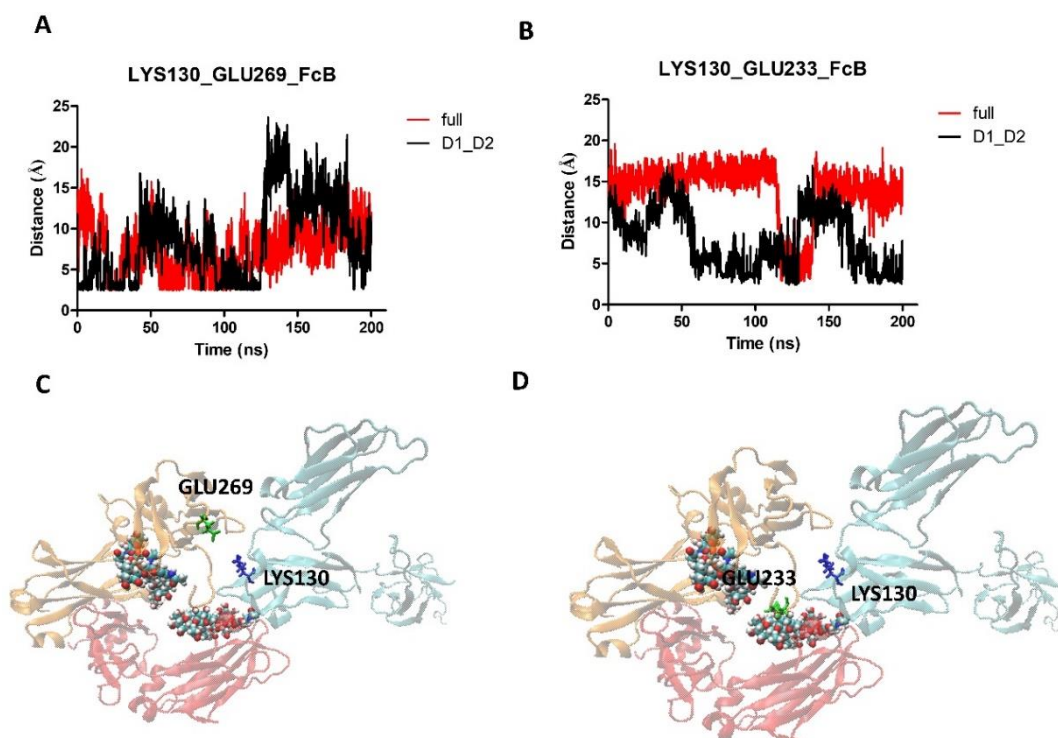
Figure 25. The evaluation of LYS130: GLU269FcB and LYS130: GLU233FcB salt bridge interactions on the full and truncated model.

In addition, the interprotein interaction was analyzed and showed similar results to the literature(J. Lu et al. 2015). Figure 26 presented the salt bridge interactions between D1 and D2 domains within the FcγRI ectodomain. GLU37:HIS125 interaction was reported as 2.8 Å distance(J. Lu et al. 2015). GLU37:LYS128 was evaluated in our model and presented the distance around 5.0 Å (Figure 26A) The interaction patterns were similar between full and truncated models. GLU99:ARG122 distance was reported as 3.4 Å and our results presented around 5.0 Å distance value (Figure 26B). The reason for the variation is that our model included the missing residues at C-terminal (6X-His tag). The truncated model seemed more stable and reduced fluctuation pattern over 200 ns MD trajectories.
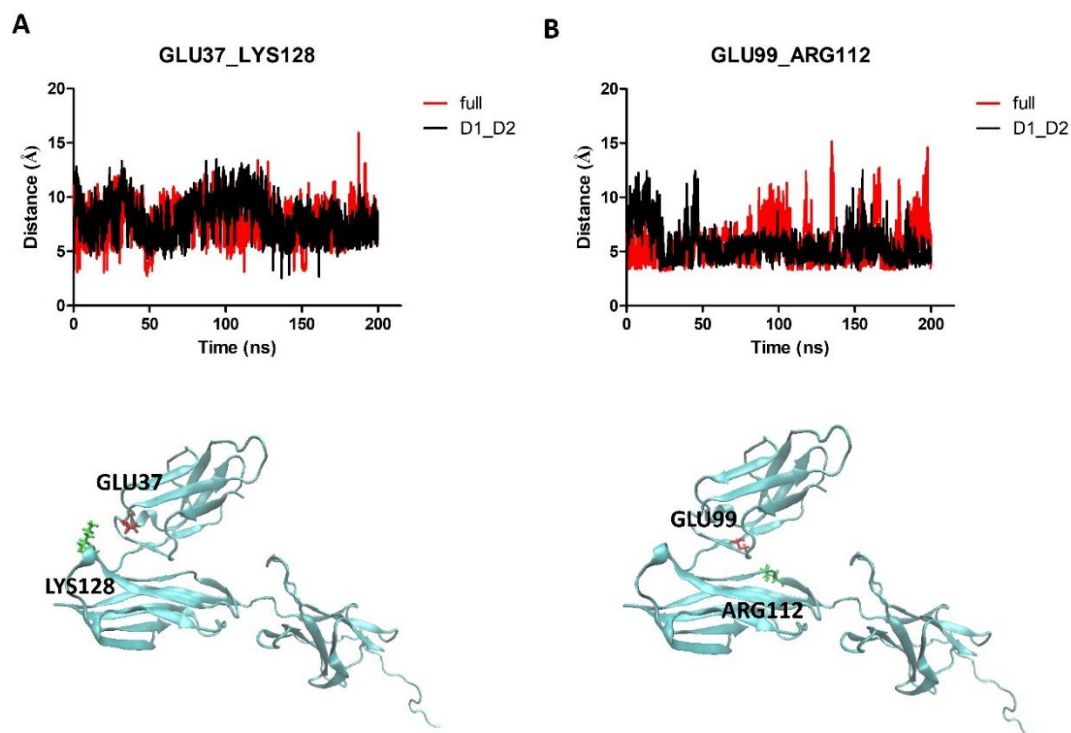
Figure 26 The salt bridge interaction analysis between D1 and D2 domains in FcγRI ectodomain on the full and truncated model.

In Figure 27, the interactions between D2 and D3 domains were given for the full model since the truncated version of it did not comprise the D3 domain. The findings were correlated with the literature, which was indicated as 3.2 Å for GLU116:LYS271 and GLU187:LYS271 interactions.
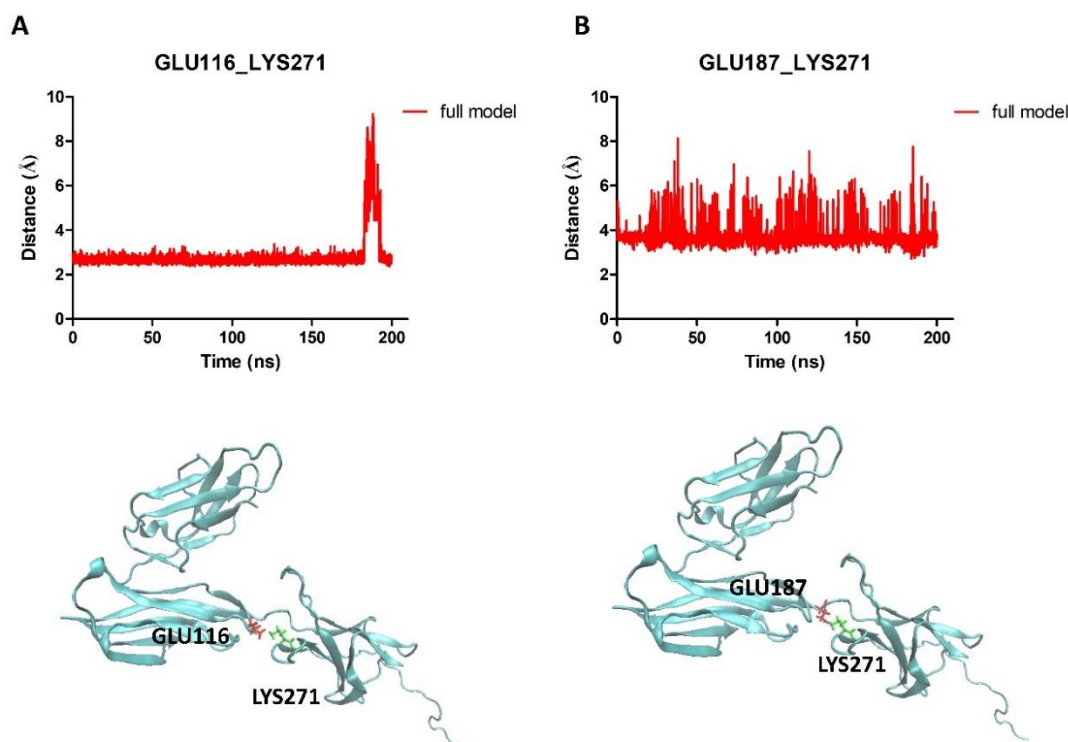
Figure 27. The salt bridge interaction analysis between D2 and D3 domains in FcγRI ectodomain on the full model.

The salt bridge analysis was evaluated for $C_H2$ and $C_H3$ domains for the full and truncated model. For the $C_H2$ domain, ASP249_LYS246 FcA interaction distance in the full model was found nearly 2-fold higher than the truncated model (Figure 28A). ASP249_LYS246 FcB interaction in the truncated model presented a more stable and reduced distance with a 5.0 Å value till 100 ns. However, there was no difference between both models for 200ns results, as displayed in Figure 28A. ASP280_LYS319 interaction did not contribute variations within the two models (Figure 28B). For the $C_H3$ domain, ASP399FcB_LYS349FcA interactions were weakened in the truncated model and increased the distance in comparison to the full model over 200ns (Figure 29A). As shown in Figure 29B, ASP356FcB_LYS439FcA interactions presented a similar pattern in further 200 ns simulation results.
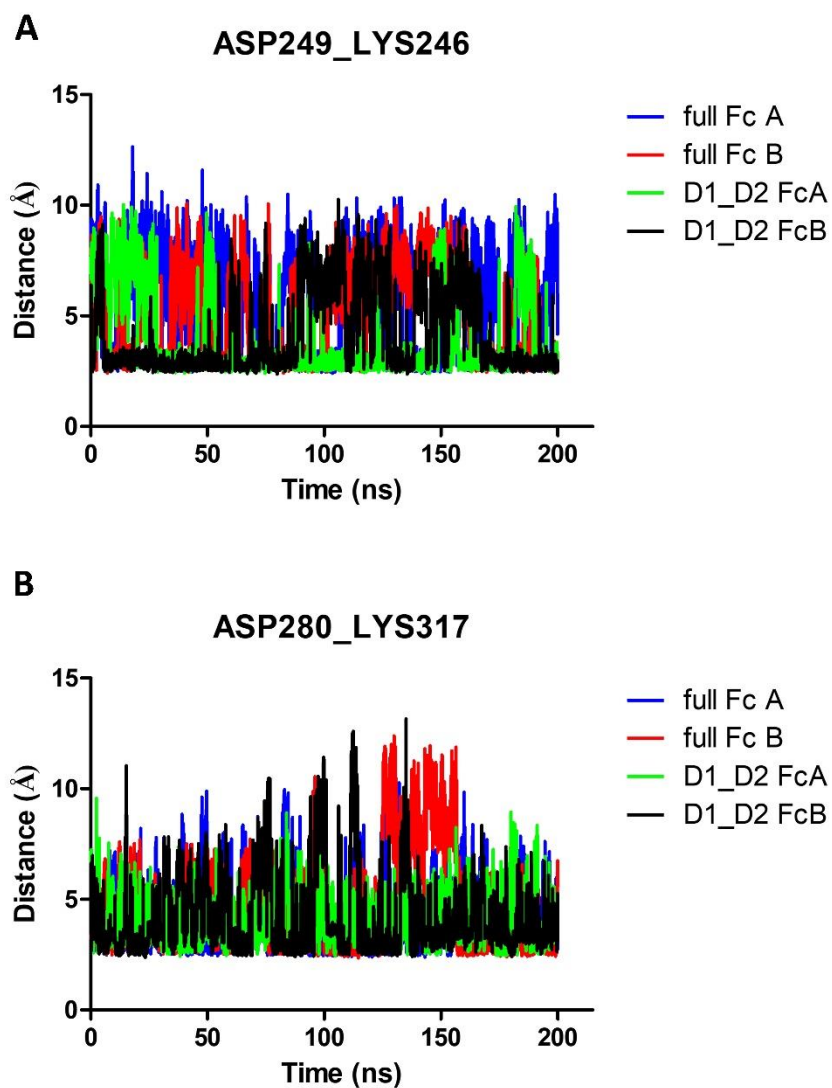
Figure 28. The salt bridge interaction analysis of $C_H2$ domains in Fc chains on the full and truncated model.
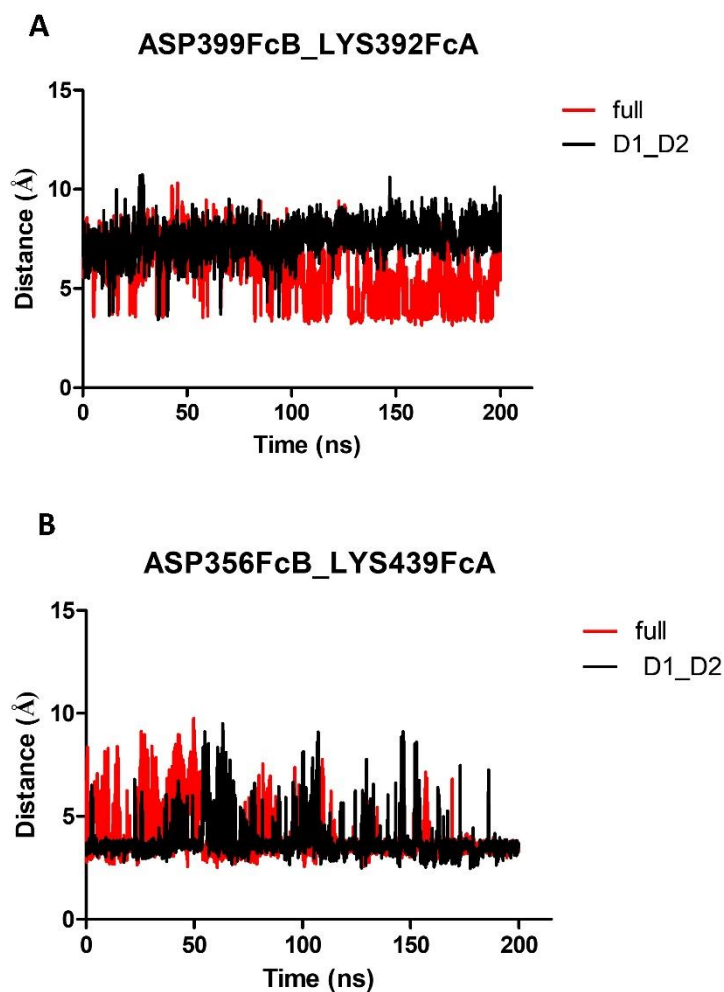
Figure 29. The salt bridge interaction analysis of $C_H3$ domains in Fc chains on the full and truncated model.

### 4.3.3 Single residue RMSD & RMSF results

The single residue RMSD and RMSF values were analyzed to evaluate the behavior of the critical residues within the Fc and FcγRI structure. LYS128 and LYS130 are in the binding surface of FcγRI and form H-bonds and salt bridge interactions with the Fc region of IgGs. RMSD plots showed reduced value with the truncated model (Figure 30A and 30B), but RMSF results indicated that there is no difference between the full and truncated model (Figure 30C and Figure 30D).
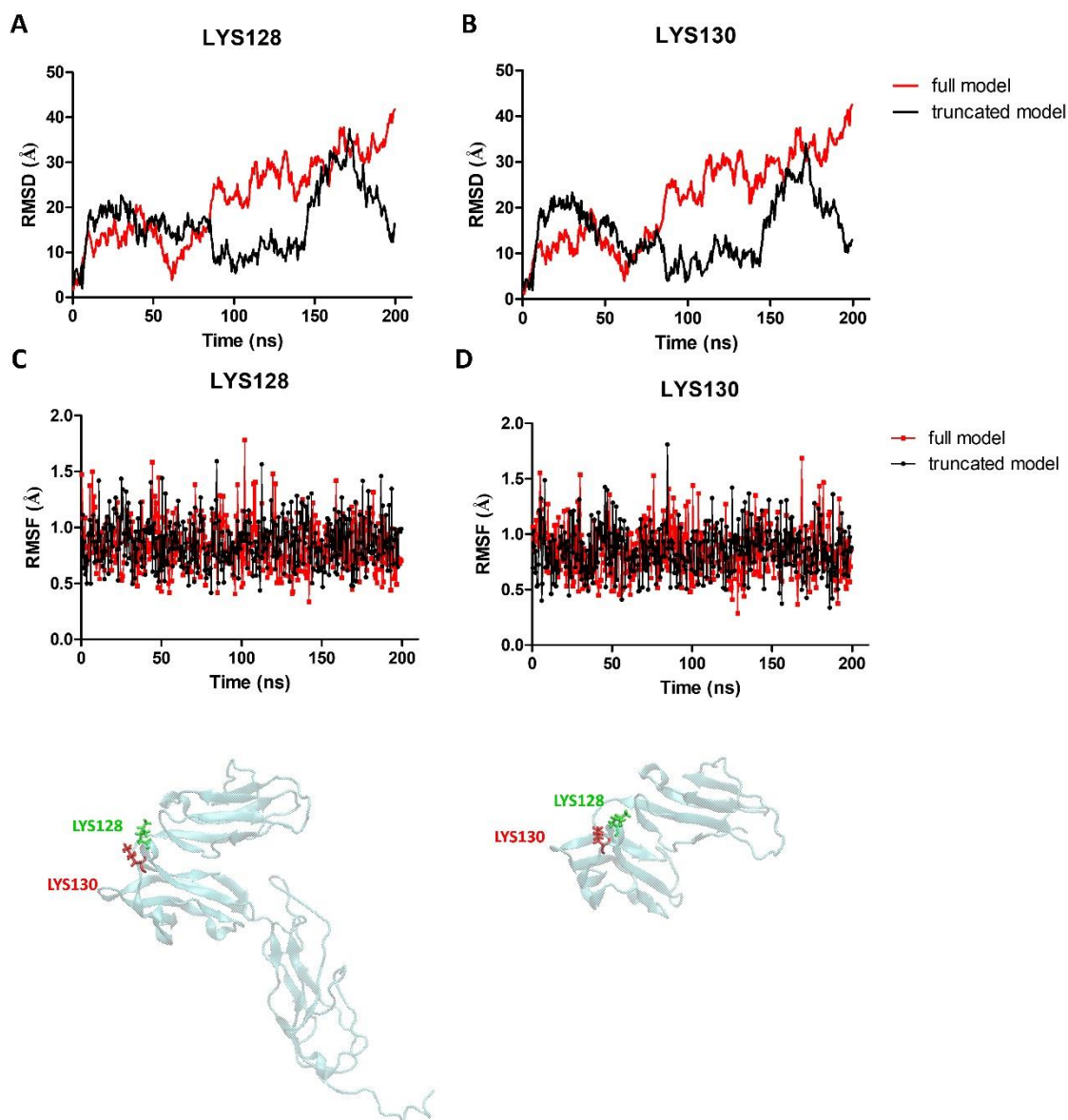
Figure 30. Single residue RMSD and RMSF plots in FcγRI ectodomain on the full and truncated models A)RMSD plot of LYS128 residue B) RMSD plot of LYS130 residue C) RMSF plot of LYS128 D) RMSF plot of LYS130 residue.

KHR motif residues which are LYS173, HIS174, and ARG175 in FcγRI ectodomain were evaluated for single residue RMSD and RMSF. Results showed that there is no difference between both models in terms of conformation stability and flexibility (Figure 31).
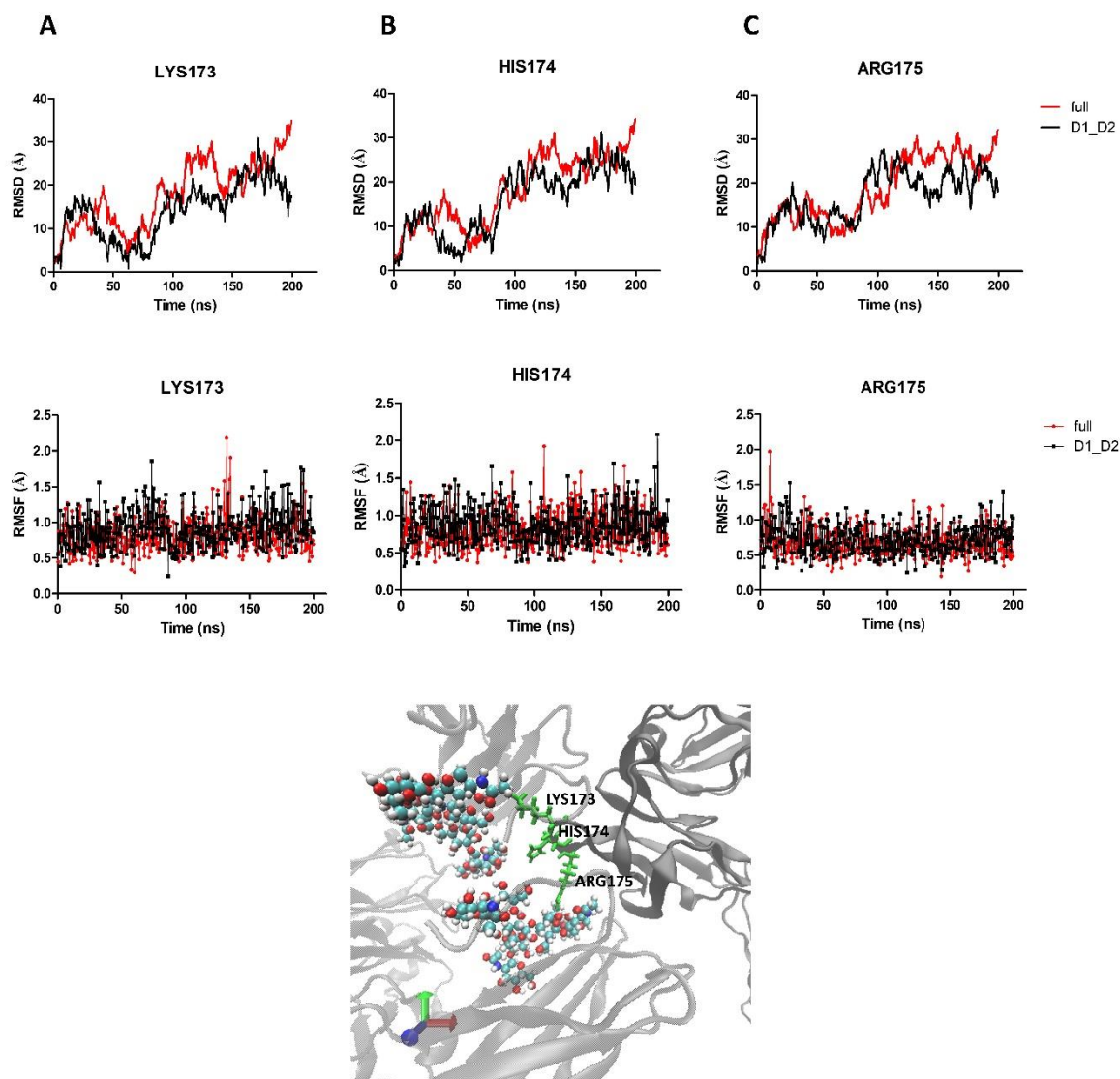
Figure 31. Single residue RMSD and RMSF plots in key residues within the FcγRI ectodomain on the full and truncated models A) LYS173 RMSD and RMSF plots B) HIS174 RMSD and RMSF plots C) ARG175 RMSD and RMSF plots.
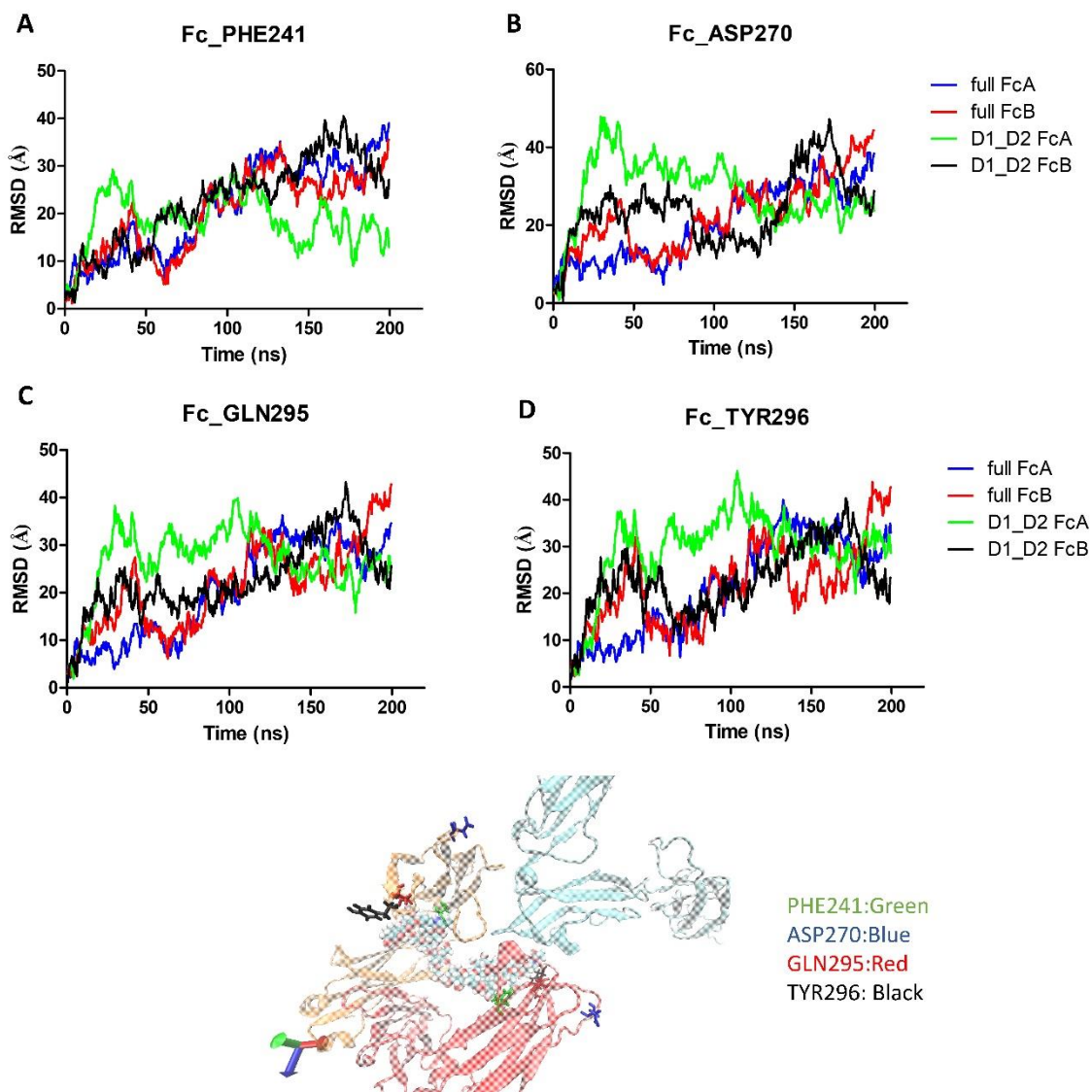
Figure 32. Single residue RMSD plots in key residues within the Fc chains on the full and truncated models A) PHE241 B) ASP270 C) GLN295 D) TYR296 RMSD plots.
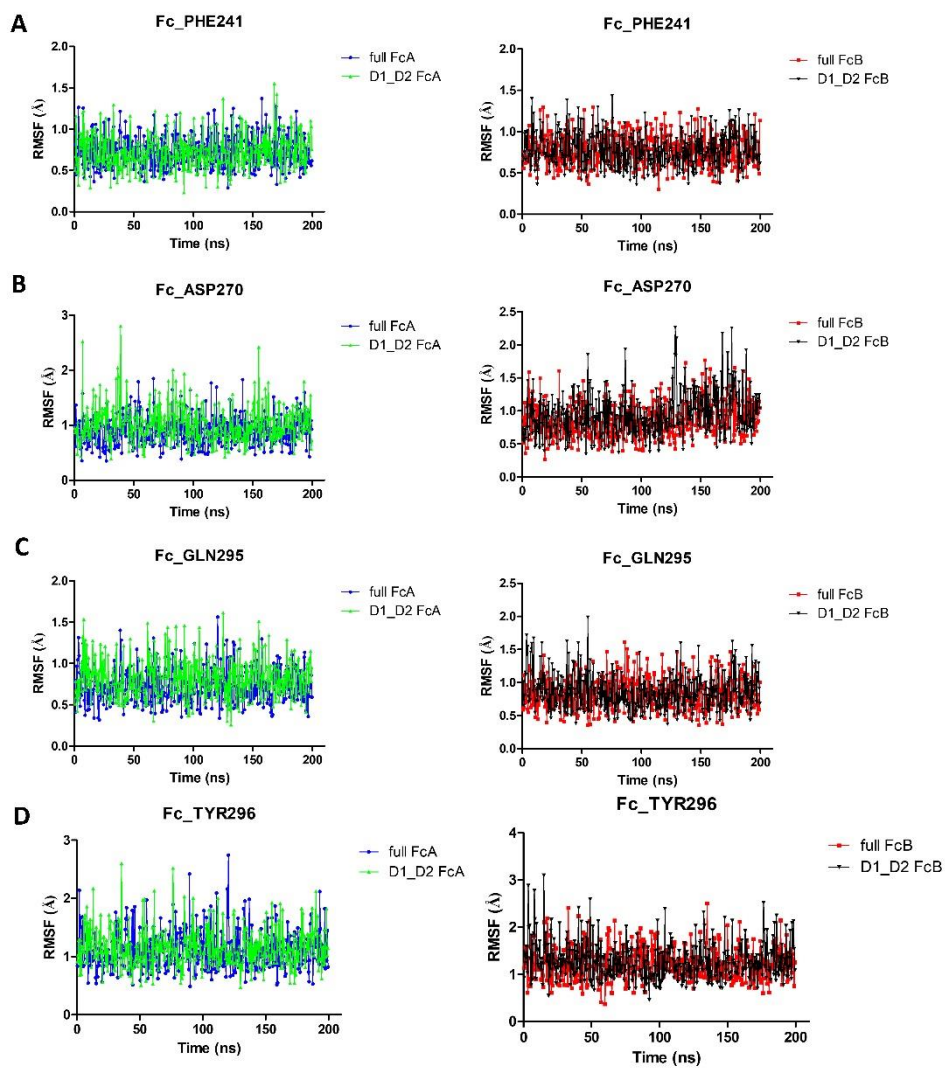
Figure 33. Single residue RMSF plots in key residues within the Fc chains on the full and truncated models A) PHE241 B) ASP270 C) GLN295 D) TYR296 RMSF plots.
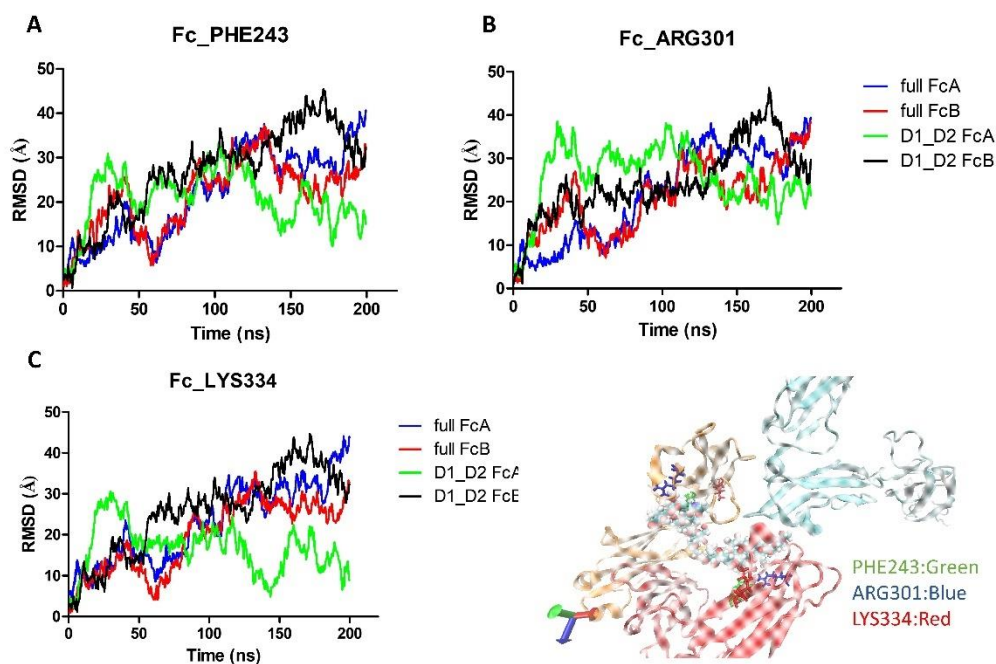
Figure 34. Single residue RMSD plots in key residues within the Fc chains on the full and truncated models A) PHE243 B) ARG301 C) LYS334 RMSD plots.

FcA chains in the truncated model had about 30 Å distance and reduced below this value over time, while in the full model, RMSD values were increased. Residues in the FcB chain showed higher RMSD values in the truncated model. Besides, RMSD profiles were similar in FcA and FcB chains in the full model. In contrast to that, The truncated model showed different patterns for FcA and FcB chains. Single residue RMSF patterns did not present any dissimilarity between the full and truncated models. As previous results, we could indicate that the change in the conformation was caused by the Cα backbone, not their R-groups.
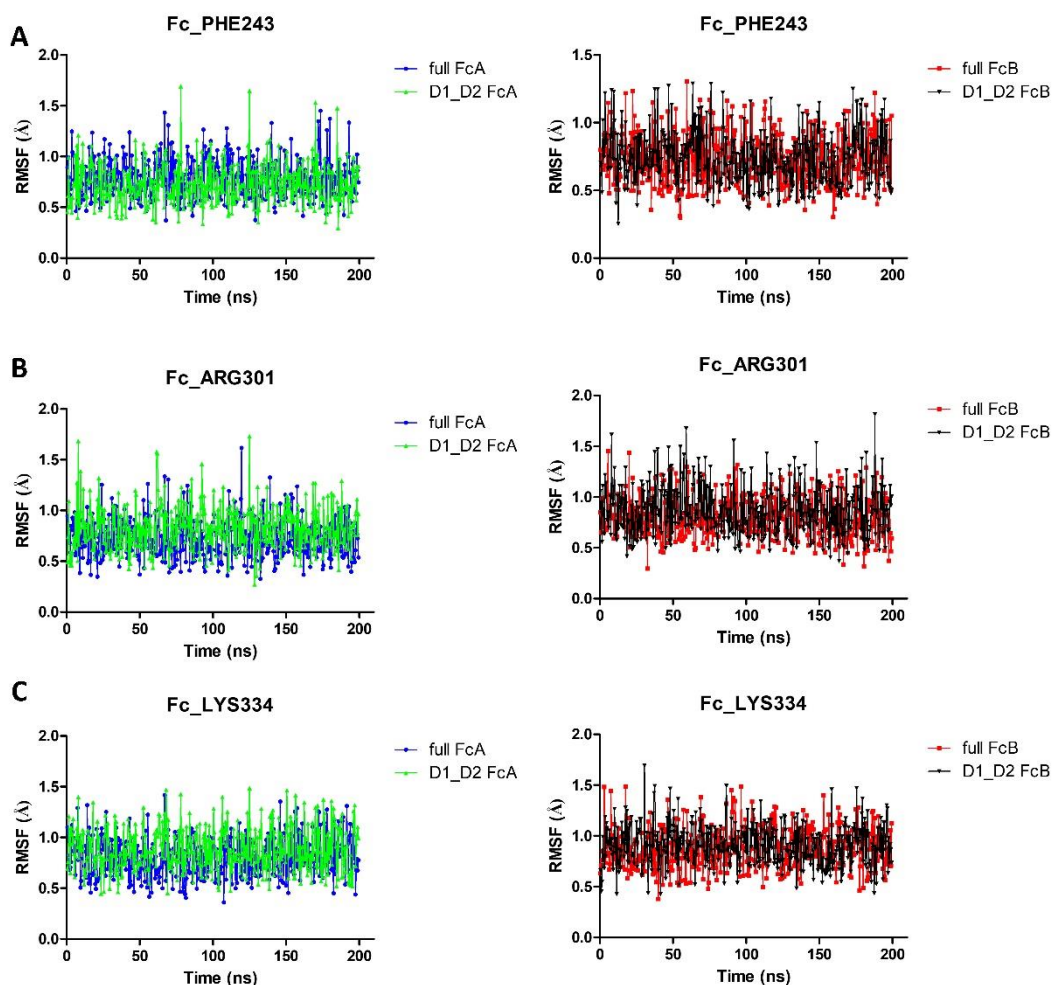
Figure 35. Single residue RMSF plots in key residues within the Fc chains on the full and truncated models A) PHE243 B) ARG301 C) LYS334 RMSF plots.

### 4.3.4 Dihedral Angle Results

Next step, the secondary structure of the residues was evaluated according to the single RMSD results. For this, Dihedral angle calculations were performed by VMD Tcl script. TY296 residue in Fc A chains showed similar movement in shifted periods. The angle movement at the beginning of the full model was the same in 50 to 100 ns in the truncated model (Figure 36A). The dihedral angle of TY296 residue in the FcB chain differed between the two models (Figure 36B). TYR296 changed mostly from -70 to -50 angle values in the full model. In the truncated model, most movements occurred at 180 to -180. For residues PHE241 and LYS334, the dihedral angle did not change between the two models, as displayed in Figure 36C and Figure 36D.

70
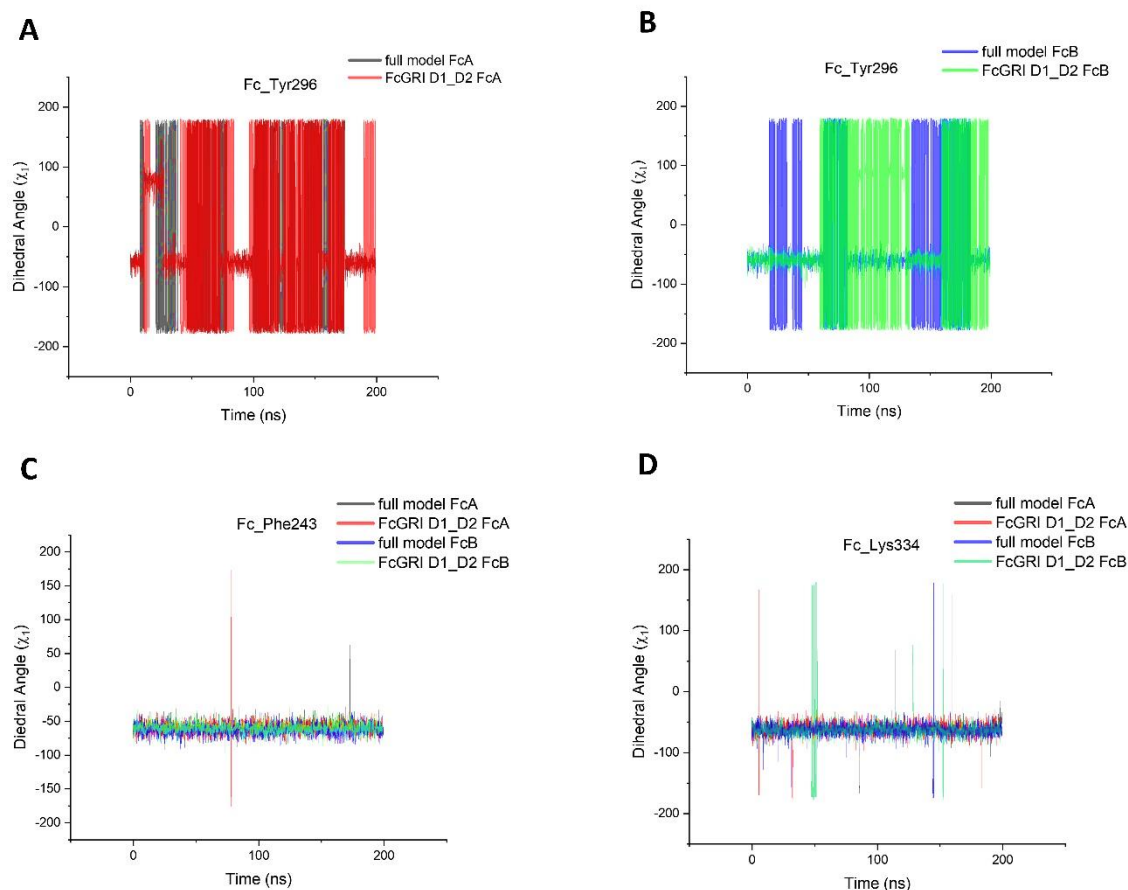
Figure 36. The comparison for dihedral angle plots on the full and truncated models A) The dihedral plot for TYR296 residue within FcA chains over 200 ns simulation runs B) The dihedral plot for TYR296 residue within FcB chains over 200 ns simulation runs C) The dihedral plot for PHE243 residue within Fc chains over 200 ns simulation runs D) The dihedral plot for LYS334 residue within Fc chains over 200 ns simulation runs.

As can be seen in Figures 37A and Figure 37B, ASP270 residue in both FcA and FcB chains presented a varied dihedral angle upon 200 ns. The truncated model remained nearly - $70.0°$ and presented changes between $170.0°$ and $-170.0°$ from 100 to 130 ns. The full model presented the movements mostly between $170.0°$ and $-170.0°$. For the FcB chain, the dihedral angle movements started with a value of $170.0°$ and $-170.0°$ for a short period. For most of the simulation period, it remained at -70.0°. GLN295 residue did not differ for the dihedral angle between FcA and FcB chain on both models and presented a value nearly at -60.0°(Figure 37C). The difference was observed for PHE241 residue in FcA for the full model. It was shifted from -50.0° to 50.0° after 180 ns(Figure 37D). ARG301 residue in the FcA chain presented different movements. The full model had a value of $-170.0°$ for most of the period, the truncated model changed between $170.0°$ to $-170.0°$ and $70.0°$(Figure 38A). For the FcB chain, the full model altered

71

between 170.0° to −170.0°. In the truncated model, the dihedral angle remained at nearly a value of 70.0°(Figure 38B).
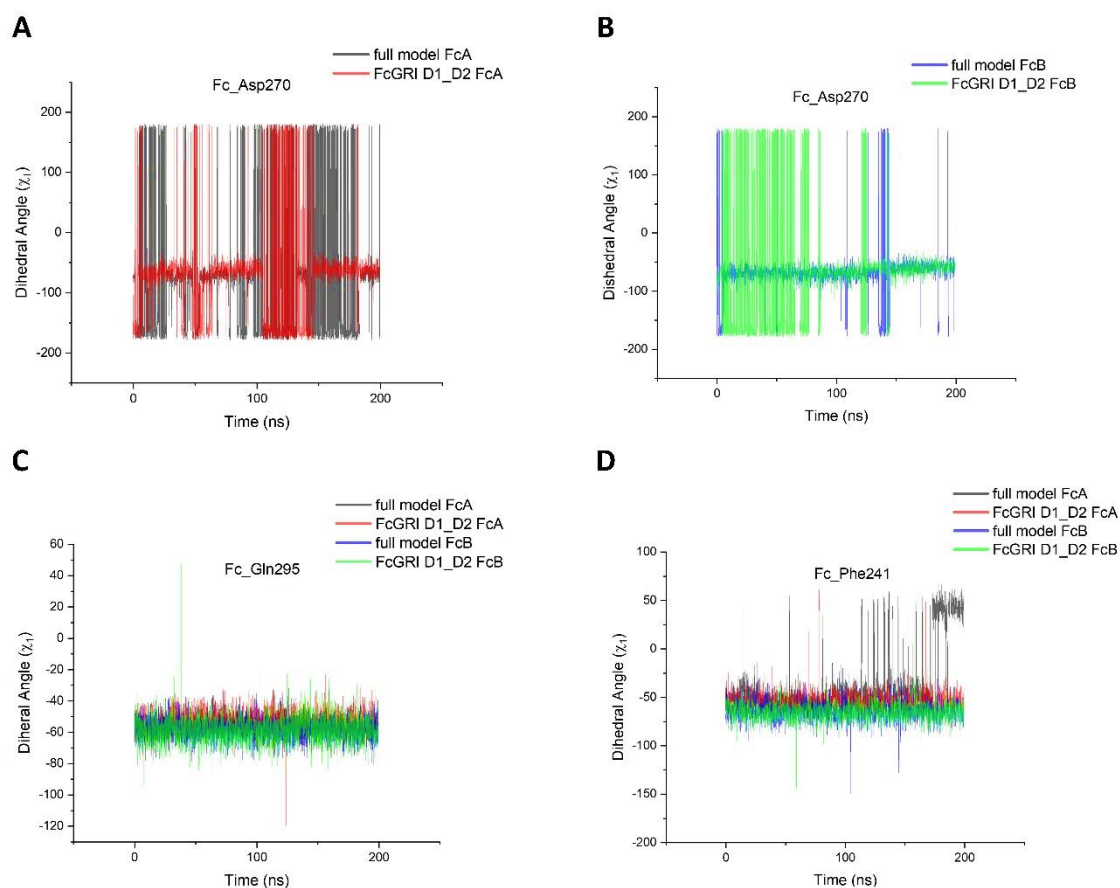


Figure 37. The comparison for dihedral angle plots on the full and truncated models A) The dihedral plot for ASP270 residue within Fc A chains over 200 ns simulation runs B) The dihedral plot for ASP270 residue within Fc B chains over 200 ns simulation runs C) The dihedral plot for GLN295 residue within Fc chains over 200 ns simulation runs D) The dihedral plot for PHE241 residue within Fc chains over 200 ns simulation runs.
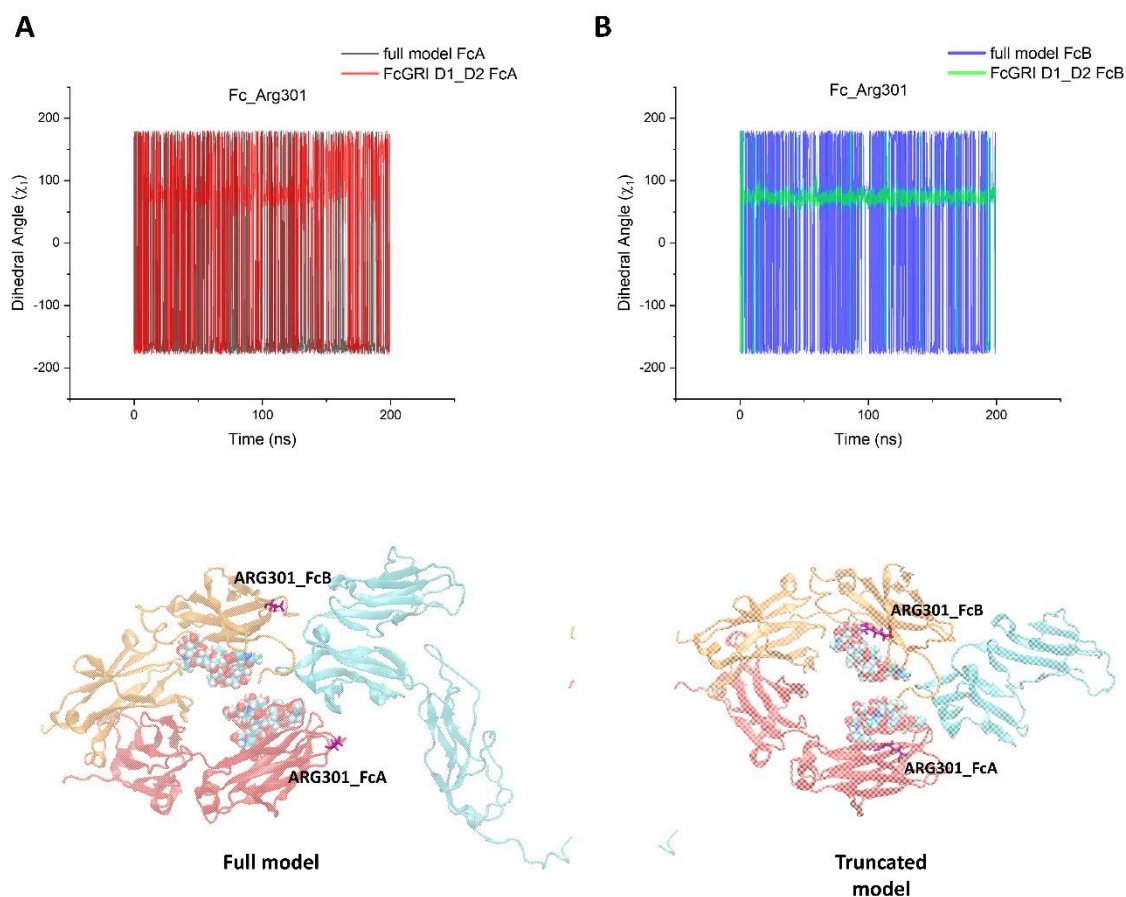
Figure 38. The comparison for dihedral angle plots on the full and truncated models A) The dihedral plot for ARG301 residue within Fc A chains over 200 ns simulation runs B) The dihedral plot for ARG301 residue within Fc B chains over 200 ns simulation runs.

### 4.3.5 Calculation of destabilization tendency with FoldX

The stability of the protein complex was evaluated with FoldX plug-in which was performed through YASARA. FoldX measured the change in $\Delta G$ (kcal/mol) between the folded and unfolded states during MD simulation periods on both models. As shown in Figure 39, the full model had higher energy and was less stable in comparison to the truncated model over both durations. Kralj et al(Kralj et al. 2021). studied Fc$\gamma$RIIa and Fc$\gamma$RIIIa interactions with Fc and full-length antibodies via MD studies(Kralj et al. 2021). According to free energy calculations, Fc$\gamma$RIIa and Fc$\gamma$RIIIa contributed to interactions with the Fab region of the IgGs and resulted in enhanced binding activity for IgGs. Especially, the $C_H1$ domain within the Fab region of the antibody was responsible for the binding interactions by forming many H-bonds. An MD study for Fc$\gamma$RI evaluated four types of structures which were free antibody, free Fc$\gamma$RI, antibody: Fc$\gamma$RI complex, and

antigen:antibody: FcγRI complex. They indicated that the conformation of the Fc region of the antibody altered to facilitate the FcγRI interactions upon the antigen binding(Zhao, Nussinov, and Ma 2019).
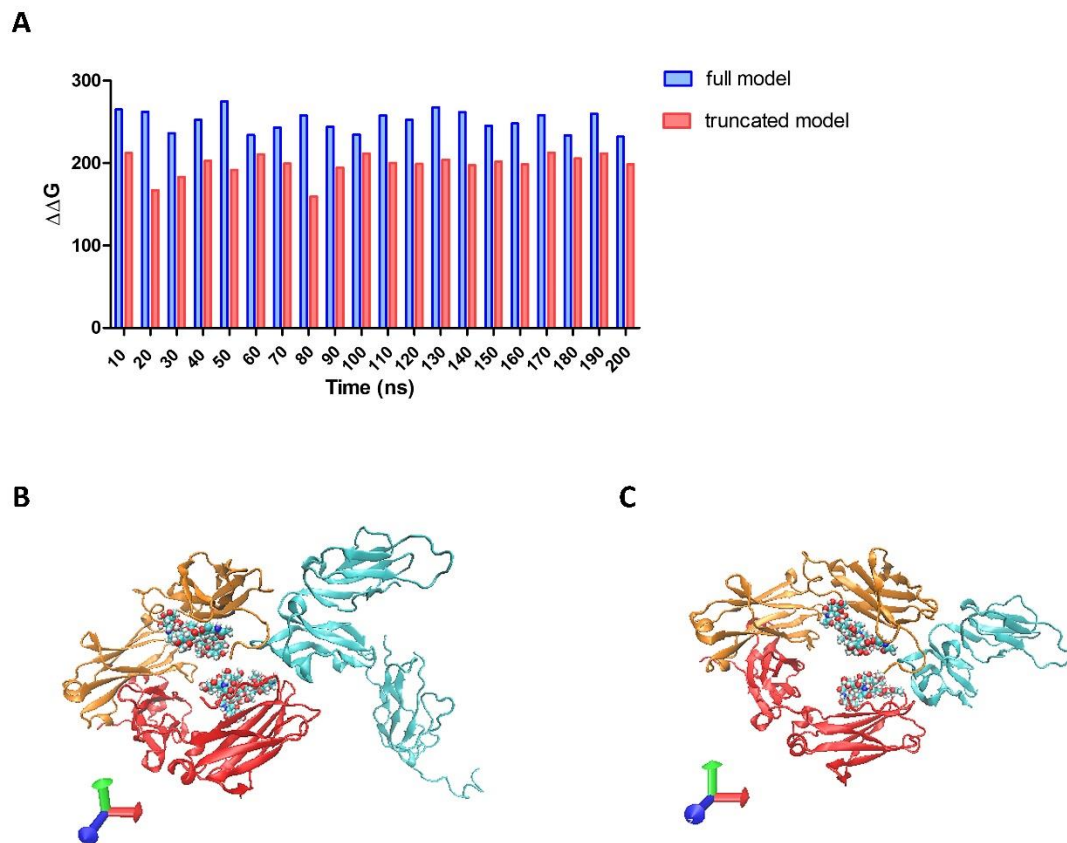


Figure 39. The change in destabilization tendency of the full and truncated models.
A) Calculation of destabilization tendency over 200 ns simulation B) Full model and
C)Truncated model systems.

In the last part of this thesis, MD simulations were conducted to reveal alterations in the Fc: FcγRI structure in terms of backbone properties, flexibility, salt bridge interactions, and secondary structure in the presence and absence of D3 domain in the FcγRI ectodomain The protein complex, Fc: FcγRI, showed variation in the absence of D3 domain in FcγRI structure. As expected, backbone properties and flexibility contributed to high RMSD & RMSF values for the D3 domain. Also, Fc chains in the same model presented alteration over simulation runs for RMSD and RMSF patterns indicating asymmetry in line with the literature. Also, the Critical binding motif, KHR, in the D2 domain of FcγRI

contributed to fluctuations and alterations in the distance for the salt bridge interaction between FcγRI and Fc chains for full and truncated models. ASP270, TYR296, and ARG301 residues in Fc chains that are known for contributing interaction with glycans contributed variation in the secondary structure based on the dihedral angle calculations. Finally, the changes in the stabilization tendency were calculated for both models. According to the results, the truncated model had lower $\Delta\Delta G$ (kcal/mol) values compared to the full model. The flexibility and mobility of the D3 domain could provide a high association with IgGs and other signaling molecules on the cell surface. The truncated FcγRI could offer a potential IgG1 capture and sensing application due to its higher stability than its full form of it.

# 5. Conclusion & Future Work

FcγRI has the highest affinity toward IgG1 molecules and binding occurs through a 1:1 binding ratio with high specificity. Since the importance of IgG1 antibodies in the field of therapeutics, biosensing, and analytical applications, FcγRI could serve as an alternative to commonly used other ligands (Protein A, Protein G, etc.) As a potential site-directed ligand molecule, FcγRI protein was evaluated for the IgG1 binding capacity through performing SPR assays. Three clinically approved IgG1 sub-type monoclonal antibody samples were utilized for the binding analysis. The antibody binding capacity was compared in parallel with the commonly used Protein A ligand. Initially, SPR assays were conducted in varied FcγRI configurations as in-surface (amine coupling, streptavidin-biotin, and His capture) and in-solution (through Protein L ligand). Amine coupling and streptavidin-biotin assay was not optimized due to the random coupling of FcγRI protein disrupting the IgG1 binding activity and the regeneration issue between IgG1 and FcγRI ectodomain, respectively. Further, His Tagged FcγRI protein was captured through anti-His immobilized chip surface and IgG1 samples injected on both FcγRI and Protein A surface. In this configuration, Antibody binding capacity was found higher in the Protein A surface than that of the FcγRI capture surface due to the 5 Ig binding sites of Protein A. In addition to that, IgG1 binding capacity was analyzed with crude and varied IgG1 monomer content samples through those ligand surfaces. The monomer content of IgG1 fractions was determined by performing the

SEC-HPLC method. The results indicated that protein A affected by the monomer content of the samples in which the highest antibody binding response was obtained with the purest (AVT) antibody solution. For FcγRI, the binding response was independent of the monomer content of the sample solutions.

Protein L ligand was used to test FcγRI and Protein A free-in solution orientation which IgG1 sample solutions were captured through their Fab region in Protein L immobilized chip surface and Protein A and FcγRI solution injected into those surfaces. In contrast to the on-surface configuration, FcγRI resulted in a higher antibody binding response than Protein A surface. Also, The steady-state and kinetics results led to pM range $K_D$ values on both ligand surfaces. All these results confirm that the orientation and capture strategy have a significant impact on the binding interactions and affinity for IgG1 and ligand interactions on the chip surface. As a further experiment, IgG1 binding ability could be enhanced through efficient capture strategy and protein engineering techniques in the structure of the FcγRI ligand.

Experimental assays were complemented with a computational method to evaluate the binding interactions in a dynamic system. The literature already mentioned in detail the critical residues in both FcγRI and Fc chains structure for the binding interactions. FcγRI ectodomain has a distinct property from other FcγRs due to an extra third domain in the ectodomain structure. The exact role of this domain is not fully understood. It is suggested as a flexible linker molecule for the IgG binding on the cell surface. Therefore, we focused on the structure and functional information about the D3 domain in FcγRI structure by performing MD simulations. The mobility and flexibility patterns were evaluated for each domain in FcA, FcB, and FcγRI and FcγRI: Fc protein complex on the full and truncated systems. RMSD and RMSF patterns were differed between the full and truncated model in which domain in Fc chain within the truncated model contributed higher backbone mobility than the full model. As expected D3 domain in FcγRI structure and Fc: FcγRI complex in the full model resulted in high mobility and flexibility due to the D3 domain. The absence of D3 domain had an impact on the salt bridge interactions between FcγRI and Fc chain, especially in KHR motif in the D2 domain of FcγRI structure. The single residue RMSD & RMSF values resulted in decreased RMSD pattern but there was no difference in RMSF values between the full and truncated models. The critical residues in Fc chains were analyzed for the change in the dihedral angle measurements. Three of them, which are

ASP270, TYR296, and ARG301 residues, presented changes in the dihedral angle measurements. Finally, the full and truncated models were subjected to calculations for their change in the destabilization tendency through the FoldX plug-in in the YASARA program. The results showed that the truncated model had higher stability than the full model.

For future contributions, the truncated FcγRI could be optimized for the recombinant production form of it for analytical applications. Recombinant truncated FcγRI production could offer advantage in comparison to the full form of it in terms of recovery and protein yield. In addition to that, genetic modification in FcγRI structure and alternative immobilization techniques could be utilized for the enhanced binding capacity for IgG1 antibodies. Together with these outcomes, FcγRI ectodomain has a potential IgG1 capture ligand in purification, sensing, and other analytical applications.

## REFERENCES

Alejandra, Waller-pulido et al. 2023. "Production of Monoclonal Antibodies for Therapeutic Purposes : A Review." *International Immunopharmacology* 120.

Anderson, Kyle W. W. et al. 2022. "HDX-MS and MD Simulations Provide Evidence for Stabilization of the IgG1—FcγRIa (CD64a) Immune Complex Through Intermolecular Glycoprotein Bonds." *Journal of Molecular Biology* 434(2): 167391. https://doi.org/10.1016/j.jmb.2021.167391.

Arney, J Winston, and Kevin M Weeks. 2022. "RNA − Ligand Interactions Quantified by Surface Plasmon Resonance with Reference Subtraction." *Biochemistry* 61: 1625–32.

Arya, Sunil K., and Pedro Estrela. 2017. "Electrochemical Immunosensor for Tumor Necrosis Factor-Alpha Detection in Undiluted Serum." *Methods* 116: 125–31. http://dx.doi.org/10.1016/j.ymeth.2016.12.001.

Asaoka, Y et al. 2012. "Engineering of Recombinant Human Fcγ Receptor I by Directed Evolution." *Protein Engineering, Design & Selection* 25(12): 835–42.

Asaoka, Yoshiharu et al. 2013. "The Binding of Soluble Recombinant Human Fc Gamma Receptor I for Human Immunoglobulin G Is Conferred by Its First and Second Extracellular Domains." *Molecular Immunology* 54(3–4): 403–7. http://dx.doi.org/10.1016/j.molimm.2013.01.007.

Bailey, Mark J, Felix Broecker, Paul E Leon, and Gene S Tan. 2018. "A Method to Assess Fc-Mediated Effector Functions Induced by Influenza Hemagglutinin Specific Antibodies." *Journal of Visualized Experiments* (132): 1–5.

Barhoumi, Lassaad et al. 2018. "A Novel Chronoamperometric Immunosensor for Rapid Detection of TNF-A in Human Saliva." *Sensors and Actuators, B: Chemical* 266: 477–84. https://doi.org/10.1016/j.snb.2018.03.135.

Baydemir, Gozde, Francesca Bettazzi, Ilaria Palchetti, and Diego Voccia. 2016. "Strategies for the Development of an Electrochemical Bioassay for TNF-Alpha Detection by Using a Non-Immunoglobulin Bioreceptor." *Talanta* 151: 141–47. http://dx.doi.org/10.1016/j.talanta.2016.01.021.

Boesch, Austin W. et al. 2018. "Enrichment of High Affinity Subclasses and Glycoforms from Serum-Derived IgG Using FcγRs as Affinity Ligands." *Biotechnology and Bioengineering* 115(5): 1265–78.

Brooks, B R et al. 2009. "CHARMM : The Biomolecular Simulation Program." *Journal of Computational Chemistry* 30: 1545-1614.

Brown, Eric P. et al. 2017. "Multiplexed Fc Array for Evaluation of Antigen-Specific Antibody Effector Profiles." *Journal of Immunological Methods* 443: 33–44.

———. 2018. "Optimization and Qualification of an Fc Array Assay for Assessments of Antibodies against HIV-1/SIV." *Journal of Immunological Methods* 455(January): 24–33. https://doi.org/10.1016/j.jim.2018.01.013.

Bruggeman, Christine W et al. 2017. "Enhanced Effector Functions Due to Antibody Defucosylation Depend on the Effector Cell Fcγ Receptor Profile." *The Journal of Immunology* 199(1): 204–11.

Bustos, Rosa Helena et al. 2018. "Label-Free Quantification of Anti-TNF-α in Patients Treated with Adalimumab Using an Optical Biosensor." *Sensors* 18(3).

Cain, Paul et al. 2023. "Impact of IgG Subclass on Monoclonal Antibody Developability." *mAbs* 15(1). https://doi.org/10.1080/19420862.2023.2191302.

Cambay, Florian et al. 2020. "Impact of IgG1 N-Glycosylation on Their Interaction with Fc Gamma Receptors." *Current Research in Immunology* 1(June): 23–37.

Champion, Thierry, and Alain Beck. 2013. "Capture of the Human IgG1 Antibodies by Protein A for the Kinetic Study of H-IgG/FcγR Interaction Using SPR-Based Biosensor Technology." In *Methods in Molecular Biology*, , 331–43.

Chen, Xiujuan, Ying Wang, Ying Wang, and Yifeng Li. 2020. "Protein L Chromatography: A Useful Tool for Monitoring/Separating Homodimers during the

Purification of IgG-like Asymmetric Bispecific Antibodies." *Protein Expression and Purification* 175(May): 105711.

Cytiva. *Biacore Concentration Analysis Handbook*.

Darden, Tom, Hsing Lee, and Lee G Pedersen. 2005. "Particle Mesh Ewald: An Nlog(N) Method for Ewald Sums in Large Systems." *Journal of Chemical Physics* 103: 8577–93.

Deng, Fei, Laicong Qiao, and Yi Li. 2022. "A Fluorescent Immunosensor on Optical Fibre for the Multiplex Detection of Proinflammatory Cytokines." *Sensing and Bio-Sensing Research* 37(May): 0–5.

Ding, Li et al. 2022. "Advances in IgA Glycosylation and Its Correlation with Diseases." *Frontiers in Chemistry* 10(September): 1–17.

Dorion-Thibaudeau, July et al. 2014. "Towards the Development of a Surface Plasmon Resonance Assay to Evaluate the Glycosylation Pattern of Monoclonal Antibodies Using the Extracellular Domains of CD16a and CD64." *Journal of Immunological Methods* 408: 24–34.

Dorion-Thibaudeau, July, Yves Durocher, and Gregory. De Crescenzo. 2017. "Quantification and Simultaneous Evaluation of the Bioactivity of Antibody Produced in CHO Cell Culture—The Use of the Ectodomain of FcγRI and Surface Plasmon Resonance-Based Biosensor." *Molecular immunology* 82: 46-49.

Essman, U et al. 1993. "A Smooth Particle Mesh Ewald Method." *Journal of Chemical Pysics* 10092(April): 10089–92.

Forest-Nault, Catherine et al. 2021. "On the Use of Surface Plasmon Resonance Biosensing to Understand Igg-FcγR Interactions." *International Journal of Molecular Sciences* 22(12).

Gao, Shunxiang et al. 2022. "A Biolayer Interferometry-Based, Aptamer–Antibody Receptor Pair Biosensor for Real-Time, Sensitive, and Specific Detection of the Disease Biomarker TNF-α." *Chemical Engineering Journal* 433(P2): 133268. https://doi.org/10.1016/j.cej.2021.133268.

Ghose, Sanchayita, Brian Hubbard, and Steven M. Cramer. 2006a. "Binding Capacity Differences for Antibodies and Fc-Fusion Proteins on Protein A Chromatographic Materials." *Biotechnology and Bioengineering* 96(4): 768–79.

———. 2006b. "Binding Capacity Differences for Antibodies and Fc-fusion Proteins on Protein A Chromatographic Materials." *Biotech Bioengineering* 96(4): 768–79. https://doi.org/10.1002/bit.21044.

Ghosh, Shreya et al. 2018. "Rapid Detection of Tumor Necrosis Factor-Alpha Using Quantum Dot-Based Optical Aptasensor." *IEEE Transactions on Nanobioscience* 17(4): 417–23.

Guerois, Raphael, Jens Erik Nielsen, and Luis Serrano. 2002. "Predicting Changes in the Stability of Proteins and Protein Complexes : A Study of More Than 1000 Mutations." *Journal of Molecular Biology* 2836(02): 369–87.

Hatayama, Kouta, Yoshiharu Asaoka, Megumi Hoya, and Teruhiko Ide. 2012. "Effective Expression of Soluble Aglycosylated Recombinant Human Fcγ Receptor i by Low Translational Efficiency in Escherichia Coli." *Applied Microbiology and Biotechnology* 94(4): 1051–59.

Hayes, Jerrard M. et al. 2016. "Fc Gamma Receptors: Glycobiology and Therapeutic Prospects." *Journal of inflammation research* 9: 209–19. https://pubmed.ncbi.nlm.nih.gov/27895507/.

———. 2017. "Identification of Fc Gamma Receptor Glycoforms That Produce Differential Binding Kinetics for Rituximab." *Molecular and Cellular Proteomics* 16(10): 1770–88.

Helena, Marcela et al. 2018. "Boosting Half-Life and Effector Functions of Therapeutic Antibodies by Fc-Engineering : An Interaction-Function Review." *International Journal of Biological Macromolecules* 119: 306–11. https://doi.org/10.1016/j.ijbiomac.2018.07.141.

Horiuchi, Takahiko et al. 2010a. "Transmembrane TNF-α: Structure, Function and Interaction with Anti-TNF Agents." *Rheumatology* 49(7): 1215–28. https://doi.org/10.1093/rheumatology/keq031.

———. 2010b. "Transmembrane TNF-α: Structure, Function and Interaction with Anti-TNF Agents." *Rheumatology* 49(7): 1215–28.

Humphrey, William, Andrew Dalke, and Klaus Schulten. 1996. "VMD : Visual Molecular Dynamics." *Journal of Molecular Graphics* 7855(December 1995): 33–38.

Irani, Vashti et al. 2015. "Molecular Properties of Human IgG Subclasses and Their Implications for Designing Therapeutic Monoclonal Antibodies against Infectious Diseases." *Molecular Immunology* 67(2): 171–82. http://dx.doi.org/10.1016/j.molimm.2015.03.255.

Jang, Dan-in et al. 2021. "The Role of Tumor Necrosis Factor Alpha ( TNF- α ) in Autoimmune Disease and Current TNF- α Inhibitors in Therapeutics." *International Journal of Molecular Sciences* 22(2719): 2–16.

Jefferis, Roy, and John Lund. 2002a. "Interaction Sites on Human IgG-Fc for FcγR: Current Models." *Immunology Letters* 82(1–2): 57–65.

———. 2002b. "Interaction Sites on Human IgG-Fc for FcγR: Current Models." *Immunology Letters* 82(1–2): 57–65.

Jo, Sunhwan, Kevin C Song, Heather Desaire, and Alexander D Mackerell. 2011. "Glycan Reader : Automated Sugar Identification and Simulation Preparation for Carbohydrates and Glycoproteins." *Journal of Computational Chemistry* 32: 3135–41.

Jung, Sang Taek, Tae Hyun Kang, and George Georgiou. 2010. "Efficient Expression and Purification of Human Aglycosylated Fc g Receptors in Escherichia Coli." 107(1): 21–30.

Kaplon, Hélène et al. 2023. "Antibodies to Watch in 2023." *mAbs* 15(1). https://doi.org/10.1080/19420862.2022.2153410.

Karlsson, Robert, Ewa Pol, and Åsa Frostell. 2016. "Comparison of Surface Plasmon Resonance Binding Curves for Characterization of Protein Interactions and Analysis of Screening Data." *Analytical Biochemistry* 502: 53–63.

Karplus, M., and J. Kuriyan. 2005. "Molecular Dynamics and Protein Function." *Proceedings of the National Academy of Sciences of the United States of America* 102(19): 6679–85.

Kim, Bo Yeong, Han Byeol Lee, and Nae Eung Lee. 2019. "A Durable, Stretchable, and Disposable Electrochemical Biosensor on Three-Dimensional Micro-Patterned Stretchable Substrate." *Sensors and Actuators, B: Chemical* 283(March 2018): 312–20. https://doi.org/10.1016/j.snb.2018.12.045.

Kim, Chloe, Justin F Galloway, Kwan Hyi Lee, and Peter C Searson. 2014. "Universal Antibody Conjugation to Nanoparticles Using the Fcγ Receptor I (FcγRI): Quantitative Profiling Of Membrane Biomarkers." *Bioconjugate Chemistry*.

Kim, Seokkyun et al. 2017. "Drifts in ADCC-Related Quality Attributes of Herceptin®: Impact on Development of a Trastuzumab Biosimilar." *mAbs* 9(4): 704–14.

Kiyoshi, Masato et al. 2015. "Structural Basis for Binding of Human IgG1 to Its High-Affinity Human Receptor FcγRI." *Nature Communications* 6: 4–6.

———. 2018. "Assessing the Heterogeneity of the Fc-Glycan of a Therapeutic Antibody Using an Engineered FcγReceptor IIIa-Immobilized Column." *Scientific Reports* 8(1): 1–11.

Knapp, Bernhard, Nadja Lederer, Ulrich Omasits, and Wolfgang. Schreiner. 2010.

"VmdICE A Plug-in for Rapid Evaluation of Molecular Dynamics Simulations Using VMD." *Journal of Computational Chemistry* 31(16): 2868-2873.

Kralj, Sebastjan et al. 2021. "Molecular Dynamics Simulations Reveal Interactions of an IgG1 Antibody With Selected Fc Receptors." *Frontiers in Chemistry* 9(July): 1–11.

Krieger, Elmar, Günther Koraimann, and Gert. Vriend. 2002. "Increasing the Precision of Comparative Models with YASARA NOVA a Self-parameterizing Force." *PROTEINS: Structure, Function, and Genetics* 402: 393-402. https://doi.org/10.1002/prot.10104.

Lee, Jong Ah Joanne et al. 2019. "Demonstration of Functional Similarity of a Biosimilar Adalimumab SB5 to Humira ®." *Biologicals* 58(May 2018): 7–15.

Lee, Jumin et al. 2016. "CHARMM-GUI Input Generator for NAMD, GROMACS, AMBER, OpenMM, and CHARMM/OpenMM Simulations Using the CHARMM36 Additive Force Field." *Journal of Chemical Theory and Computation* 12: 405–13.

Li, Haimei et al. 2021. "Quench-Release-Based Fluorescent Immunosensor for the Rapid Detection of Tumor Necrosis Factor α." *ACS Omega* 6(46): 31009–16.

Liu, Jennifer et al. 2016. "Assessing Analytical Similarity of Proposed Amgen Biosimilar ABP 501 to Adalimumab." *BioDrugs* 30(4): 321–38.

Lu, Jinghua et al. 2011. "Crystal Structure of Fc Gamma Receptor I and Its Implication in High Affinity Gamma -Immunoglobulin Binding." *The Journal of Biological Chemistry* 286(47): 40608–13.

———. 2015. "Structure of FcγRI in Complex with Fc Reveals the Importance of Glycan Recognition for High-Affinity IgG Binding." *Proceedings of the National Academy of Sciences of the United States of America* 112(3): 833–38.

Lu, Ruei-Min et al. 2020. "Development of Therapeutic Antibodies for the Treatment of Diseases." *Journal of Biomedical Sciences* 27(1): 1–30. https://doi.org/10.1186/s12929-019-0592-z.

Lyu, Xiaochen et al. 2022. "The Global Landscape of Approved Antibody Therapies." *Antibody Therapeutics* 5(4): 233–57.

Macri, Christophe, Huw Morgan, Jose A. Villadangos, and Justine D. Mintern. 2021. "Regulation of Dendritic Cell Function by Fc-γ-Receptors and the Neonatal Fc Receptor." *Molecular Immunology* 139: 193–201.

Martinez-Perdiguero, Josu, Aritz Retolaza, Luis Bujanda, and Santos Merino. 2014. "Surface Plasmon Resonance Immunoassay for the Detection of the TNFα Biomarker in Human Serum." *Talanta* 119: 492–97.

http://dx.doi.org/10.1016/j.talanta.2013.11.063.

Marušič, Jaka et al. 2012. "Recognition of Human Tumor Necrosis Factor α (TNF-α) by Therapeutic Antibody Fragment: Energetics and Structural Features." *Journal of Biological Chemistry* 287(11): 8613–20.

Mckeating, Kristy S. et al. 2019. "Antifouling Lipid Membranes over Protein a for Orientation-Controlled Immunosensing in Undiluted Serum and Plasma." *ACS Sensors* 4(7): 1774–82.

Murphy, Kenneth, and Casey Weaver. 2017. *Janeway's Immunobiology, Ninth Edition*. 9th ed. Garland Science: New York.

Oganesyan, Vaheh et al. 2015. "Structural Insights into the Interaction of Human IgG1 with FcγRI: No Direct Role of Glycans in Binding." *Acta Crystallographica Section D: Biological Crystallography* 71: 2354–61.

Ogura, Takeharu, Yoshiyuki Tanaka, and Hiromu Toyoda. 2016. "Whole Cell-Based Surface Plasmon Resonance Measurement to Assess Binding of Anti-TNF Agents to Transmembrane Target." *Analytical Biochemistry* 508: 73–77. http://dx.doi.org/10.1016/j.ab.2016.06.021.

Paetz, Antje et al. 2005. "Recombinant Soluble Human Fcγ Receptor I with Picomolar Affinity for Immunoglobulin G." *Biochemical and Biophysical Research Communications* 338(4): 1811–17.

Park, Sang-jun et al. 2017. "Structural Bioinformatics Glycan Reader Is Improved to Recognize Most Sugar Types and Chemical Modifications in the Protein Data Bank." *Bioinformatics* 33(June): 3051–57.

Park, Sang-jun Jun et al. 2019. "CHARMM-GUI Glycan Modeler for Modeling and Simulation of Carbohydrates and Glycoconjugates." *Glycobiology* 29(4): 320–31.

Patel, Rekha, Alyssa Neill, Hongcheng Liu, and Bruce Andrien. 2015. "IgG Subclass Specificity to C1q Determined by Surface Plasmon Resonance Using Protein L Capture Technique." *Analytical Biochemistry* 479: 15–17.

van der Poel, Cees E., Robbert M. Spaapen, Jan G. J. van de Winkel, and Jeanette H. W. Leusen. 2011. "Functional Characteristics of the High Affinity IgG Receptor, FcγRI." *The Journal of Immunology* 186(5): 2699–2704.

Pruna, Raquel et al. 2018. "Novel Nanostructured Indium Tin Oxide Electrode for Electrochemical Immunosensors: Suitability for the Detection of TNF-α." *Electrochimica Acta* 283: 1632–39.

Robinett, Ryan A. et al. 2018. "Dissecting FcγR Regulation through a Multivalent Binding

Model." *Cell Systems* 7(1): 41-48.e5. https://doi.org/10.1016/j.cels.2018.05.018.

Schroeder, Harry W, and Lisa Cavacini. 2010. "Structure and Function of Immunoglobulins." *J Allergy Clin Immunol* 125(202).

Schymkowitz, Joost et al. 2005. "The FoldX Web Server : An Online Force Field." *Nucleic Acids Research* 33: 382–88.

Seo, Neungseon et al. 2018. "Analytical and Functional Similarity of Amgen Biosimilar ABP 215 to Bevacizumab." *mAbs* 10(4): 678–91. https://www.tandfonline.com/doi/full/10.1080/19420862.2018.1452580 (November 21, 2019).

Shields, Robert L et al. 2001. "High Resolution Mapping of the Binding Site on Human IgG1 for FcγRI, FcγRII, FcγRIII, and FcRn and Design of IgG1 Variants with Improved Binding to the FcγR *." *The Journal of Biological Chemistry* 276(9): 6591–6604.

Taeye, Steven W De, Theo Rispens, and Gestur Vidarsson. 2019. "The Ligands for Human IgG and Their E Ff Ector Functions." *Antibodies* 14: 1–18.

Takakura, Michiko, Minoru Tada, and Akiko Ishii-Watabe. 2017. "Development of Cell-Based Assay for Predictively Evaluating the FcγR-Mediated Human Immune Cell Activation by Therapeutic Monoclonal Antibodies." *Biochemical and Biophysical Research Communications* 485(1): 189–94. http://dx.doi.org/10.1016/j.bbrc.2017.02.050.

Tebbey, Paul W. et al. 2015. "Consistency of Quality Attributes for the Glycosylated Monoclonal Antibody Humira® (Adalimumab)." *mAbs* 7(5): 805–11.

Temming, A Robin et al. 2021. "C-Reactive Protein Enhances IgG-Mediated Cellular Destruction Through IgG-Fc Receptors in Vitro." *Frontiers in Immunology* 12(March): 1–17.

The Antibody Society. 2022. "Therapeutic Monoclonal Antibodies Approved or in Review in the EU or US." (date accessed); www.antibodysociety.org/resources/approved-antibodies. .

Thomann, Marco et al. 2015a. "In Vitro Glycoengineering of IgG1 and Its Effect on Fc Receptor Binding and ADCC Activity." *PLoS ONE* 10(8): e0134949.

———. 2015b. "In Vitro Glycoengineering of IgG1 and Its Effect on Fc Receptor Binding and ADCC Activity." *PLOS ONE* 10(8): e0134949. https://journals.plos.org/plosone/article?id=10.1371/journal.pone.0134949 (August 17, 2021).

Upton, Rosie et al. 2016. "Orthogonal Assessment of Biotherapeutic Glycosylation: A Case Study Correlating N-Glycan Core Afucosylation of Herceptin with Mechanism of Action." *Analytical Chemistry* 88(20): 10259–65.

Vargas, Eva et al. 2022. "Using Cell Membranes as Recognition Layers to Construct Ultrasensitive and Selective Bioelectronic Affinity Sensors." *Journal of the American Chemical Society* 144(38): 17700–708.

Vidarsson, Gestur, Gillian Dekkers, and Theo Rispens. 2014. "IgG Subclasses and Allotypes : From Structure to Effector Functions." *Frontiers in Immunology* 5(October): 1–17.

Wang, Wei, and Qing Chen. 2022. "Antigen Improves Binding of IgGs to Fc γ Rs in SPR Analysis." *Analytical Biochemistry* 640: 114411. https://doi.org/10.1016/j.ab.2021.114411.

Wang, Wei, Sandra Thiemann, and Qing Chen. 2022. "Utility of SPR Technology in Biotherapeutic Development : Qualification for Intended Use." *Analytical Biochemistry* 654(April): 114804. https://doi.org/10.1016/j.ab.2022.114804.

Wang, Yuye et al. 2021. "Targeted Sub-Attomole Cancer Biomarker Detection Based on Phase Singularity 2D Nanomaterial-Enhanced Plasmonic Biosensor." *Nano-Micro Letters* 13(1): 1–11. https://doi.org/10.1007/s40820-021-00613-7.

van de Winkel, Jan G.J., and Peter J.A. Capel. 1993. "Human IgG Fc Receptor Heterogeneity: Molecular Aspects and Clinical Implications." *Immunology Today* 14(5): 215–21.

Xie, Liqi et al. 2020. "Demonstrating Analytical Similarity of Trastuzumab Biosimilar HLX02 to Herceptin® with a Panel of Sensitive and Orthogonal Methods Including a Novel FcγRIIIa Affinity Chromatography Technology." *BioDrugs* 34(3): 363–79. https://doi.org/10.1007/s40259-020-00407-0.

Yagati, Ajay Kumar, Min Ho Lee, and Junhong Min. 2018. "Electrochemical Immunosensor for Highly Sensitive and Quantitative Detection of Tumor Necrosis Factor-α in Human Serum." *Bioelectrochemistry* 122: 93–102. https://doi.org/10.1016/j.bioelechem.2018.03.007.

Zhang, Erhui et al. 2020. "Quality by Design–Based Assessment for Analytical Similarity of Adalimumab Biosimilar HLX03 to Humira®." *AAPS Journal* 22(3): 1–14.

Zhao, Jun, Ruth Nussinov, and Buyong Ma. 2019. "Antigen Binding Allosterically Promotes Fc Receptor Recognition." *mAbs* 11(1): 58–74.

Zhu, Han et al. 2022. "Aptamer-Assisted Protein Orientation on Silver Magnetic

Nanoparticles: Application to Sensitive Leukocyte Cell-Derived Chemotaxin 2 Surface Plasmon Resonance Sensors." *Analytical Chemistry* 94(4): 2109–18.

APPENDIX A

Parameters for glycan molecules within Fc chains

```
RESI BGLCNA           0.000  ! 2-acetyl-2-deoxy-beta-D-glucosamine
                             ! (beta N-acetylglucosamine or GlcNAc)
GROU                         !
ATOM C1   CC3162    0.340    !                    O6-HO6
ATOM H1   HCA1      0.090    !                    |
ATOM O1   OC311    -0.650    !                H61-C6-H62
ATOM HO1  HCP1      0.420    !                    |
ATOM C5   CC3163    0.110    !                 H5-C5---O5
ATOM H5   HCA1      0.090    !          H4    /        \      O1-HO1
ATOM O5   OC3C61   -0.400    !           \ / HO3         \  /
GROU                         !            C4 |           C1
ATOM C2   CC3161    0.070    !           / \ O3    H2  / \
ATOM H2   HCA1      0.090    !      HO4-O4   \|    | |/      H1
ATOM N    NC2D1    -0.470    !            C3---C2
ATOM HN   HCP1      0.310    !            |    |
GROU                         !            H3   N-HN
ATOM C    CC2O1     0.510    !                 /
ATOM O    OC2D1    -0.510    !              O=C    HT1
GROU                         !                 \  /
ATOM CT   CC331    -0.270    !              HT2-CT
ATOM HT1  HCA3      0.090    !                  \
ATOM HT2  HCA3      0.090    !                   HT3
ATOM HT3  HCA3      0.090    !
GROU                         !
ATOM C3   CC3161    0.140    !
ATOM H3   HCA1      0.090    !
ATOM O3   OC311    -0.650    !
ATOM HO3  HCP1      0.420    !
GROU                         !
ATOM C4   CC3161    0.140    !
ATOM H4   HCA1      0.090
ATOM O4   OC311    -0.650
ATOM HO4  HCP1      0.420
GROU
ATOM C6   CC321     0.050
ATOM H61  HCA2      0.090
ATOM H62  HCA2      0.090
ATOM O6   OC311    -0.650
ATOM HO6  HCP1      0.420
!
BOND C1   O1        C1   H1       O1   HO1      C1   O5        C1
C2
BOND C2   H2        C2   N        N    HN       C2   C3        C3
H3
BOND C3   O3        O3   HO3      C3   C4       C4   H4        C4
O4
BOND O4   HO4       C4   C5       C5   H5       C5   C6        C6
H61
BOND C6   H62       C6   O6       O6   HO6      C5   O5        N    C
BOND C    O         C    CT       CT   HT1      CT   HT2       CT
HT3
IMPR C CT N  O
IMPR N C  C2 HN
!    I    J    K    L     R(IK)   T(IKJ)   PHI    T(JKL)   R(KL)
IC      O1   C2  *C1   H1  1.3949  109.50  118.29  110.11   1.1152
```

```
IC      O1    O5    *C1    C2    1.3949   110.13   120.34   109.32   1.5156
IC       N    C3    *C2    H2    1.4607   113.70  -119.19   107.08   1.1227
IC       N    C1    *C2    C3    1.4607   112.62  -127.32   109.20   1.5149
IC      O3    C4    *C3    H3    1.4246   110.45   117.60   108.58   1.1171
IC      O3    C2    *C3    C4    1.4246   111.13   123.24   110.86   1.5168
IC      O4    C5    *C4    H4    1.4204   110.47  -117.94   108.07   1.1172
IC      O4    C3    *C4    C5    1.4204   110.88  -123.03   110.79   1.5206
IC      C6    O5    *C5    H5    1.5134   108.06   117.57   109.86   1.1171
IC      C6    C4    *C5    O5    1.5134   113.35   119.99   108.45   1.4386
IC      O6    H62   *C6    H61   1.4280   109.26  -117.58   107.87   1.1141
IC      O6    C5    *C6    H62   1.4280   111.18  -121.26   110.14   1.1132
IC      O5    C1    C2     C3    1.4220   109.32    58.90   109.20   1.5149
IC      C1    C2    C3     C4    1.5156   109.20   -52.68   110.86   1.5168
IC      C2    C3    C4     C5    1.5149   110.86    52.13   110.79   1.5206
IC      C3    C4    C5     O5    1.5168   110.79   -56.10   108.45   1.4386
IC      C4    C5    O5     C1    1.5206   108.45    64.09   111.47   1.4220
IC      C5    O5    C1     C2    1.4386   111.47   -66.18   109.32   1.5156
IC      C4    C5    C6     O6    1.5206   113.35  -179.21   111.18   1.4280
IC      O5    C1    O1     HO1   1.4220   110.13    53.79   107.03   0.9601
IC      C1    C2    N      HN    1.5156   112.62   -21.73   117.18   0.9940
IC      C2    C3    O3     HO3   1.5149   111.13     0.20   109.43   0.9762
IC      C3    C4    O4     HO4   1.5168   110.88    45.93   106.90   0.9672
IC      C5    C6    O6     HO6   1.5134   111.18   -58.35   108.74   0.9641
IC       C    N     C2     C3    1.3365   123.04   -84.98   113.70   1.5149
IC       C    C2    *N     HN    1.3365   123.04  -171.85   117.18   0.9940
IC      CT    C     N      C2    1.4798   117.02  -173.18   123.04   1.4607
IC       N    CT    *C     O     1.3365   117.02   178.97   121.63   1.2235
IC       O    C     CT     HT1   1.2235   121.63   116.39   110.28   1.1105
IC       O    C     CT     HT2   1.2235   121.63    -3.06   109.29   1.1121
IC       O    C     CT     HT3   1.2235   121.63  -122.59   110.33   1.1105
PATC FIRS NONE LAST NONE

RESI BMAN              0.000  ! 4C1 beta-D-mannose
                              !
GROU                          !
ATOM C1   CC3162    0.340  !                      O6-HO6
ATOM H1   HCA1      0.090  !                      |
ATOM O1   OC311    -0.650  !                 H61-C6-H62
ATOM HO1  HCP1      0.420  !                      |
ATOM C5   CC3163    0.110  !                 H5-C5---O5
ATOM H5   HCA1      0.090  !           H4   /        \    O1-HO1
ATOM O5   OC3C61   -0.400  !            \  /  HO3 HO2  \  /
GROU                          !            C4  |    |   C1
ATOM C2   CC3161    0.140  !            / \ O3   O2 / \
ATOM H2   HCA1      0.090  !        HO4-O4  \|    | /    H1
ATOM O2   OC311    -0.650  !                C3---C2
ATOM HO2  HCP1      0.420  !                |     |
GROU                          !                H3    H2
ATOM C3   CC3161    0.140  !
ATOM H3   HCA1      0.090  !
ATOM O3   OC311    -0.650  !
ATOM HO3  HCP1      0.420  !
GROU
ATOM C4   CC3161    0.140
ATOM H4   HCA1      0.090
ATOM O4   OC311    -0.650
ATOM HO4  HCP1      0.420
GROU
ATOM C6   CC321     0.050
```

```
ATOM H61    HCA2     0.090
ATOM H62    HCA2     0.090
ATOM O6     OC311   -0.650
ATOM HO6    HCP1     0.420
!
BOND C1    O1        C1    H1        O1    HO1        C1    O5         C1
C2
BOND C2    H2        C2    O2        O2    HO2        C2    C3         C3
H3
BOND C3    O3        O3    HO3        C3    C4         C4    H4         C4
O4
BOND O4    HO4       C4    C5        C5    H5         C5    C6         C6
H61
BOND C6    H62       C6    O6        O6    HO6        C5    O5
!     I     J     K     L      R(IK)    T(IKJ)     PHI    T(JKL)     R(KL)
IC   O1    C2   *C1    H1     1.4147   114.01   123.87   115.47    1.1241
IC   O1    O5   *C1    C2     1.4147   102.76   121.94   110.36    1.5194
IC   O2    C3   *C2    H2     1.4714   110.16   123.24   108.47    1.1051
IC   O2    C1   *C2    C3     1.4714   114.57   122.69   107.36    1.5071
IC   O3    C4   *C3    H3     1.3878   111.68   114.99   113.62    1.1108
IC   O3    C2   *C3    C4     1.3878   109.74   124.46   111.76    1.5071
IC   O4    C5   *C4    H4     1.3992   108.74  -119.41   104.60    1.1086
IC   O4    C3   *C4    C5     1.3992   114.29  -123.16   110.67    1.5450
IC   C6    O5   *C5    H5     1.5345   108.55   116.69   108.96    1.0801
IC   C6    C4   *C5    O5     1.5345   111.73   122.98   113.28    1.4134
IC   O6    H62  *C6    H61    1.4228   107.34  -116.56   114.05    1.1041
IC   O6    C5   *C6    H62    1.4228   116.50  -120.25   107.28    1.1156
IC   O5    C1    C2    C3     1.4381   110.36    63.05   107.36    1.5071
IC   C1    C2    C3    C4     1.5194   107.36   -55.99   111.76    1.5071
IC   C2    C3    C4    C5     1.5071   111.76    49.25   110.67    1.5450
IC   C3    C4    C5    O5     1.5071   110.67   -49.18   113.28    1.4134
IC   C4    C5    O5    C1     1.5450   113.28    56.65   110.70    1.4381
IC   C5    O5    C1    C2     1.4134   110.70   -64.29   110.36    1.5194
IC   C4    C5    C6    O6     1.5450   111.73  -168.80   116.50    1.4228
IC   O5    C1    O1    HO1    1.4381   102.76   -14.89   110.00    0.9891
IC   C1    C2    O2    HO2    1.5194   114.57   -31.81   104.69    0.9864
IC   C2    C3    O3    HO3    1.5071   109.74    46.67   101.47    0.9688
IC   C3    C4    O4    HO4    1.5071   114.29    42.72   117.62    0.9726
IC   C5    C6    O6    HO6    1.5345   116.50   -62.83   105.97    0.9733
PATC  FIRS NONE LAST NONE
RESI AMAN              0.000 ! 4C1 alpha-D-mannose
                            !
GROU                        !
ATOM C1     CC3162   0.340 !                        O6-HO6
ATOM H1     HCA1     0.090 !                         |
ATOM O1     OC311   -0.650 !                    H61-C6-H62
ATOM HO1    HCP1     0.420 !                         |
ATOM C5     CC3163   0.110 !                    H5-C5---O5
ATOM H5     HCA1     0.090 !              H4   /        \    H1
ATOM O5     OC3C61  -0.400 !                \ / HO3 HO2 \  /
GROU                        !                C4  |    |   C1
ATOM C2     CC3161   0.140 !               / \  O3   O2 / \
ATOM H2     HCA1     0.090 !          HO4-O4  \|    | /    O1-HO1
ATOM O2     OC311   -0.650 !                  C3---C2
ATOM HO2    HCP1     0.420 !                  |     |
GROU                        !                 H3    H2
ATOM C3     CC3161   0.140 !
ATOM H3     HCA1     0.090 !
ATOM O3     OC311   -0.650 !
```

89

```
ATOM HO3  HCP1      0.420  !
GROU
ATOM C4   CC3161    0.140
ATOM H4   HCA1      0.090
ATOM O4   OC311    -0.650
ATOM HO4  HCP1      0.420
GROU
ATOM C6   CC321     0.050
ATOM H61  HCA2      0.090
ATOM H62  HCA2      0.090
ATOM O6   OC311    -0.650
ATOM HO6  HCP1      0.420
!
BOND C1   O1        C1   H1        O1   HO1       C1   O5        C1
C2
BOND C2   H2        C2   O2        O2   HO2       C2   C3        C3
H3
BOND C3   O3        O3   HO3       C3   C4        C4   H4        C4
O4
BOND O4   HO4       C4   C5        C5   H5        C5   C6        C6
H61
BOND C6   H62       C6   O6        O6   HO6       C5   O5
!    I    J    K    L       R(IK)   T(IKJ)    PHI     T(JKL)   R(KL)
IC   O1   C2   *C1  H1     1.3975  110.50  -118.09   109.89   1.1050
IC   O1   O5   *C1  C2     1.3975  108.93  -123.71   113.70   1.4876
IC   O2   C3   *C2  H2     1.4750  107.62   114.46   115.21   1.1022
IC   O2   C1   *C2  C3     1.4750  114.83   120.80   109.00   1.5586
IC   O3   C4   *C3  H3     1.4261  109.30   119.59   108.95   1.1150
IC   O3   C2   *C3  C4     1.4261  109.19   118.55   107.65   1.5049
IC   O4   C5   *C4  H4     1.3887  107.72  -127.19   110.85   1.1254
IC   O4   C3   *C4  C5     1.3887  108.42  -117.81   110.46   1.5035
IC   C6   O5   *C5  H5     1.4825  112.02   117.79   109.03   1.1288
IC   C6   C4   *C5  O5     1.4825  112.70   127.52   112.13   1.4375
IC   O6   H62  *C6  H61    1.4292  107.96  -123.56   113.24   1.1140
IC   O6   C5   *C6  H62    1.4292  109.39  -114.45   102.63   1.1098
IC   O5   C1   C2   C3     1.3632  113.70   56.64    109.00   1.5586
IC   C1   C2   C3   C4     1.4876  109.00  -56.11    107.65   1.5049
IC   C2   C3   C4   C5     1.5586  107.65   55.76    110.46   1.5035
IC   C3   C4   C5   O5     1.5049  110.46  -54.16    112.13   1.4375
IC   C4   C5   O5   C1     1.5035  112.13   53.40    114.61   1.3632
IC   C5   O5   C1   C2     1.4375  114.61  -55.52    113.70   1.4876
IC   C4   C5   C6   O6     1.5035  112.70  -173.75   109.39   1.4292
IC   O5   C1   O1   HO1    1.3632  108.93   53.42    107.62   0.9615
IC   C1   C2   O2   HO2    1.4876  114.83  -137.09   114.41   1.0113
IC   C2   C3   O3   HO3    1.5586  109.19   60.11    113.74   0.9944
IC   C3   C4   O4   HO4    1.5049  108.42   42.16    103.57   0.9552
IC   C5   C6   O6   HO6    1.4825  109.39  -84.75    103.86   0.9396
PATC FIRS NONE LAST NONE
RESI BFUC              0.000  ! beta-L-fucose
                             !
GROU                         !
ATOM C1   CC3162    0.340  !
ATOM H1   HCA1      0.090  !
ATOM O1   OC311    -0.650  !                          H5
ATOM HO1  HCP1      0.420  !                          |
ATOM C5   CC3163    0.110  !                       C5---O5
ATOM H5   HCA1      0.090  !           H4   /|        \    H1
ATOM O5   OC3C61   -0.400  !            \ / C6  HO2 \  /
GROU                         !             C4       |   C1
```

90

```
ATOM C2    CC3161    0.140  !                    / \ H3   O2 / \
ATOM H2    HCA1      0.090  !          HO4-O4   \|    | /   O1-HO1
ATOM O2    OC311    -0.650  !                   C3---C2
ATOM HO2   HCP1      0.420  !                   |    |
GROU                        !              HO3-O3    H2
ATOM C3    CC3161    0.140  !
ATOM H3    HCA1      0.090  !         n.b.: H61, H62, and H63 are
attached to C6
ATOM O3    OC311    -0.650  !
ATOM HO3   HCP1      0.420  !
GROU
ATOM C4    CC3161    0.140
ATOM H4    HCA1      0.090
ATOM O4    OC311    -0.650
ATOM HO4   HCP1      0.420
GROU
ATOM C6    CC331    -0.270
ATOM H61   HCA3      0.090
ATOM H62   HCA3      0.090
ATOM H63   HCA3      0.090
!
BOND C1    O1          C1    H1          O1    HO1          C1    O5           C1
C2
BOND C2    H2          C2    O2          O2    HO2          C2    C3           C3
H3
BOND C3    O3          O3    HO3         C3    C4           C4    H4           C4
O4
BOND O4    HO4         C4    C5          C5    H5           C5    C6           C6
H61
BOND C6    H62         C6    H63         C5    O5
!      I      J      K      L      R(IK)     T(IKJ)     PHI     T(JKL)    R(KL)
IC    O1     C2    *C1     H1     1.4115    105.82   -120.26   110.81   1.0905
IC    O1     O5    *C1     C2     1.4115    113.00   -118.92   111.32   1.5218
IC    O2     C3    *C2     H2     1.4190    110.99    116.97   108.77   1.0892
IC    O2     C1    *C2     C3     1.4190    111.74    123.77   110.04   1.5167
IC    O3     C4    *C3     H3     1.4198    108.29   -120.00   108.28   1.0957
IC    O3     C2    *C3     C4     1.4198    111.19   -120.00   110.08   1.5102
IC    O4     C5    *C4     H4     1.4163    108.82   -120.00   109.07   1.0972
IC    O4     C3    *C4     C5     1.4163    111.43   -120.00   108.83   1.5171
IC    C6     O5    *C5     H5     1.5099    105.42   -117.88   109.66   1.0926
IC    C6     C4    *C5     O5     1.5099    112.84   -117.26   109.77   1.4384
IC    H63    H62   *C6     H61    1.0900    111.42    118.10   108.62   1.0873
IC    H63    C5    *C6     H62    1.0900    111.44    123.18   108.72   1.0943
IC    O5     C1     C2     C3     1.4059    111.32    -53.56   110.04   1.5167
IC    C1     C2     C3     C4     1.5218    110.04     54.55   110.08   1.5102
IC    C2     C3     C4     C5     1.5167    110.08    -57.15   108.83   1.5171
IC    C3     C4     C5     O5     1.5102    108.83     58.25   109.77   1.4384
IC    C4     C5     O5     C1     1.5171    109.77    -59.84   114.27   1.4059
IC    C5     O5     C1     C2     1.4384    114.27     57.30   111.32   1.5218
IC    C4     C5     C6     H63    1.5171    112.84    -60.00   111.44   1.0900
IC    O5     C1     O1     HO1    1.4059    113.00    -60.00   108.04   0.9634
IC    C1     C2     O2     HO2    1.5218    111.74     60.00   105.37   0.9665
IC    C2     C3     O3     HO3    1.5167    111.19     60.00   106.26   0.9641
IC    C3     C4     O4     HO4    1.5102    111.43     60.00   105.89   0.9645
```